ABSTRACT

Title: **PHYSICS-BASED MODEL-GUIDED MACHINE LEARNING ANALYSIS OF WRIST BALLISTOCARDIOGRPHY FOR CUFF-LESS BLOOD PRESSURE MONITORING**

Peyman Yousefian
Doctor of Philosophy, 2019

Directed by: Associate Professor Jin-Oh Hahn, Mechanical Engineering Department

Abstract: Cuff-less blood pressure (BP) monitoring technology is being widely pursued today. In this research we investigated the wrist ballistocardiogram (BCG) as a limb BCG, to develop a scientific basis to use the limb BCG to for cuff-less BP monitoring. In our study, we pursue two alternative approaches to the use of wrist BCG signal for BP monitoring: (1) use of the wrist BCG as proximal timing in pulse transit time (PTT) based methods; (2) use of wrist BCG wave features for BP monitoring. In this regard, the physics-based model is developed to elucidate the mechanism responsible for the generation of the BCG signal at the body's extremity limb locations. The developed and experimentally validated mathematical model can predict the limb BCG in responses to the arterial BP waves in the aorta. The model suggests that the limb BCG waveform reveals the timings and amplitudes associated with the aortic BP waves and it exhibits meaningful morphological changes in response to the alterations in the CV risk predictors. Such understanding combined with machine learning techniques has helped us to extract viable features, and construct predictive models that can estimate BP. The findings of this study show that limb BCG has the potential to realize convenient cuff-less BP monitoring. First, it is a strong candidate to extract the proximal timing for PTT based methods. Second, BCG wave features are associated with BP and it could be used for BP monitoring. Third, we can combine the PTT with BCG wave features to achieve more comprehensive prediction models with superior performance.

PHYSICS-BASED MODEL-GUIDED MACHINE LEARNING ANALYSIS OF WRIST BALLISTOCARDIOGRPHY FOR CUFF-LESS BLOOD PRESSURE MONITORING

by

Peyman Yousefian

Dissertation submitted to the Faculty of the Graduate School of the
University of Maryland, College Park, in partial fulfillment
of the requirements for the degree of
Doctor of Philosophy
2019

Advisory Committee:

Associate Professor Jin-Oh Hahn, Chair

Professor Alison B. Flatau, Dean's Representative

Professor Balakumar Balachandran

Professor Amr M. Baz

Professor Nikhil Chopra

Dedication

To my family.

Acknowledgements

Foremost, I would like to express my sincere gratitude to my advisor Prof. Hahn for the continuous support of this research. His guidance helped me in all the time of research. Besides my advisor, I would like to thank my fellow coworkers: Sungtae Shin, and Azin Mousavi for the human subject experiments and data collection.

Table of Contents

List of Figures

List of Tables

1. Introduction

Cardiovascular disease (CVD) is a leading cause of mortality and morbidity that produces immense health and economic impacts in the United States and globally[1]. Considering its prevalence and implications on the quality of life and healthcare cost, one ideal solution to effective prevention and treatment of CVD is to enable ubiquitous surveillance and monitoring of CV risk predictors based on ultra-convenient techniques. However, the majority of state-of-the-art techniques for non-invasive measurement and assessment of CV risk predictors suffer from inconvenience. Indeed, techniques such as carotid-femoral tonometry for pulse wave velocity measurement[2]–[7], flow-mediated dilatation for endothelial function assessment[8]–[11], and ankle-brachial index for peripheral artery disease screening[12]–[14] necessitate at least a subset of the following inconvenience and discomfort: trained operators, specialized costly equipment, access to privately sensitive body sites, and interventions.

The BCG, defined as the body movement in response to the blood ejected by the heart, is increasingly receiving interest as an emerging modality equipped with the great potential to realize ultra-convenient CV health monitoring and assessment by virtue of its direct relationship to CV functions[15] and its amenity to ultra-convenient measurement. Indeed, early investigations have demonstrated that the BCG may have clinical value due to the close association between its waveform morphology and various cardiac events[16]–[21]. In addition, rapid advances in the electronics and wearable technology opened up the possibility to ultra-conveniently measure the BCG during daily activities[22]–[30]. These unique advantages combined, recent applications of the BCG to CV health monitoring have reported success in estimating a range of CV parameters and risk predictors: heart rate[22], [23], pulse transit time and pulse wave velocity[24], [31]–[34], arterial BP[28], [30], [32], [33], stroke volume and cardiac output[29], [32], and cardiac contractility[35]–[37] to list a few.

Despite the reasonable success and demonstrated promise, there are a few critical challenges common to most, if not all, prior endeavors on the BCG-based CV health monitoring. One salient challenge is that prior endeavors lack in rigor in terms of insights related to the physical meaning of the BCG. In the absence of established physical understanding of the BCG, most prior efforts have pursued brute-force data-driven approaches in which the association between a set of subjectively selected features in the BCG waveform versus the target CV parameters and risk predictors of interest was sought [27]–[30], [37]. The other salient challenge is that the BCG waveform morphology is known to exhibit large variability with respect to the measurement instruments, postures, and

locations [36], [38], [39]. These challenges altogether complicate the interpretation of the successful data-driven associations obtained in prior works, as well as hamper the seamless translation and generalization of the compelling findings obtained for the BCG pertaining to a specific instrument, posture, and location to other instruments, postures, and locations. It is contended that a viable solution to address these challenges is to drastically enhance the physiological understanding of the BCG, its association with the underlying CV physiology, and its variability with respect to the alterations in the instrument, posture, and location. Such physical insights, if established and properly integrated with the ongoing success of the data-driven BCG-based approaches to CV health monitoring, may open up new opportunities toward next generation of BCG-based CV healthcare techniques embedded with transparency, interpretability, and robustness against the external variability.

Currently, the most popular approach to cuff-less BP monitoring is based on the principle of PTT [40]. PTT is the time delay for the pressure wave to travel between two arterial sites. An increase in BP causes PTT to decline, as artery stiffens with an increase in BP, thereby increasing the velocity of travel of the pressure wave. Hence, PTT is often inversely correlated with BP. One main drawback of the PTT approach, especially from a convenience standpoint, is that it requires the instrumentation of two arterial pulse waveforms to compute PTT. In the past, this requirement has been fulfilled by measuring arterial pulse waveforms from two distinct locations in the body (e.g., from carotid and femoral arteries for the well-known carotid-femoral PTT [41]), which is quite inconvenient and cumbersome. Hence, a recent effort to enable ultra-convenient BP monitoring has focused on the development of techniques to infer BP from a single wearable device. Some of these efforts employ multiple pulse waveforms from a single device (e.g., an electrocardiogram and a photoplethysmogram (PPG) at an extremity site [42], [43], or multiple PPGs within a known short distance [44]) to still leverage the PTT principle for BP monitoring, while some other efforts strive to infer BP from the analysis of a single pulse waveform [45]–[47]. In both cases, PPG has been the preferred choice of modality for arterial pulse measurement due to its amenity to easy placement and stable instrumentation.

It is demonstrated that the whole-body BCG measured with, e.g., a weighing scale-like platform, may be leveraged in conjunction with a second pulse waveform (e.g., PPG at an extremity location) for PTT-based BP monitoring [31], [48]. It is also demonstrated that whole-body BCG alone may suffice for cuff-less BP monitoring, where previous studies attempted the use of waveform features in the whole-body BCG that (at least qualitatively) represent aortic PTT and distal aortic pulse pressure (PP) to achieve independent monitoring of diastolic (DP) and systolic (SP) BPs [33].

Despite the potential of the whole-body-BCG signal to improve the cuff-less BP monitoring techniques explored thus far, there are still extra rooms for improvement both in convenience and accuracy. In terms of convenience, the measurement of whole-body BCG may require bulky devices such as scale and bed. Hence, a viable option to improve convenience may be to explore wearables that can be worn on limb locations (e.g., wrist watch and arm band) for instrumentation of the BCG. In terms of accuracy, whole-body BCG measurement systems like scales are dependent on load measurement techniques. In these techniques, deflection of a beam supporting the body mass is measured using a strain gauge. It is possible that the dynamic of the scale affects the body motion and consequently changes the morphology and accuracy of the BCG signal. We can avoid such a problem by measuring the wrist BCG with a small accelerometer.

Motivated by the above rationale, this research is coordinated in the following sequence. First, we need to understand the origin of the limb BCG. In this regard, the mechanical model of the whole body in response to the blood extraction by heart is developed in chapter 3. The model is analyzed to understand the BCG signal morphology and discover any meaningful association of the features in the signal with heart-related activities, like aortic BP timings or amplitudes. The model illustrates that there are some features in the BCG signal that could be used as a proximal timing to calculate PTT. In addition, it is also discovered that there are some features inside the BCG signal that are representative of PTT. For example, J-K interval in wrist BCG is highly correlated with aortic PTT. In the next chapters, we will use these findings to develop physics-based BP predictors.

In the next chapters, we develop predictive models to estimate BP by levering the physics-based insights discovered in chapter 3, as well as using machine learning techniques to select and create predictors using BCG and PPG signals. In chapter 4, limb BCG-based PTT is constructed for BP estimation, using the Physics-based insights obtained in the previous chapter. In this chapter, we compare the performance of the wrist-based BCG with whole-body-based BCG as proximal timing and illustrate that wrist BCG could serve as superior proximal timing in PTT calculation. In chapter 5, the idea of only using BCG signal to estimate the BP is examined, as a more convenient alternative compared to the PTT method that needs two BCG and PPG signals. In chapter 6, a hybrid model is examined, in which both PTT and BCG-based features are utilized. In chapter 7, subject-specific models are examined for both BCG-based and hybrid approach. Chapter 8 concludes the thesis, and chapter 9 explains the limitations of this work and suggests future works.

2. Concepts and Literature Review

In this section, a quick introduction of the BP waveform and classical BP monitoring methods are presented. Then basic concepts of the novel methods for noninvasive continuous monitoring of BP is reviewed. In this regard, three physiological signal will be used to estimate BP.

- ECG (Electrocardiogram): is a time variant voltage produced by the myocardium during the cardiac cycle. It contains P, QRS, and T peaks which reflect rhythmic electrical depolarization and repolarization of the myocardium, representing the contraction of the arteria and ventricles.
- PTT (Pulse Transit Time): is the time taken for the arterial pulse pressure wave to travel from proximal to a peripheral site. The PTT is believed to be inversely correlated with the BP [49].
- PPG (Photoplethysmography): indicated the amount of the oxygen in artery by emitting a light to the artery and measuring the reflected or transmitted value of the light.
- BCG (Ballistocardiography): measures the reactionary forces of the body in response to cardiac ejection of blood into aorta [2].

The next sections will discuss how to use each or combination of the mentioned signals to estimate the blood pressure.

2.1. BP Waveforms

According to the illustrated diagram of blood circulation in Fig. 2.1. , oxygenized blood in the lungs is pumped by the left side of the heart through aorta to reach into various body organs. Then it returns to the right side of the heart through veins and is pumped into the lungs. As blood flows through the systemic circulation, pressure decreases progressively because of the resistance to blood flow. Thus, it is highest in the aorta, and lowest when it returns to the heart.

Blood flow can be expressed by the following equation:

$$Q = \frac{\Delta P}{R} \qquad \text{Eq. 2.1}$$

in which Q is flow or cardiac output (ml/min), ΔP is pressure gradient (mm Hg), and R is resistance (mm Hg/mL/min). The equation can be rewritten as

$$\text{Cariac Output} = \frac{\text{Mean arterial pressure - Right arterial pressure}}{\text{Total peripheral resistance (TPR)}} \qquad \text{Eq. 2.2}$$

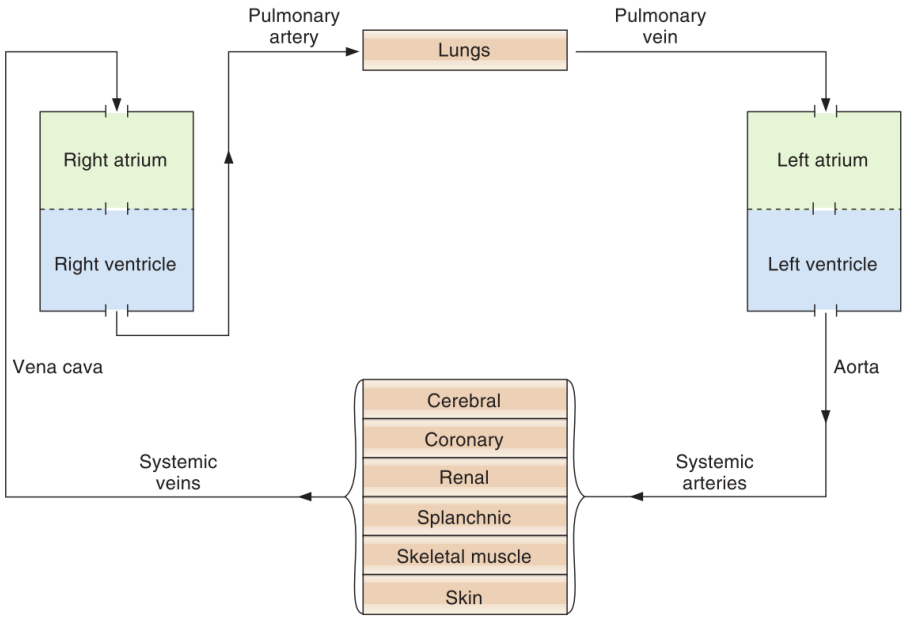

Fig. 2.1. Circuitry of the cardiovascular system [50].

Blood flow in the vessels can be either laminar or turbulent. Laminar flow is streamlined in a straight line, while the turbulent flow is not. Reynold's number predicts whether it is laminar or turbulent, increases with blood velocity and decreases with viscosity. At high Reynold's numbers, there is a tendency for turbulent, which causes audible vibrations called bruits.

As mentioned earlier, arterial blood pressure is not constant during cardiac cycle. As illustrated in It is pulsatile and varies over time and location. Systolic pressure is the highest arterial blood pressure during a cardiac cycle. Systolic BP is measured when the blood is ejected into the arterial system after the heart contraction (systole in Fig. 2.3). Contrary to systolic BP, diastolic pressure is the lowest arterial pressure during the cardiac cycle. Diastolic BP is measured when the heart is relaxed (diastole in Fig. 2.3) and blood is returned to the heart via the veins. The difference between the systolic and diastolic pressure is known as pulse pressure. As blood is ejected from the left ventricle into the arterial system, arterial pressure increases because of the low capacitance of the arteries. Stroke volume is the most important determinant of pulse pressure [50].

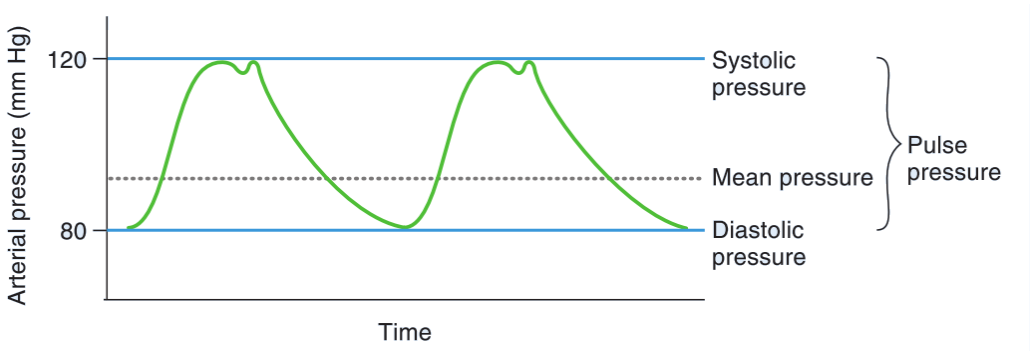

Fig. 2.2. A typical human blood pressure waveform [50].

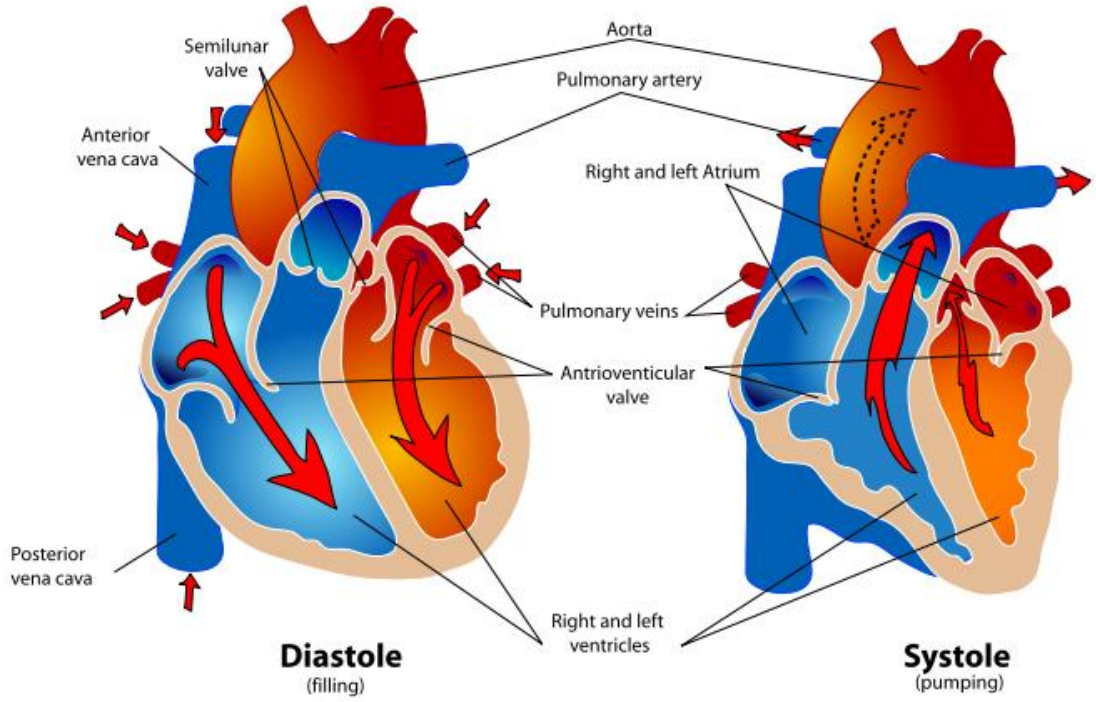

Fig. 2.3. Human heart in systole and diastole [51].

2.2. Introduction to Conventional BP Measurement Methods

Among the several BP monitoring methods [2], Cathetherication is the most accurate method to measure the BP. In this method, the invasive catheter provides access to the arterial system. A strain gauge contacts the fluid and measures the pressure waves generated in the arterial system by cardiac contractions [52]. In addition, several non-invasive techniques are available for measuring BP (including auscultation [53] and

oscillometry [54], [55] used in patient care; and volume clamping [56], [57] and tonometry [58], [59] used in research). In this section a brief introduction of each method is presented.

Auscultation: in this method, the operator puts an air cuff around the arm and pumps it up to cut of the blood flow in the artery with the pressure extracted by the cuff. Then they start to release the pressure in the cuff. As the pressure decreases, the blood starts to flow again, where the operator hears a sound known as Korotkoff sound. The pressure at which blood starts flowing, is the measure of the maximum output pressure of the heart or systolic BP. Then, the operator continues to release the pressure slowly, and consequently the sound in the cuff is gradually decreased. It continues to the point that the sound stops. The point at which the sound stops, in which the turbulent flow is turned into the laminar flow, is indicator of the diastolic BP [53]. This method requires a great deal of training and is subjected to the expertise of the examiner.

Oscillometric: This method is similar to the auscultation method. In this method small fluctuation of the cuff are measured rather than Korotkoff sounds to detect the systolic, mean, and diastolic blood pressure [19].

Volume clamp method: this method is based on transforming the information of the volume of blood in the artery to pressure. Increasing of the pressure inside the artery will cause increase in the volume of the blood. as illustrated in Fig. 2.4, an external pressure is inserted to the artery, to counter balance the internal pressure to maintain the constant volume. In such condition, the inserted external pressure is equal to the blood pressure in the artery. A PPG sensor on the finger measures the volume of the blood, and an air cuff installed on the finger provides the required external pressure [60].

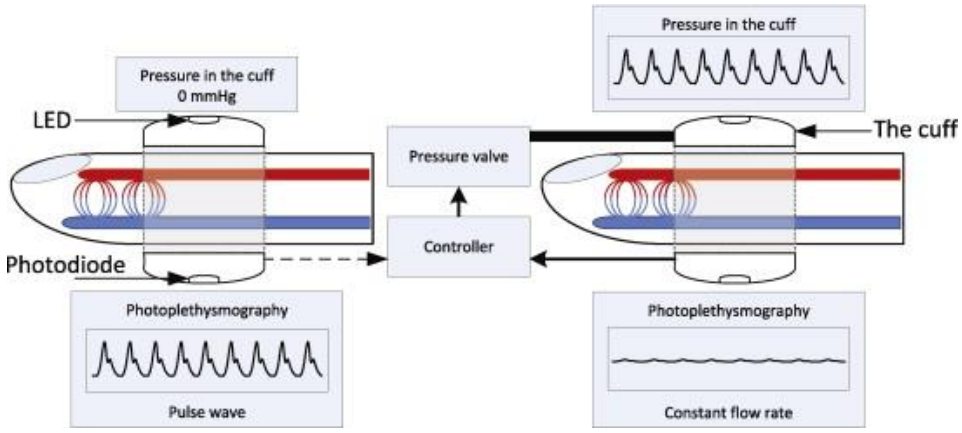

Fig. 2.4- Working principal of the volume clamp method to measure BP [60].

Tonometry: in this method, pressure sensor is pressed on an artery which is located near the surface to detect blood pressure. In this measurement, the upper part of the blood vessel is made flat by pushing it with appropriate strength. As depicted in Fig. 2.5, at the flat area of the blood vessel, the tension force of the blood vessel is normal to the direction of the force due to blood pressure. So it will not counter act the blood pressure, and the sensor can directly measure the pressure [61].

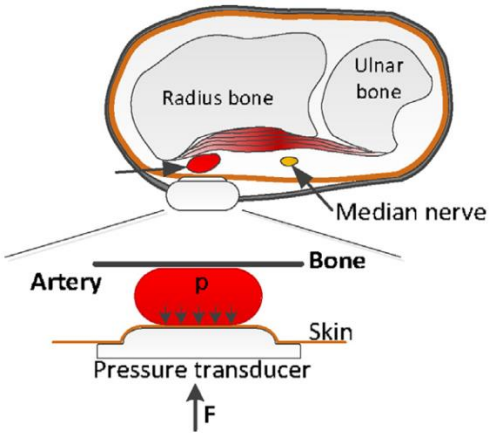

Fig. 2.5- Working principle of the tonometry method [60].

2.3. Association of BP and PTT

PTT is defined as the time delay that pulse pressure needs to travel between two locations in the body Fig. 2.6(a). Given that the velocity of the pressure pulse is a function of the pressure of the fluid, and increases as the pressure goes up, PTT is inversely related to the BP. It means that for higher blood pressure we expect shorter PTT, and vice versa. Hence, PTT contains information about the BP, and makes it possible to estimate it noninvasively and cuff-less. As shown in Fig. 2.6(b) BP is correlated to PTT, however we should note that BP is not the only factor that affects PTT [2].

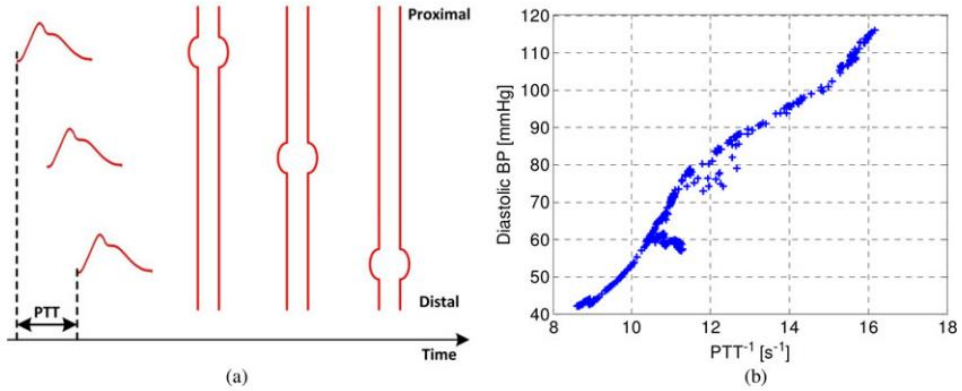

Fig. 2.6- PTT as an indicator of the blood pressure level. (a) PTT is defined as the time delay for the pressure pulse to travel between two arterial locations. (b) Higher blood pressure pulse needs less time to travel between two locations, thus PTT is inversely correlated to BP [2].

Reference [62] introduced a simple physical model to describe the relationship between PTT and BP. The introduced model simplifies the body structure and defines BP as a function of PTT based on the fundamental physics and the conservation of energy. It assumes laminar blood flow from the heart chamber to fingertip through a rigid pipe, representing the artery. The model estimates the pulse velocity by dividing the distance between heart and fingertip by the PTT. Then it uses the approximate pulse transit velocity to estimate the blood pressure.

$$F.d = \frac{1}{2}mv^2 + mgh \qquad \text{Eq. 2.3}$$

where the left side is the work done by heart and the right side is the total energy of the blood traveling from the heart to the fingertip. The force is equal to the blood pressure multiplied by arterial cross section area, and velocity can be estimated by PTT. The following equation can be derived by replacing the corresponding terms and simplification as explained in [62].

$$BP = \frac{A}{PTT^2} + B = \frac{1}{1.4}\rho\frac{d^2}{PTT^2} + \frac{\rho gh}{0.7} \qquad \text{Eq. 2.4}$$

where d is the distance between heart and fingertip, ρ is the density of the blood, h is the height difference between the heart and fingertip, g is the gravity constant. Since the presented model assumes laminar and non-pulsatile flow, it is more appropriate to describe diastolic BP. Since the systolic pressure is highly correlated with mean BP and diastolic BP, PTT can be used to infer systolic BP, as well.

While the previous model, gives a simple physical interpretation of the BP and PTT relationship using the conversion of the energy law, it doesn't consider any details like the effect of the artery compliance. In this regard, more comprehensive models are presented to consider mechanical elements affecting the relationship between BP and PTT. A comprehensive summary of the available models is reported in [2]. In this regard, two model is required to describe BP and PTT relationship: (1) the relationship between BP and arterial elasticity, known as arterial wall models, (2) the relationship between arterial elasticity with wave propagation speed and consequently PTT, known as wave propagation models. Some of the derived models are as below equations:

$$BP = K_1 \ln\left(PTT\right) + K_2 \qquad \text{Eq. 2.5}$$

$$BP = \frac{K_1}{PTT} + K_2 \qquad \text{Eq. 2.6}$$

$$BP = \frac{K_1}{\left(PTT - K_2\right)^2} + K_3 \qquad \text{Eq. 2.7}$$

Among the introduced models, experimental studies have shown that 1/PTT is linearly related to BP over a wide range of BP change.

As mentioned above, PTT is the time delay that BP waveform takes to travel from one location to another. So we need to measure timing of BP pulse at two different locations, and then calculate PTT using the time difference between them. To get long PTTs, it is better to choose one location closer to the heart, also known as proximal location, and choose the other one from distant locations like limbs or fingers, which is known as distal location. In the following subsections, the signals that can be used to measure distal and proximal timings are discussed.

2.3.1. PPG Distal Timing

PPG signal can be used as a waveform to indicate the arrival of BP pulse. There are two type of PPG measurement modes, reflection and transmission mode. In reflection mode, a light emitting diode (LED) is used to illuminate the skin. Variation of the blood volume changes the light absorption, and consequently reflected light. A photodetector placed on the same side of the emitter, measures the reflected light and monitors the blood volume changes. A common problem of PPG sensors is their depth insensitivity. As shown in Fig. 2.7, there is various composition of blood vessels under the skin, containing capillaries, arterioles, and arteries. Each layer of the structure, has different order of getting blood waves.

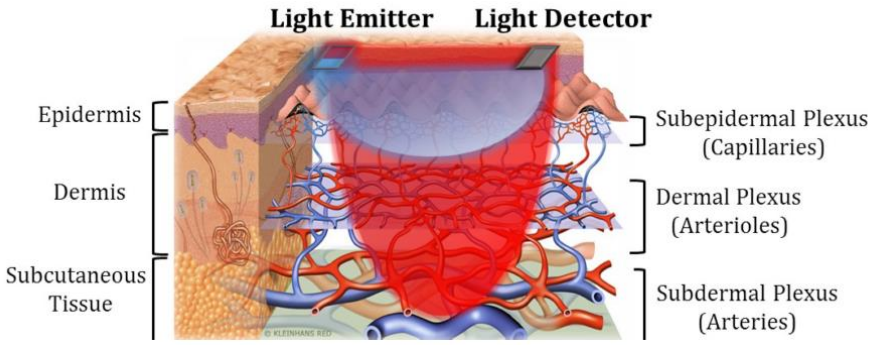

Fig. 2.7- Schematic of skin vasculature and multi wavelength reflectance PPT measurement [63].

As depicted in Fig. 2.8, red PPG light, which has large wavelength, can go through deeper layers of the body. On the other hand, green light with shorter wavelength will be absorbed quickly and only collects information from upper layers. As a result, green PPG is most likely to contain blood volume information only from capillary blood. However, the red PPG collects information from all of the mentioned underlying structures, i.e. capillaries, arterioles, and arteries. Therefore, as illustrated in Fig. 2.9, the red PPG signal will include mixed pulsation information from layers and may led to inaccurate estimation results [63]. In small arteries, smooth muscle contraction and relaxation can cause variation in arterial stiffness, and thus PTT, that are independent of BP [64].

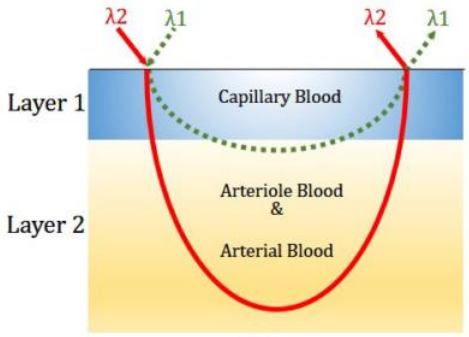

Fig. 2.8- Interaction of the PPG signal and tissue, with two different lights. Red light with large wavelength has information from deeper layers, compared to the green light with shorter wavelength and only collects information from capillary layer [63].

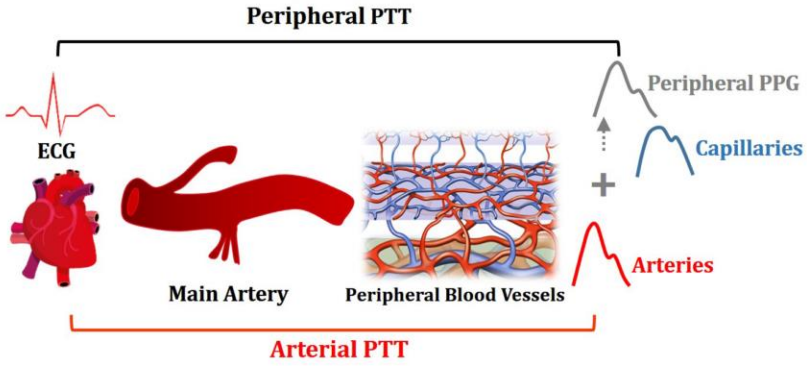

Fig. 2.9- Illustration of the PPG signal with large wavelength, which contains pulsation time from different layers [63].

The PTT based method for cuff-less BP monitoring contains three main steps [2]: (1) measurement of arterial waveforms in two distinct locations, preferably one proximal and one distal; (2) estimation of the PTT as the time delay between two corresponding points of the signal, preferably foot location of the signal; (3) calibration of PTT in time unites to BP in pressure units (usually from ms to mmHg).

2.3.2. ECG Proximal Timing

ECG signal provides the timing of cardiac electrical activity, which happens before the mechanical contraction of the heart muscle. The time delay between the ECG waveform and distal arterial waveform is called pulse arrival time (PAT). As mentioned before, to calculate wave propagation speed, we are interested in PTT, which represents the timing between mechanical contraction of the heart and distal arterial waveform. The relationship between PAT and PTT is:

$$PAT = PET + PTT \qquad \text{Eq. 2.8}$$

where PET, the pre-ejection period, is the amount of time delay that the heart takes to do mechanical contraction and generate the systolic pulse, after getting electrical excitation represented by the BCG R peak. Pre-ejection period (PEP) can be considerable part of the PAT, and can range from 10 to 35% of the PTT [65]. This results in the major limitation of the PAT method, which is its subjectivity to the time required for electrical excitation of the heart. Since the R peak marks the electric excitation of the heart contraction, there is a small delay before mechanical contraction, PEP. Since we cannot noninvasively measure the PEP, it would be a source of the error in PAT. It is speculated to become more significant in subjects with low heart rate [62].

2.3.3. BCG Proximal Timing

BCG signal indicates the acceleration of the body due to the internal force created by the heart when ejects blood into aorta. Basically there is two methods to measure this signal: (1) measuring the force exerted by the body into its support on the ground, like weight scale, bed, chairs. (2) measuring the acceleration of the body by attaching an accelerometer. In both methods, we can get information about the proximal waveform, from distal locations. A typical whole body BCG waveform in illustrated in Fig. 2.10.

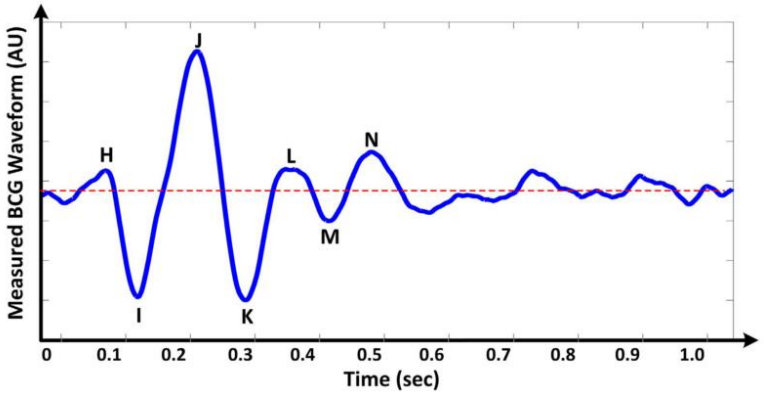

Fig. 2.10. Typical whole body BCG waveform [66].

In reference [67], a model is presented to describe the mechanism behind the BCG waveform. They mathematically modeled the BCG waveform as an instantaneous force in the head-to-foot direction by analyzing the equilibrium of forces exerted on the blood in the main artery of the body, the aorta. As depicted in Fig. 2.11, the model contains two tubes in cascade, representing the ascending and descending part of the aorta. Pressure gradient in each of the tubes results in mechanical force that is inserted into the body:

$$F_{BCG} = A_D \delta P_{12}(t) + A_A \delta P_{10}(t) \qquad \text{Eq. 2.9}$$

In which A_D and A_A represent the average cross sectional areas of the descending and ascending aorta, respectively, and $\delta P_{ij}(t) = P_i(t) - P_j(t)$ constitute the BP gradients.

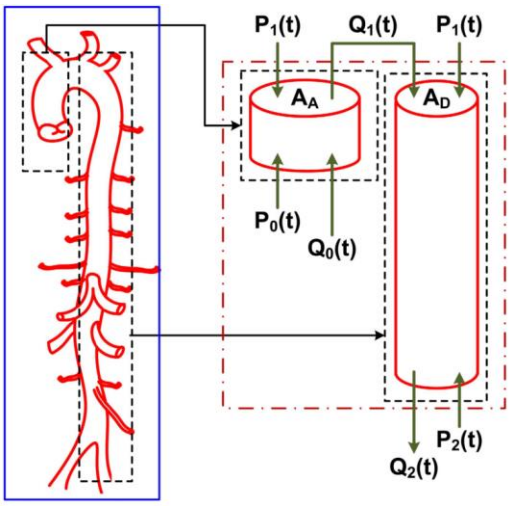

Fig. 2.11- Simplified model of the aorta to describe the BCG waveform. The left and right tubes represent the ascending and descending parts of the aorta [67].

Fig. 2.12 illustrates how BP waveforms at inlet, apex, and outlet of aorta, denoted by P_0, P_1, P_2 respectively, build up the BCG waveform. According to the presented model and figure we can realize that I-wave initiation corresponds approximately to the foot of the P_0, denoting the pressure rise up at the inlet of the aorta or beginning of the mechanical contraction of the heart. The figure also shows that the J-wave peak corresponds approximately to the foot of the P_2 or outlet of the aorta. As a result, the time interval between the I-wave's initiation and J-wave's peak may represent the aortic pulse transit time [67].

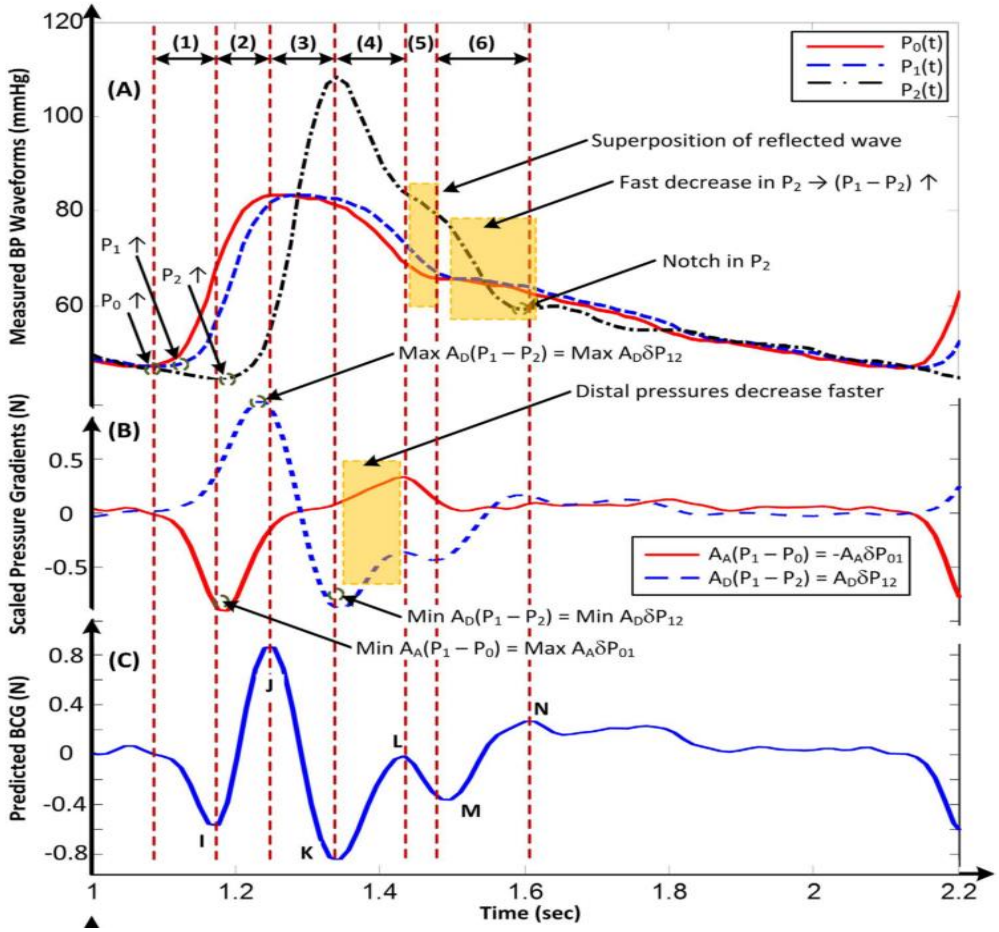

Fig. 2.12- Measured BP waveforms in different locations of the aorta, and corresponding predicted BCG waveform. (A) BP waveforms at inlet, apex, and outlet of aorta; (B) Force gradient in ascending and descending part of aorta; (C) Predicted BCG form [67].

Calculating PTT using the BCG waveform as the proximal timing, has some advantages to PAT using the ECG. BCG signal is more convenient to measure than ECG. It can be easily measured from distal locations, and the sensor doesn't need to be located nearby the heart. Furthermore, because the BCG signal is associated with the mechanical contraction of the heart, it is not subjected to the error caused by PET. In [64], PTT measurement from a weighing scale is compared to the PAT measurements. Their results show that weighing scale-based PTT measurements tracks the BP changes in individual subjects significantly better than the conventional PAT method. They have accomplished their experiments in various interventions, in which BP is changed via different physiologic mechanisms.

However, the BCG is more convenient for measurement and is not subjected to the PET error, it has some shortcomings and technical difficulties to implement. (i) BCG signal has low signal to noise ratio, thus needs comprehensive signal processing practices. (ii) It is

subjected to delays due to inertia and dynamics of the human body, in response to the excitation force created by blood ejection by heart, thus it is subjected to the physical properties of the subject. (iii) it is highly susceptible to motion artifacts and small movements due to physiological activities like breathing.

2.4. Association of BP and BCG Waveform

In section 2.3.3, a typical BCG waveform and the principal mechanism responsible for the genesis of it is explained. According to the presented model, the BCG wave is formed due to the interaction between two aortic BP waves: (i) the gradient of the BP between aortic inlet and arch, generated by the ascending aortic; (ii) the gradient of the BP between aortic arch and outlet, generated by the descending aortic. The physical insight obtained from the presented physical model makes it possible to extract features in BCG signal that are directly correlated to the blood pressure. As a result, we can estimate blood pressure only by pulse wave analysis (PWA) of the BCG signal.

According to the presented model in [66] and Fig. 2.12, the beginning of the aortic inlet BP wave approximately corresponds to the initiation of the first major wave (called I-wave). In addition, peak of the second major wave, J-wave, corresponds to the beginning of the aortic outlet BP wave. So we can consider the time interval between I-peak, or initiation of the I-wave (known as H-peak), and J-peak as the aortic PTT. Therefor H-J and I-J interval in the BCG signal can be considered as the required time delay for BP foot (corresponding to diastolic BP) to travel from aortic inlet to outlet, aortic PTT, which is a well-known surrogate of DP [67].

Another important insight from the BCG model is about the meaning of the difference between amplitudes of the J-peak and K-peak, named as J-K amplitude. First, according to Fig. 2.12, J-peak corresponds to the beginning of the aortic outlet BP wave (P_2), also known as diastolic BP. Second, the K-peak corresponds to the maximum aortic outlet BP, also known as systolic BP. Given that P_0 and P_1 are approximately constant during J-peak to K-peak interval, we can conclude that the J-K amplitude is only due to the change of P_2 from diastolic to systolic BP, which is known as pulse pressure (PP) [67].

It is illustrated that I-J interval and J-K amplitude are strong candidates to correlate with DP and PP, respectively. The experimental results in [66] confirms validity of the above insight derived from physical modeling. The achieved results can leverage BP monitoring in two ways. First, it is possible to integrate the J-K amplitude information, which provides PP estimation, with the information from estimated DP from PTT measurement. It can

result in estimation of DP and SP. The second is to estimate both DP and SP only using BCG signal. In this discipline, DP is estimated directly from PPT information measured by I-J interval, and we can combine estimated DP and PP from BCG PWA to monitor SP [66].

2.5. Conclusion

All of the non-invasive techniques to measure BP employ an inflatable cuff. For this reason, oscillometric and other cuff-based devices do not afford ubiquitous BP monitoring capabilities. That is, people in low resource settings may not have any access to such devices; others must go out of their way (e.g., to a pharmacy) to use these devices; and even people who own a device cannot carry it with them wherever they go. In general, the cuff based methods are less accessible, reliable, and infrequent for continuous BP monitoring [62]. As a result, a reliable cuff-less technology for continuous BP monitoring is being widely pursued today.

Much of the cuff-less blood pressure monitoring efforts are based on the principle of PTT [40]. PTT is the time delay for the pressure wave to travel between two arterial sites. An increase in BP causes PTT to decline, as artery stiffens with an increase in BP, thereby increasing the velocity of travel of the pressure wave. Hence, PTT is often inversely correlated with BP. Further, PTT may be simply determined from the time interval between proximal and distal arterial waveforms. Therefore, PTT carries the major advantage of possibly offering passive BP monitoring without using a cuff.

Most previous studies of BP measurement via PTT have used the time delay between an ECG waveform and an arterial waveform from an arm, especially a finger blood volume waveform via a PPG sensor, as a convenient surrogate of PTT [40]. However, these PAT measurements have a major shortcoming: PAT includes the pre-ejection period in addition to PTT. Since the PEP component depends on the electromechanical functioning of the heart, it can change independently of PTT and thus BP. For example, PEP changes in the same direction as PTT during exercise [68] but in the opposite direction to PTT during vasoconstriction [69]. Note that several studies of PAT have demonstrated good correlation with BP by employing only exercise-induced BP change [40].

Even though PTT based method is a convenient BP monitoring method compared to cuff-based methods, there are still several limitations to the PTT method. First, most of PTT techniques employ single surrogate of BP, to monitor both DP and SP. Given that the BP waveform levels, i.e. DP, SP, PP, and MP can be independent of each other, we need more than one surrogate to estimate them independently. Second, this method requires the

placement of at least to sensors on the body to measure ECG as proximal, and PPG as distal timing. Thus, the convenience of the PTT method can be improved by reducing the number of sensors that must be placed on the body. In addition, in conventional PTT measurement methods PPG signal is required, which is subjected to several shortcomings. Firstly, PPG is sensitive to movement and can be deteriorated at the times of vigorous muscle activity [62]. Contact pressure between the PPG emitter and the skin, is another factor that has major effect on the amplitude and quality of the signal, especially for shorter range PPGs like green. Lower contact pressure, will result in law amplitude signal. On the other hand, high pressure can damage tissue and discomfort the user.

BCG signal can provide more accurate proximal time to improve some of the above mentioned shortcomings of the PTT method. To eliminate the adverse impact of PEP on PTT-BP correlation, a new approach to PTT measurement that avoids the use of ECG as proximal timing reference is required. BCG signal, which represents the acceleration of the body due to the mechanical forces produced by blood ejection by heart, can provide a proximal timing which is not subject to PEP. In this regard, a physical model is developed that explains how BCG signal is generated from aortic BP waveforms. This model provides a physical insight to extract proper features from BCG signal as the proximal timing. Experimental results show that proximal timing extracted from the BCG signal, and consequently calculate PTT is a superior indicator of BP than conventional ECG based PTT [64]. In addition to provide more accurate proximal timing than ECG signal, the extracted features from BCG signal can be directly used to estimate BP, without any need for additional signal. Previous studies show that I-J time interval is inversely correlated to DP and J-K amplitude is proportional to PP.

As mentioned above, the BCG signal is proven to carry useful information of the blood pressure waveform. However, more studies are required to develop more accurate estimators either based on the only BCG signal, or infusion of the extracted features from PPG and BCG signals. In addition, most of the previous studies are focused on the weight scale BCG. As mentioned earlier, BCG signal can be measured from any location on the body. Limbs are one of the most convenient locations to measure BCG signal. Particularly wrist BCG is convenient to measure, by means of a wrist band or smart watch. In this regard, more studies are required to discover the BP-related information within the limb BCG. This study may contain developing a physical model to describes the relationship between the limb BCG signal and blood pressure waveform.

3. Mathematical Model for Wearable BCG Analysis

3.1. Introduction

In the recent studies, it is elucidated based on a mathematical model-based analysis that the force exerted on the body due to the blood ejected by the heart (called the "force BCG") results from the arterial BP gradients in the ascending and descending aorta[70], indicating that the morphology of the BCG waveform has a close association with the underlying aortic BP waveforms. Then, in a series of subsequent work, it is illustrated that such a physical understanding may provide valuable insights in the disciplined interpretation of the BCG in terms of CV parameters and risk predictors as well as in the systematic development of the BCG-based techniques for CV health monitoring[32], [33]. However, the relationship between the force BCG and the BCG actually measured by various instruments at the limb locations still remains mysterious. Elucidating the physical mechanisms responsible for the relationship may pave the way toward understanding how the force BCG is transmitted to upper and lower limb locations through compliant joints and viscoelastic tissues to elicit the limb movement responses as well as interpreting the physiological association between the limb BCG versus the arterial BP waves, CV parameters, and CV risk predictors. Motivated by such a promise, the objective of this chapter was to conduct a rigorous mathematical model-based analysis of the association between the morphology of the arterial BP waves, force BCG, and the limb BCG. A mathematical model to predict the limb BCG responses to the arterial BP waves in the aorta was developed and experimentally validated. Then, the validated mathematical model was analyzed to discover the association between the arterial BP waves and the corresponding limb BCG waveforms as well as to predict the impact of changes in the CV risk predictors on the morphology of the limb BCG waveforms.

This chapter is organized as follows. Section 2 describes the experimental data used in this chapter, as well as the mathematical model and the details of its calibration and analysis. Section 3 summarizes the results, which are discussed and interpreted to elucidate the physiological association between the arterial BP waves and the limb BCG waveforms in Section 4. Section 5 concludes the chapter.

3.2. Methods

In an attempt to establish the physiological association between the limb BCG and the underlying arterial BP, a mathematical model that relates the arterial BP waves to the limb BCG was conceived. The validity of the mathematical model was assessed in both

qualitative and quantitative ways: (i) by investigating its efficacy in predicting morphologically correct limb BCG waveforms (qualitative), and (ii) by investigating its efficacy in predicting the absolute intervals and amplitudes associated with the experimentally observed limb BCG waves with minimal calibration (quantitative). Then, the mathematical model was simulated with the "representative" BP waves obtained from the experimental data to yield the limb BCG waveforms, which were analyzed together with the arterial BP waveforms to discover the association between the two. Details follow.

3.2.1. Experimental Data

Experimental data from our prior work were used to assess the validity of the mathematical model. Given that the mathematical model would serve as the basis to establish the association between the limb BCG and the arterial BP waves in this work, the efficacy of the mathematical model to predict physiologically plausible limb BCG waveforms when the arterial BP waves are inputted was the primary concern. Data from two prior work were leveraged to assess the validity of the mathematical model: (i) arterial BP waves measured at the ascending aorta and femoral artery (Data 1; N=20; age:64+/-9 years; gender: 17 male and 3 female), and (ii) scale displacement BCG and wrist acceleration BCG along with non-invasive brachial BP (Data 2; N=10; age: 24+/-2.3 years; gender: 4 male and 6 female; weight: 64+/-11 kg; height: 165+/-10 cm). Data 1 was collected from patients undergoing cardiac surgery with cardiopulmonary bypass under the approval of the University of Alberta Health Research Ethics Board and written informed consent. Its experimental protocol and setup are described in detail in our prior work[71], [72]. Data 2 was collected from young healthy volunteers under the approval of the University of Maryland Institutional Review Board and written informed consent[73]. In each subject, the scale displacement BCG was measured using a custom-built weighing scale while the wrist acceleration BCG was measured using a custom-built wrist-worn accelerometer. The non-invasive brachial BP wave was measured using a commercial equipment (ccNexfin, Edwards Lifesciences, Irvine, CA, USA). The measurements were simultaneously conducted while the subject stood still on the weighing scale with their arms placed at the side and the movement minimized.

It is acknowledged that the use of arterial BP and limb BCG data collected from separate studies to validate the mathematical model is not ideal. However, considering that the intended context of use of the mathematical model in this work is to predict physiologically realistic BCG waveforms rather than to precisely reproduce the experimentally observed BCG waveforms, the use of such data was regarded as acceptable.

Before its application to the mathematical model for analysis, the two data were standardized by scaling the arterial BP waves in Data 1 such that its group-average mean and diastolic levels were matched to the corresponding levels associated with Data 2.

3.2.2. Mathematical Model

A mathematical model to predict the BCG waveforms at the upper and lower limb locations in response to the heartbeat was conceived by integrating a mechanistic model translating the heartbeat-induced aortic BP waves to the force exerted on the body (called hereafter the "force BCG") with a multi-degree-of-freedom (multi-DOF) mass-damper-spring model representing the vibrational transmission in the body in the head-to-foot direction (Fig. 3.1(a)). The former was adopted from our prior work[70], which predicts the force BCG from three aortic BP waves: aortic inlet BP, aortic arch BP, and aortic outlet BP (Fig. 3.1(b)). In brief, the force BCG is the outcome of the interaction between the three aortic BP waves:

$$F_{BCG}(t) = A_D[P_1(t) - P_2(t)] - A_A[P_0(t) - P_1(t)] \quad (1)$$

where F_{BCG} is the force BCG exerted on the body, P_0, P_1, and P_2 are aortic inlet, arch, and outlet BP waves, respectively, and A_A and A_D are the ascending aortic and descending aortic areas. The latter was developed to fulfill two objectives: (i) to predict the vertical limb movements (i.e., the limb BCG) from the force BCG exerted on the upper torso; and (ii) to be minimally complex. An iterative trial and error process yielded a 4-DOF linear lumped parameter model consisting of four mass elements representing the upper torso (m_1), upper limbs (m_2), internal organs (m_3), and lower limbs (m_4), as well as the associated coupling elements to connect these masses (six dampers and six springs) (Fig. 3.1(b)). In this way, the essential behavior of the body in transmitting the force induced by the arterial BP waves to the upper (e.g., arm and wrist) and lower (e.g., leg and foot) limb sites may be captured.

To account for the fact that the measurement of the lower-limb BCG often requires a dedicated instrument (e.g., a weighing scale[26], [35]), an additional mass-damper-spring dynamics (associated with the mass element m_5 in Fig. 3.1(b)) was augmented to the above-mentioned mathematical model of the human body, so that the dynamic response characteristics of the instrument for the lower-limb BCG may also be accommodated in predicting the lower-limb BCG waveform (Fig. 3.1(b)).

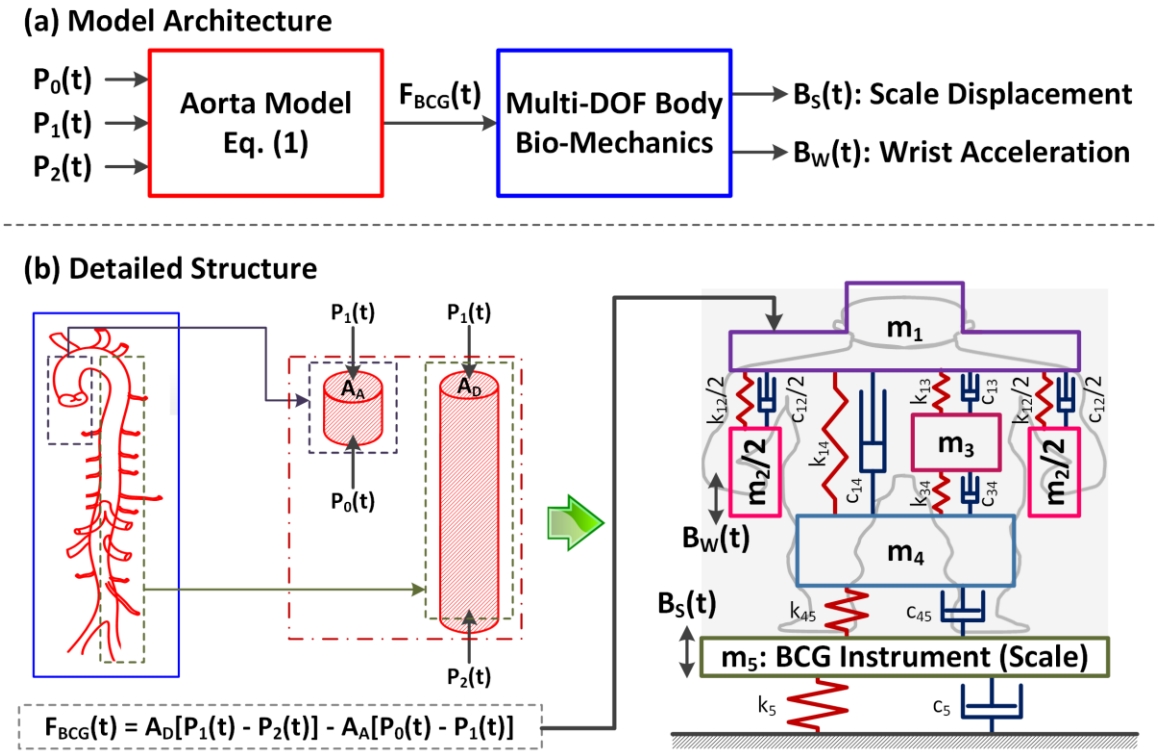

Fig. 3.1: A mathematical model to predict BCG waveforms at the upper and lower limb locations in response to the heartbeat. (a) Model architecture: A mechanistic model that translates the heartbeat-induced aortic BP waves to the force exerted on the body (called the force BCG) is integrated with a multi-degree-of-freedom (multi-DOF) mass-damper-spring model that represents the vibrational transmission in the body in the head-to-foot direction. (b) Detailed structure: The BP waves are inputted to the lumped-parameter mechanistic model of the aorta (1) to yield the force BCG. The force BCG subsequently excites the upper torso (m_1) in the multi-DOF vibrational transmission model of the body to produce the corresponding movement (i.e., the BCG) of the upper limbs (m_2) and lower limbs (m_4). The lower limb BCG is measured as the resulting movement of the instrument (m_5). Hence, the mathematical model predicts the scale displacement BCG as the displacement associated with m_5, and the wrist acceleration BCG as the acceleration associated with m_2.

Using the experimental data described in Section 2.1, the mathematical model was simulated as follows. The BP waves were inputted to the lumped-parameter mechanistic model of the aorta (1) to yield the force BCG. The force BCG subsequently excited the upper torso (m_1) in the multi-DOF vibrational transmission model of the body to produce the corresponding movements (i.e., the BCG) of the upper limbs (m_2) and lower limbs (m_4). The lower limb BCG was measured as the resulting movement of the instrument (m_5). Hence, the mathematical model predicts the scale displacement BCG as the displacement associated with m_5, and the wrist acceleration BCG as the acceleration associated with m_2.

3.2.3. Parametric Sensitivity Analysis

To understand the overall variability of the limb BCG waveforms with respect to the variability in the bio-mechanical characteristics of the body as well as to determine the list of parameters in the mathematical model to calibrate using the experimental data, parametric sensitivity analysis was conducted as follows.

First, nominal parameter values for the mathematical model were determined. The parameters associated with the lumped-parameter mechanistic model of the aorta were adopted from the physically relevant values reported in the literature[70]. The parameters associated with the multi-DOF vibrational transmission model of the body were derived from the parameter values reported in a prior work on a comprehensive 16-DOF vibrational transmission model of human body[74] via a standard model reduction procedure[75]. Specifically, the 16-DOF vibrational transmission model was reduced to the 4-DOF vibrational transmission model in Fig. 1 so that (i) m_1 corresponds to the mass of the head and upper torso; (ii) m_2 corresponds to the mass of the upper arms, elbows, forearms, and hands; (iii) m_3 corresponds to the mass of the internal organs; and (iv) m_4 corresponds to the mass of the thighs, shanks, and feet. The damping and stiffness parameters c_{12} and k_{12} associated with m_2 as well as c_{45} and k_{45} associated with m_4 were determined in such a way that the resulting fundamental resonance frequencies and amplitudes associated with m_2 and m_4 were matched to those associated with the corresponding subsystems in the 16-DOF vibrational transmission model[75]. On the other hand, the damping and stiffness parameters c_{14} and k_{14} connecting m_1 and m_4 as well as c_{13}, c_{34}, k_{13}, and k_{34} connecting m_3 to m_1 and m_4 were adopted directly from the respective values associated with the 16-DOF vibrational transmission model[74].

Nominal parameter values associated with the instrument dynamics were assigned so that (i) m_5 is the mass of the scale used to measure the lower-limb BCG in our prior work[73]; (ii) k_5 and c_5 yields the critically damped 1-DOF dynamics with the natural frequency reported in a prior study[26]. Second, the resulting 5-DOF vibrational transmission model was transformed into the transfer functions relating the force BCG to the scale displacement BCG and the wrist acceleration BCG:

$$\mathrm{B_S}(\mathrm{s}) = \mathrm{H_S}(\mathrm{s})\mathrm{F_{BCG}}(\mathrm{s}), \qquad \mathrm{B_W}(\mathrm{s}) = \mathrm{H_W}(\mathrm{s})\mathrm{F_{BCG}}(\mathrm{s}) \tag{2}$$

where $\mathrm{B_S}(\mathrm{s})$ and $\mathrm{B_W}(\mathrm{s})$ are the scale displacement and wrist acceleration BCG, and $\mathrm{H_S}(\mathrm{s})$ and $\mathrm{H_W}(\mathrm{s})$ are the associated transfer functions. Third, parametric sensitivity

functions were analytically computed in the frequency domain as the partial derivatives of $H_S(s)$ and $H_W(s)$ with respect to the parameters therein:

$$S_{S,\theta}(j\omega) = \frac{\theta_0}{H_S(j\omega)|_{\theta=\theta_0}} \frac{\partial H_S(j\omega)}{\partial \theta}\bigg|_{\theta=\theta_0}, \qquad S_{W,\theta}(j\omega) = \frac{\theta_0}{H_W(j\omega)|_{\theta=\theta_0}} \frac{\partial H_W(j\omega)}{\partial \theta}\bigg|_{\theta=\theta_0} \tag{3}$$

where $S_{S,\theta}(j\omega)$ and $S_{W,\theta}(j\omega)$ denote the parametric sensitivity functions associated with $H_S(s)$ and $H_W(s)$, respectively, and $\theta \in \{\{m_i\}_{i=1}^5, k_{12}, k_{13}, k_{14}, k_{34}, k_{45}, c_{12}, c_{13}, c_{14}, c_{34}, c_{45}, k_5, c_5\}$ while θ_0 is the nominal value of θ. Fourth, the sensitivity of the BCG morphology to the mass, damping, and stiffness parameters was analyzed in the frequency domain by way of the Bode magnitude plots of the parametric sensitivity functions. Finally, the results of this analytical parametric sensitivity analysis was confirmed by time-domain numerical simulation of the mathematical model, by examining and comparing the changes in the morphology of the scale displacement and wrist acceleration BCG waveforms entailed by the perturbations in the mass, damping, and stiffness parameters of the same percentage amount (+/-20%).

3.2.4. Model Calibration

To evaluate the predictive capability of the mathematical model in Fig. 3.1 with respect to the experimental data described in Section 2.1, the mathematical model was calibrated to the experimental data. Considering that the primary role of the mathematical model is to provide the basis to elucidate the association between the limb BCG and the arterial BP waves, it is required that the mathematical model be able to predict typical limb BCG waveforms when typical arterial BP waveforms are inputted. Considering that a large portion of the nominal parameter values obtained for the mathematical model in Section 2.3 (e.g., the values of the mass parameters $\{m_i\}_{i=1}^5$ and the stiffness parameters $k_{12}, k_{13}, k_{14}, k_{34}, k_{45}$) may be physically appropriate to represent the body of an average subject according to the existing literature, the mathematical model was calibrated by optimizing a minimal set of parameters whose values are unknown and at the same time exert a large impact on the BCG morphology. Based on this rationale, all the mass and stiffness parameters with physical relevance ($\{m_i\}_{i=1}^5$ as well as $k_{12}, k_{13}, k_{14}, k_{34}, k_{45}$) were fixed to the nominal values, whereas c_5 and k_5 (which are unknown) as well as high-sensitivity damping parameters (determined by the parametric sensitivity analysis) were calibrated to minimize the discrepancy between the experimental versus model-predicted BCG waveforms.

The calibration was performed specifically as follows. First, representative arterial BP waves were derived as the average of the arterial BP waveforms associated with all subjects in Data 1. Second, typical model-predicted BCG waveforms were derived using these arterial BP waveforms and the mathematical model in Fig. 3.1. The typical force BCG was computed as the output of the mechanistic model of the aorta (1) when the representative arterial BP waveforms were inputted. Then, the typical scale displacement and wrist acceleration BCG waveforms were computed by inputting the typical force BCG to the transfer functions $H_S(s)$ and $H_W(s)$. Third, the parameters c_5 and k_5 as well as the high-sensitivity damping parameters determined by the parametric sensitivity analysis were optimized in such a way that the difference between the experimental versus model-predicted BCG was minimized in terms of the amplitudes of the primary waves associated with the scale displacement (I, J, and K waves[70]) and wrist acceleration (J, K, and L waves[30]) BCG. For this purpose, representative wave amplitudes corresponding to the experimental BCG were derived as the average of the wave amplitudes associated with all subjects in Data 2. Then, the above-listed parameters were tuned by formulating and solving a numerical optimization problem to minimize the following penalty J using MATLAB and its Optimization Toolbox (MathWorks, Natick, MA):

$$J = J_S + J_W = \underbrace{\left[\left(\frac{I_S^{(M)} - I_S^{(E)}}{I_S^{(E)}}\right)^2 + \left(\frac{J_S^{(M)} - J_S^{(E)}}{J_S^{(E)}}\right)^2 + \left(\frac{K_S^{(M)} - K_S^{(E)}}{K_S^{(E)}}\right)^2\right]}_{J_S} + \underbrace{\left[\left(\frac{J_W^{(M)} - J_W^{(E)}}{J_W^{(E)}}\right)^2 + \left(\frac{K_W^{(M)} - K_W^{(E)}}{K_W^{(E)}}\right)^2 + \left(\frac{L_W^{(M)} - L_W^{(E)}}{L_W^{(E)}}\right)^2\right]}_{J_W} \quad (4)$$

where I, J, K, and L are the amplitudes associated with the I, J, K, and L waves, the subscripts S and W denote the scale displacement and wrist acceleration, and the superscripts E and M denote experimental and model-predicted, respectively.

3.2.5. Model Analysis

The mathematical model was subsequently used to assess the validity with respect to the experimental data, as well as to elucidate the physiological association between the limb BCG and the underlying arterial BP waves. Details follow.

The validity of the mathematical model was assessed with respect to the experimental data in two ways: pre-calibration qualitative assessment and post-calibration quantitative

assessment. In the pre-calibration qualitative assessment, the mathematical model was evaluated for its ability to predict the presence of the primary waves in the scale displacement (I, J, and K waves) and wrist acceleration (J, K, and L waves) BCG. For the sake of this assessment, the un-calibrated mathematical model, equipped with the nominal parameter values obtained in Section 2.3, was excited with the arterial BP waves associated with all subjects in Data 1 to simulate the corresponding scale displacement and wrist acceleration BCG waveforms. Then, the number of subjects in which the presence of each of the primary waves was predicted in the simulated BCG waveforms was counted. In the post-calibration quantitative assessment, the mathematical model was evaluated for its ability to reproduce quantitatively correct BCG waveforms. For the sake of this assessment, the calibrated mathematical model was excited with the arterial BP waves associated with all subjects in Data 1 to simulate the corresponding scale displacement and wrist acceleration BCG waveforms. Then, the distributions of the primary wave-to-wave intervals (I-J and J-K intervals in the scale displacement BCG as well as J-K and K-L intervals in the wrist acceleration BCG) and wave-to-wave amplitudes (I-J and J-K amplitudes in the scale displacement BCG as well as J-K and K-L amplitudes in the wrist acceleration BCG) were computed (in terms of mean and standard error (SE)). These distributions were subsequently compared with the corresponding distributions obtained directly from the experimental BCG waveforms associated with all subjects in Data 2.

The physiological association between the limb BCG and the arterial BP waves was investigated in two ways. First, given that the primary constituents of the force BCG are the ascending aortic and descending aortic BP gradients[70], the scale displacement and wrist acceleration BCG waveforms were decomposed into the components originating from the ascending and descending aortic BP gradients, and how each of these BP gradients are transformed into the BCG waveforms was investigated. The mathematical model is linear and the superposition principle applies. Hence, the decomposition reduces to simulating the mathematical model with the ascending and descending aortic BP gradients one at a time. This analysis was especially beneficial in scrutinizing the effect of individual arterial BP wave (P_0, P_1, and P_2) on the BCG waveforms in that it enables how each arterial BP wave evolves into component waveform for the BCG; in contrast, direct analysis of the relationship between the combined ascending and descending aortic BP gradients and the resulting BCG waveforms may not yield much physiological insights due to the complex interaction among the three arterial BP waves. Second, the mathematical model was used to study the impact of the pulse wave velocity and pulse pressure amplification (which are well known CV risk predictors) on the morphology of the BCG waveforms. By using the representative arterial BP waves used in the calibration, the alterations in the pulse wave velocity and pulse pressure amplification were simulated by perturbing the time intervals and relative amplitudes between P_0, P_1, and P_2. Specifically,

an increase (or decrease) in the pulse wave velocity was realized by decreasing (or increasing) the time intervals between P_0 and P_1 as well as between P_0 and P_2 by the same percentage amount, while an increase (or decrease) in the pulse pressure amplification was realized by increasing (or decreasing) the pulse amplitude of P_2 while maintaining the pulse amplitudes of P_0 and P_1. The representative arterial BP waves associated with the perturbations up to +/-20% in both pulse wave velocity and pulse pressure amplification were created. The nominal and perturbed representative arterial BP waves were inputted to the mathematical model to predict the resulting limb BCG waveforms. Then, the changes in the wave-to-wave intervals and amplitudes in the limb BCG in response to the alterations in the pulse wave velocity and pulse pressure amplification were investigated.

3.3. Results

Fig. 3.2 shows the representative (i.e., group-averaged) arterial BP waves as well as typical pre-calibration model-predicted scale displacement and wrist acceleration BCG waveforms. Overall, the mathematical model conceived in this chapter adequately predicted the overall morphology of the scale displacement and wrist acceleration BCG waveforms even without calibration to the experimental data. In particular, the presence of the primary waves (i.e., the I, J, and K waves in the scale displacement BCG as well as the J, K, and L waves in the wrist acceleration BCG) were observed in 95% of the subjects simulated with the experimental arterial BP waveforms (the K wave in the scale displacement BCG and the K and L waves in the wrist acceleration BCG were not clearly predicted in one subject). In addition, the BCG waveforms predicted by the 4-DOF mathematical model was almost identical to those predicted by the 16-DOF vibrational model[74]. Hence, it was concluded that the mathematical model used in this chapter is able to capture the essential characteristics associated with the transmission of the heartbeat-induced body movement throughout the body.

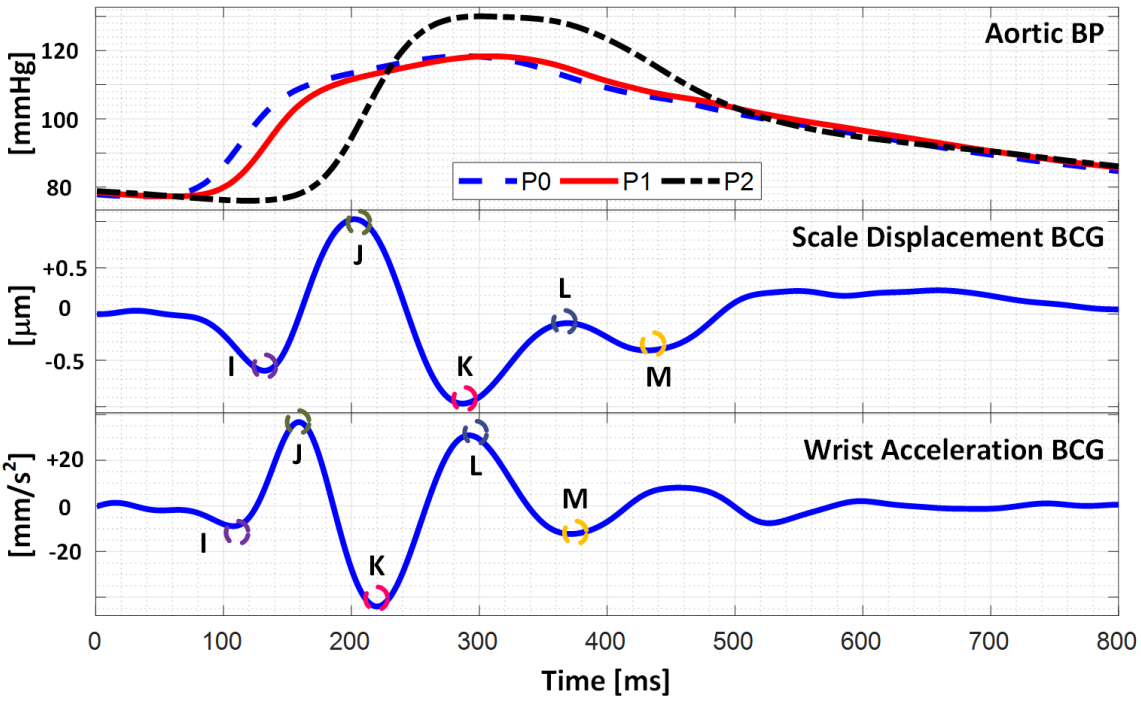

Fig. 3.2: Representative arterial BP waves as well as pre-calibration model-predicted scale displacement and wrist acceleration BCG waveforms.

The parametric sensitivity analysis indicated that the most critical mass, damping, and stiffness parameters influencing the morphology of the scale displacement BCG turned out to be the arm mass ($\mathbf{m_2}$), spinal damping ($\mathbf{c_{14}}$), and scale stiffness ($\mathbf{k_5}$) parameters, while the most critical mass, damping, and stiffness parameters influencing the morphology of the wrist acceleration BCG turned out to be the arm mass ($\mathbf{m_2}$), spinal damping ($\mathbf{c_{14}}$), and arm stiffness ($\mathbf{k_{12}}$) parameters. Guided by these findings and motivated by the goal of predicting "typical" BCG waveforms, the mathematical model was calibrated by tuning $\mathbf{c_{14}}$ as well as $\mathbf{c_5}$ and $\mathbf{k_5}$ to minimize the discrepancy between the experimental versus model-predicted BCG wave amplitudes (see Section 2.4). Table 3.1 summarizes the parameter values in the mathematical model thus calibrated using the experimental arterial BP and limb BCG waveforms.

Table 3.1: Mathematical model parameter values calibrated using experimental arterial BP and limb BCG waveforms.

Mass [kg]		Damping [N·s/m]		Stiffness [kN/m]	
m_1	9.0	c_{12}	271	k_{12}	40.7
m_2	8.0	c_{13}	53	k_{13}	3.15
m_3	23	c_{14}	1056	k_{14}	31.3
m_4	25	c_{34}	32	k_{34}	2.28
m_5	2.5	c_{45}	1141	k_{45}	425.3
		c_5	722	k_5	833.0

Table 3.2: Wave-to-wave intervals and amplitudes in experimental and model-predicted BCG (mean+/-SE).

(a) Scale displacement BCG

	Wave-to-Wave Intervals		Wave-to-Wave Amplitudes	
	I-J [ms]	J-K [ms]	I-J [μm]	J-K [μm]
Experiment (N=10)	88+/-2	88+/-3	1.72+/-0.18	1.65+/-0.20
Model (N=20)	70+/-3	92+/-6	1.63+/-0.20	1.97+/-0.15
Average Difference	18	4	0.09	0.32

(b) Wrist acceleration BCG

	Wave-to-Wave Intervals		Wave-to-Wave Amplitudes	
	J-K [ms]	K-L [ms]	J-K [mm/s^2]	K-L [mm/s^2]
Experiment (N=10)	62+/-3	80+/-3	73+/-7	52+/-4
Model (N=20)	62+/-2	70+/-3	75+/-11	64+/-8
Average Difference	0	10	2	12

Fig. 3.3 shows the representative force, scale displacement, wrist displacement, and wrist acceleration BCG waveforms predicted by the calibrated mathematical model (by inputting the representative BP waveforms) in conjunction with the representative (i.e., group-averaged) experimental scale displacement and wrist acceleration BCG waveforms, while Table 3.2 summarizes the experimental and model-predicted wave-to-wave intervals and amplitudes in the scale displacement and wrist acceleration BCG waveforms. The mathematical model predicted the primary waves in the scale displacement (I, J, and K) and wrist acceleration (J, K, and L) BCG with small time interval (26% (I-J) and 5% (J-K) for scale displacement and 0% (J-K) and 15% (K-L) for wrist acceleration) and amplitude (6% (I-J) and 16% (J-K) for scale displacement and 3% (J-K) and 19% (K-L) for wrist acceleration) errors. On the other hand, its limited ability to reproduce the secondary H wave in the

scale displacement BCG and the I wave in the wrist acceleration BCG is attributed to the fact that these waves are associated with the left ventricular activities[35] while the mathematical model can only predict the BCG waves originating from the arterial BP gradients[70].

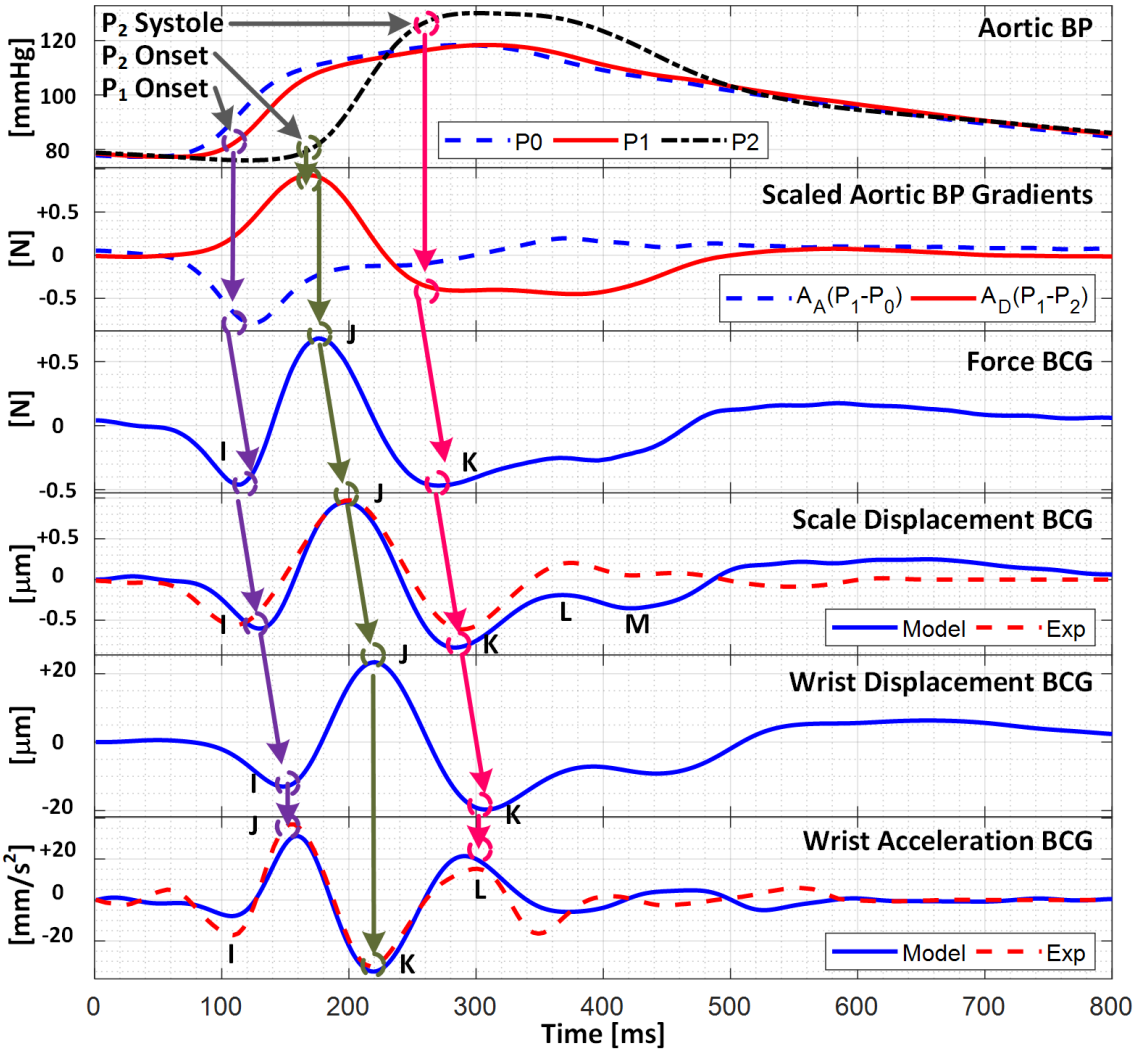

Fig. 3.3: Force, scale displacement, wrist displacement, and wrist acceleration BCG waveforms predicted by calibrated mathematical model in conjunction with representative experimental scale displacement and wrist acceleration BCG waveforms.

Fig. 3.4 shows the decomposition of the scale displacement, wrist displacement, and wrist acceleration BCG waveforms into the components associated with the ascending and descending aortic BP gradients. In both the scale and wrist displacement BCG, the falling limb of the I wave was primarily formed by the ascending aortic BP gradient, whereas the

J-K down-stroke was predominantly formed by the descending aortic BP gradient. In the wrist acceleration BCG, accordingly, the J wave was mostly formed by the ascending aortic BP gradient, while the L wave was mostly formed by the descending aortic BP gradient. The K wave, on the contrary, was formed by both BP gradients, although the descending aortic BP gradient still had larger influence than its ascending counterpart. Yet all in all, the results shown in Fig. 3.4 suggest that all the I, J, and K waves in the displacement BCG as well as the J, K, and L waves in the acceleration BCG correspond to the same extrema in the underlying aortic BP gradients, illustrating that the pairs of (i) displacement I wave-acceleration J wave, (ii) displacement J wave-acceleration K wave, and (iii) displacement K wave-acceleration L wave are associated with the same physiological origins. These relationships are illustrated in Fig. 3.3 as well as summarized in Table 3.3.

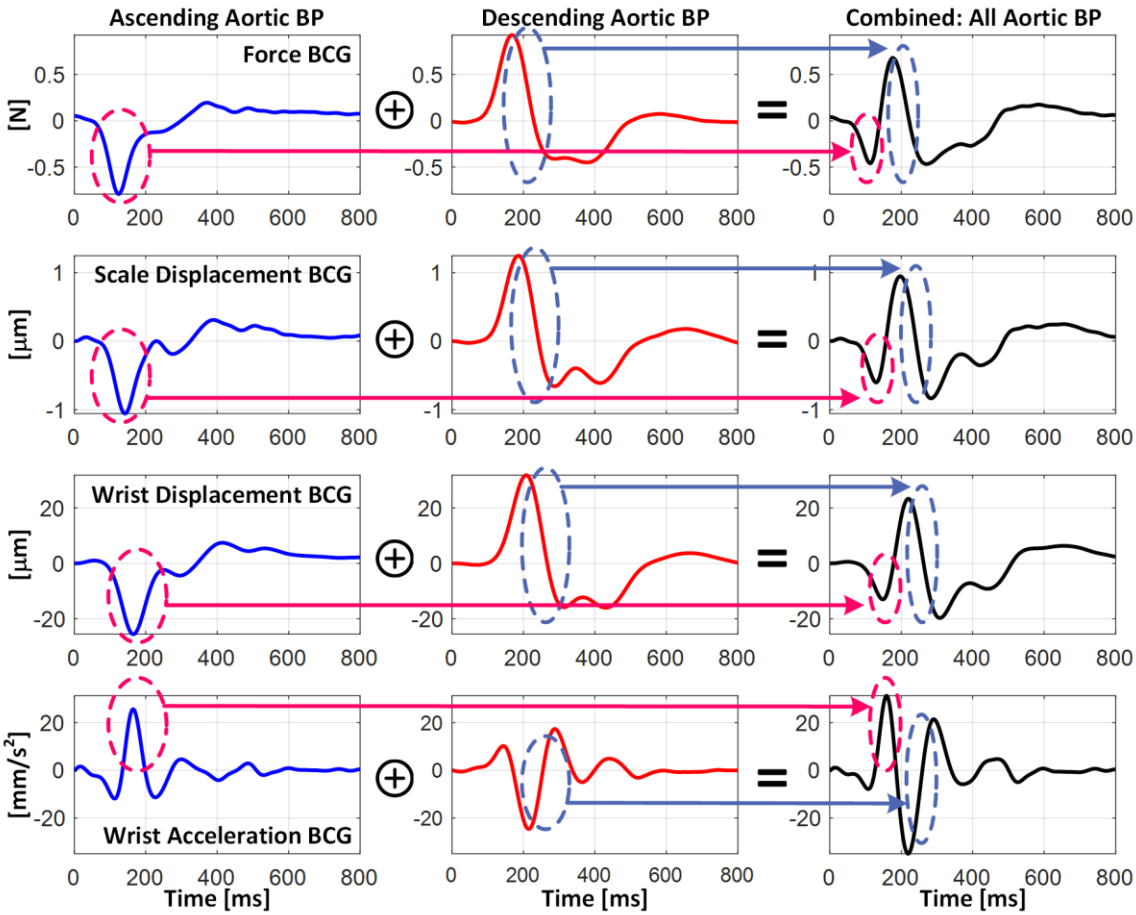

Fig. 3.4: Decomposition of scale displacement, wrist displacement, and wrist acceleration BCG waveforms into components associated with ascending and descending aortic BP gradients.

Table 3.3: Relationships between arterial BP waves, arterial BP gradients, and scale displacement and wrist acceleration BCG waves.

Arterial BP	Arterial BP Gradients	Scale Displacement BCG	Wrist Acceleration BCG
P_1 onset	Peak, P_0-P_1	I	J
P_2 onset	Peak, P_1-P_2	J	K
P_2 systole	Valley, P_1-P_2	K	L
P_1 Amplitude	Positive Amplitude, P_1-P_2	J Amplitude	K Amplitude
P_2 Amplitude	Peak-Peak Amplitude, P_1-P_2	J-K Amplitude	K-L Amplitude

Fig. 3.5 illustrates the relationship between the aortic pulse wave velocity and pulse pressure amplification versus the morphology of the limb BCG waveforms. Overall, the aortic pulse wave velocity was associated with both the wave-to-wave intervals and amplitudes in the limb BCG, whereas the aortic pulse pressure amplification was predominantly associated with the wave amplitudes in the limb BCG. In particular, an increase in the aortic pulse wave velocity yielded the corresponding decrease in (i) the I-J and I-K intervals in the scale displacement BCG, and accordingly, the J-K and J-L intervals in the wrist acceleration BCG; and (ii) the amplitudes of the I and J waves in the scale displacement BCG as well as the J wave amplitude in the wrist acceleration BCG. In addition, an increase in the aortic pulse pressure amplification yielded the corresponding increase in the J-K amplitude in the scale displacement BCG as well as the K-L amplitude in the wrist acceleration BCG.

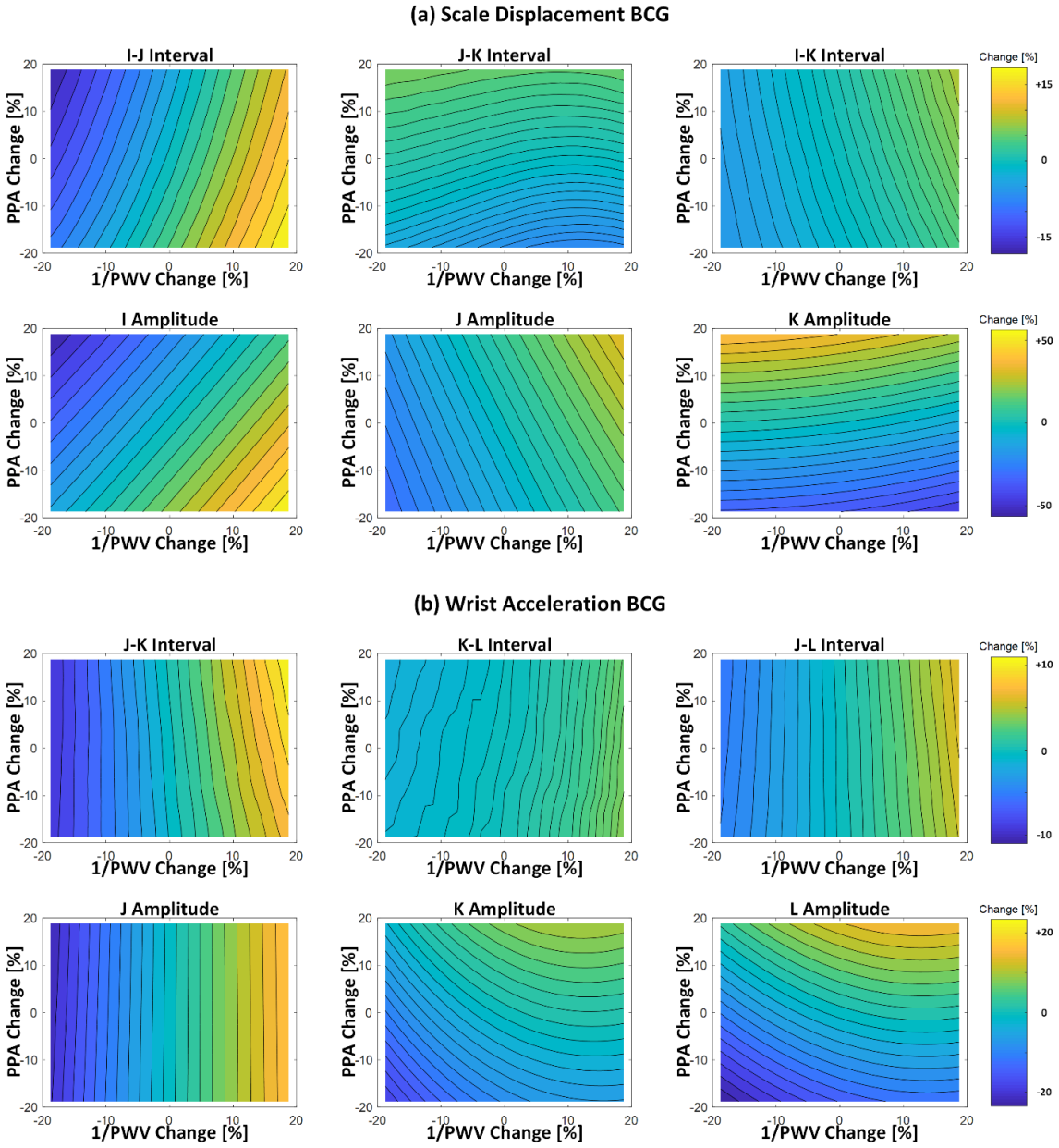

Fig. 3.5: Relationship between the aortic pulse wave velocity (PWV) and pulse pressure amplification (PPA) versus the morphology of the limb BCG waveforms. (a) Scale displacement BCG. (b) Wrist acceleration BCG.

3.4. Discussion

3.4.1. Mathematical Model: Validity and Implications

The calibrated mathematical model could faithfully reproduce the morphology of the scale displacement and wrist acceleration BCG waveforms (Fig. 3.3). In particular, the mathematical model predicted the presence of the I, J, and K waves in the scale displacement BCG as well as the J, K, and L waves in the wrist acceleration BCG. In addition, the agreement between the experimental and model-predicted wave-to-wave intervals and amplitudes were quite remarkable (Table 3.2). Considering that (i) the parameters in the mathematical model were only minimally calibrated (i.e., except for the scale-related parameters ($\mathbf{c_5}$ and $\mathbf{k_5}$), only one parameter (i.e., $\mathbf{c_{14}}$) was calibrated), (ii) they were fixed at constant values in predicting these waves associated with all subjects, and that (iii) the subjects associated with the BP waveforms used in the model prediction and those associated with the experimental BCG waveforms were largely different, the ability of the mathematical model to predict primary waves in the scale and wrist BCG with acceptable quantitative agreement with independent experimental data appears to strongly support the validity of the mathematical model in predicting the limb BCG waveforms. In fact, we speculate that a subset of the errors listed in Table 3.2 may in part be attributed to the discrepancy in the subject demographics associated with Data 1 and Data 2, and may be improved by reducing the gap associated with the subject demographics due to the following reasons. First, the model-predicted scale displacement BCG showed small I-J interval and amplitude as well as large J-K amplitude compared with its experimental counterpart, while the model-predicted wrist acceleration BCG showed large K-L amplitude compared with its experimental counterpart. Second, considering that the subjects in Data 1 may be associated with large pulse wave velocity and pulse pressure amplification compared with those in Data 2 (since the former are old and also subject to adverse CV state while the latter are young and healthy), the discrepancy in the CV state between these data may be removed by decreasing (i) the pulse wave velocity (e.g., by increasing the time interval between P_1 and P_2) and (ii) the PP amplification (e.g., by decreasing the amplitude of P_2). According to Fig. 3.5, such alterations in pulse wave velocity and pulse pressure amplification will lead to the following changes in the model predictions: (i) an increase in the I-J interval of the scale displacement BCG, thereby improving the I-J interval accuracy in Table 3.2(a); (ii) an increase in the J wave amplitude and a decrease in the K wave amplitude in the scale displacement BCG, which will increase its I-J amplitude while maintain or decrease its J-K amplitude, thereby improving the I-J and J-K amplitude accuracy in Table 3.2(a); and (iii) a decrease in the K and L waves in the wrist

acceleration BCG, which will largely decrease its K-L amplitude, thereby improving the K-L amplitude accuracy in Table 3.2(b).

The predicted BCG waveforms indicate that, as a first-order approximation, the I, J, K, and L waves in the wrist acceleration BCG may correspond to the H, I, J, and K waves in the scale and wrist displacement BCG for the following reasons. First, assuming that the body is rigid, all the body parts would undergo the same displacement, which would result in the identical scale and wrist displacement BCG waveforms. Second, considering that deriving wrist acceleration from wrist displacement involves two differentiations in time and also that differentiating twice in time leads to a phase lead of 180 degrees (along with frequency-dependent amplitude modulation), the gross morphology of the wrist acceleration BCG waveform may be derived by flipping (i.e., multiplying (-1) to) the wrist displacement BCG waveform.

Yet strictly, the body is not rigid; rather, it exhibits a complex multi-body dynamics nature comprising a number of mass, damping, and stiffness characteristics. In fact, the findings from the parametric sensitivity analysis suggest that the morphology of the limb BCG may be affected by the musculoskeletal properties of the subject, and the influence may not be negligible. In particular, both the scale displacement and wrist acceleration BCG were largely sensitive to the upper-limb properties among others. These musculoskeletal properties exerts a mechanical filtering on the force BCG produced by the heartbeat, thereby altering the limb BCG waveforms (Fig. 3.3 and Fig. 3.4). Therefore, the exact interpretation of the BCG to relate it to CV functions may require explicit account for the body dynamics.

3.4.2. Association between Limb BCG and Arterial BP Waveforms

The mathematical model could now be exploited to elucidate the association between the limb BCG waves and arterial BP waves as follows.

First, the timings associated with the aortic BP waveforms may be indirectly deciphered from the limb BCG waveforms. More specifically, our prior work elucidated that the diastolic minima pertaining to the aortic inlet (P_0) and outlet (P_2) BP waves roughly correspond to the initiation of the I wave and the peak of the J wave in the force BCG[70]. Therefore, at least in an approximate sense, the I wave in the scale displacement BCG, the I wave in the wrist displacement BCG, and the J wave in the wrist acceleration BCG may indicate the diastolic minimum pertaining to the aortic inlet BP, and likewise, Indeed, our prior experimental work suggests that the I wave in the scale displacement BCG and the J

wave of the wrist acceleration BCG can be used as the timing associated with the aortic inlet BP toward cuff-less BP monitoring[73].

Second, the I wave amplitude in the scale displacement BCG and accordingly the J wave amplitude in the wrist acceleration BCG may represent the ascending aortic BP gradient. Indeed, Fig. 3.4 illustrates that the falling limb of the I wave in the scale displacement BCG as well as the rising limb of the J wave in the wrist acceleration BCG are determined primarily by the I wave in the force BCG (or equivalently, the ascending aortic BP gradient). Considering that the amplitude of the ascending aortic BP gradient is sensitive to the perturbations in the CV risk predictors of aortic pulse wave velocity and pulse pressure amplification, these waves may be analyzed to obtain meaningful insights on these CV risk predictors (Fig. 3.5).

Third, the J-K down-stroke in the scale displacement BCG and (accordingly) the K-L up-stroke in the wrist acceleration BCG may represent the descending aortic BP gradient. Indeed, Fig. 3.4 illustrates that the J-K down-stroke in the scale displacement BCG as well as the K-L up-stroke in the wrist acceleration BCG are determined primarily by the J-K down-stroke in the force BCG (or equivalently, the descending aortic BP gradient, in that the ascending aortic BP gradient is close to zero during this phase). Hence, together with the fact that the amplitude of the descending aortic BP gradient is sensitive to the distal pulse pressure[70], these down-stroke/up-stroke portions may be analyzed to estimate distal pulse pressure.

Fourth, the J wave amplitude in the scale displacement BCG and accordingly (yet to a weaker extent) the K wave amplitude in the wrist acceleration BCG may represent the aortic pulse pressure. This speculation is plausible based on two observations: (i) the amplitude of the J wave in the force BCG may represent the aortic pulse pressure[70]; and (ii) the J wave in the scale displacement BCG and the K wave in the wrist acceleration BCG correspond approximately to the J wave in the force BCG. Hence, together with the surrogates of distal pulse pressure mentioned above (i.e., the J-K amplitude in the scale displacement BCG and the K-L amplitude in the wrist acceleration BCG), the limb BCG may provide a means to monitor another CV risk predictor of aortic pulse pressure amplification.

Finally, it must be noted that the promising potential of the limb BCG as surrogate measure of arterial BP hinges upon the significance of the mechanical filtering effect of the body. Indeed, the mechanical filtering has profound implications on the value of the limb BCG waveforms in probing arterial BP and CV functions. For example, the absolute timings

associated with the arterial BP may not be robustly determined from the limb BCG compared to the force BCG, due to the non-negligible phase lag and morphological distortion imposed by the body's mechanical filtering on the limb BCG waveforms.

Despite the confounding impact of body filtering, the mathematical model indicated that the time intervals between the primary waves in the limb BCG waveforms remained quite consistent. In particular, the I-J and J-K intervals associated with the force BCG (66+/-3 ms and 96+/-6 ms) and the scale displacement BCG (70+/-3 ms and 92+/-6 ms; Table 3.2) remained comparable. Further, these I-J and J-K intervals were also comparable to the J-K and (to a lesser extent) K-L intervals associated with the wrist acceleration BCG (62+/-2 ms and 70+/-3 ms; Table 3.2). In addition, the primary waves in both the scale (I, J, and K) and wrist (J, K, and L) BCG exhibited adequate degree of sensitivity in response to the changes in the arterial wave propagation characteristics (Fig. 3.5). Hence, the limb BCG may still possess value as surrogate measure of arterial BP and CV functions.

3.4.3. Relationship between Aortic Pulse Wave Velocity and Pulse Pressure Amplification versus Limb BCG Morphology

By leveraging and compiling the mathematical model predictions illustrated in Fig. 3.3-Fig. 3.5, the following insights on the role of the aortic pulse wave velocity and pulse pressure amplification in shaping the limb BCG waveforms may be made.

First, the aortic pulse wave velocity influences the limb BCG morphology by altering the time intervals among the aortic BP waves (i.e., P_0, P_1, and P_2 in Fig. 3.3). Regarding the wave-to-wave time intervals, the I-J and I-K intervals in the scale and wrist displacement BCG, and accordingly the J-K and J-L intervals in the wrist acceleration BCG as well, are inversely proportional to the aortic pulse wave velocity, because a decrease in the aortic pulse wave velocity results in the delay in the onset and peak timings of P_2 (which delays the timings associated with the J and K waves in the scale displacement BCG and accordingly the K and L waves in the wrist acceleration BCG). Noting that the H wave in the scale displacement BCG roughly corresponds to the initiation of its I wave (and thus, the onset of P_0[70]), the I-K and I-L intervals in the wrist acceleration BCG are also inversely proportional to the aortic pulse wave velocity. Regarding the wave amplitudes, the most salient influence of the aortic pulse wave velocity originates from the alteration of the separation between the ascending and descending aortic BP gradients. In particular, the amplitude of the I wave in the scale displacement BCG, and accordingly the amplitude of the J wave in the wrist acceleration BCG, are inversely proportional to the aortic pulse wave velocity, because a decrease in the aortic pulse wave velocity results in the greater

separation between the two aortic BP gradients, weakening the mutual cancellation between them (in other words, the primary peaks associated with the ascending and descending aortic BP gradients are better preserved, leading to the scale displacement I wave and wrist acceleration J wave with higher amplitudes). Together with the observation that the amplitude sensitivity of all the other BCG waves to perturbation in the aortic pulse wave velocity was relatively small, the I-J amplitude in the scale displacement BCG, the I-J amplitude in the wrist displacement BCG, and the J-K amplitude in the wrist acceleration BCG (which may be proportional to the I-J amplitude in the scale displacement BCG) are also inversely proportional to the aortic pulse wave velocity.

Second, the aortic pulse pressure amplification influences the limb BCG morphology by altering the relative pulse amplitudes among the aortic BP waves. Its influence is primarily on the wave amplitudes (Fig. 3.5). Specifically, an increase in the aortic pulse pressure amplification (i.e., an increase in the pulse amplitude associated with P_2 relative to P_0 and P_1) is associated with an increase in the J-K amplitude in the scale displacement BCG and accordingly the K-L amplitude in the wrist acceleration BCG, since the J-K down-stroke in the scale displacement BCG and the K-L up-stroke is the wrist acceleration BCG are determined by the level of pulse pressure associated with P_2[70].

Finally, two remarks are worth making. First, the absolute amplitude of the limb BCG waveform is directly proportional to the level of pulse pressure[70]. Hence, an overall increase in the level of pulse pressure (e.g., with aging) may increase the amplitude of the limb BCG waveform. Second, as a first-order approximation, the influence of the aortic pulse wave velocity and pulse pressure amplification on the limb BCG waveform morphology may appear de-coupled: (i) the wave-to-wave intervals are primarily affected by the aortic pulse wave velocity, and (ii) the wave amplitudes primarily altered by the aortic pulse wave velocity (scale displacement I-J and wrist acceleration J-K) and pulse pressure amplification (scale displacement J-K and wrist acceleration K-L) are distinct. However, in reality, both the aortic pulse wave velocity and pulse pressure amplification exert impacts on the limb BCG waveform morphology, and these influences can be quite convoluted (meaning that it may not be trivial to infer the alteration in the aortic pulse wave velocity and pulse pressure amplification from the rudimentary analysis of the changes in the limb BCG waveform morphology). Hence, the physiological insights obtained from the mathematical model analysis may need to be integrated with data-driven techniques (e.g., machine learning) to decipher CV states and functions from the limb BCG.

3.5. Conclusion

The physiological association between the limb BCG waveforms and the arterial BP waveforms in the aorta was elucidated. It was demonstrated that arterial BP waves in the aorta may exert profound influences on the morphology of the limb BCG waveforms, and also that the influences are subject to complex interplay between the arterial BP waves. These findings suggest that certain characteristic features in the limb BCG waveforms may serve as viable surrogates of CV function, health, and potentially CVD.

4. Wearable BCG-Based Pulse Transit Time for Cuff-Less BP Monitoring

4.1. Introduction

One of the most widely pursued operator-less and cuff-less BP monitoring techniques is based on the PTT principle [2]. PTT is the time required for an arterial wave (e.g., BP) to travel from one (usually proximal) arterial site to another (usually distal) and is known to be inversely associated with BP via nonlinear pressure-area relationship of the arterial wall [2]. Due to the inconvenience associated with the instrumentation of proximal arterial pulse signals, the vast majority of existing PTT-based BP monitoring studies have resorted to pulse arrival time (PAT) in which the R wave of the electrocardiogram (ECG) is used as the proximal timing reference [2]. PAT has shown its efficacy for association with systolic BP (SP) in many previous investigations [2]. However, PAT is composed of PTT and pre-ejection period (PEP), which does not vary consistently in response to BP. In fact, our prior work has suggested that the efficacy of PAT may be degraded under BP-perturbing interventions in which PTT and PEP vary in the opposite directions, due to the mutual cancellation of their respective changes in response to BP [32], [33]. To overcome the drawback of PAT, the ability for convenient instrumentation of arterial pulse signals as proximal timing reference for PTT is desired.

Hence, the BCG has the potential to offer convenient options for the instrumentation of proximal arterial pulse signals for constructing PTT.

Prior works suggest that characteristic features extracted from the BCG instrumented with a scale-like platform (i.e., a high-performance force plate) have the potential for convenient cuff-less BP monitoring [17], [68]. Inspired by this success with the whole-body BCG and the ultra-convenience of wearable limb BCG, the goal of this chapter was to investigate the potential of wearable limb BCG to enable cuff-less BP monitoring via PTT by investigating the association between wearable limb BCG-based PTT and BP in comparison with whole-body BCG-based PTT and PAT. To this aim, a wearable BCG-based PTT was constructed using the BCG and PPG signals instrumented by a wristband as proximal and distal timing reference (called the wrist PTT). Its efficacy as surrogate of BP was examined in comparison with PTT constructed using the whole-body BCG instrumented by a customized weighing scale (scale PTT) as well as pulse arrival time (PAT) using the experimental data collected from 23 young healthy participants under multiple BP-perturbing interventions.

4.2. Human Subject Study

Under the Institutional Review Board (IRB) approval obtained from the University of Maryland and written informed consent, 23 young healthy volunteers were recruited and studied in strict accordance with the IRB guidelines.

4.2.1. Method

In the study, the following physiological waveforms were collected from each subject: (1) an ECG measured using 3 gel electrodes in the Lead II configuration and interfaced to a wireless amplifier (BN-EL50, Biopac Systems, Goleta, CA, USA); (2) a reference BP waveform measured using a fast servo-controlled finger cuff embedded with a blood volume (PPG) waveform sensor on the ring finger of a hand to implement the volume clamp method (ccNexfin, Edwards Lifesciences, Irvine, CA, USA); (3) a whole-body BCG waveform measured using a customized weighing scale; (4) a wrist BCG and PPG waveforms measured using a custom-manufactured wristband; (5) a finger PPG waveform measured using a transmission-mode clip (TSD124A, Biopac systems, Goleta, CA, USA) placed on a free finger and interfaced to a wired amplifier (OXY100E, Biopac systems, Goleta, CA, USA). The devices were interfaced to a laptop computer via a data acquisition unit (MP150, Biopac Systems, Goleta, CA, USA) to synchronously record all the waveforms at 1 kHz sampling rate (Fig. 4.1).

The data were collected during four BP-perturbing interventions (Fig. 4.2). Each subject stood still for 1.5 min for an initial rest state (R1). Then, the subject underwent the cold pressor intervention (CP) for 2 min, in which the subject immersed free hand into ice water. Followed by standing still for 1.5 min for a second rest state (R2), the subject underwent the mental arithmetic intervention (MA) for 3 min, in which the subject repeatedly added the digits of a three-digit number and added the sum to the original number. Followed by standing still for 1.5 min for a third rest state (R3), the subject underwent the slow breathing intervention (SB) for 3 min, in which the subject took deep and slow breaths. Followed by standing still for 1.5 min for a fourth rest state (R4), the subject underwent the breath holding intervention (BH), in which the subject held breath after normal exhalation (i.e., starting from functional residual capacity (FRC)). Lastly, the subject stood still for 1.5 min for a fifth rest state (R5). The recordings were made throughout these states.

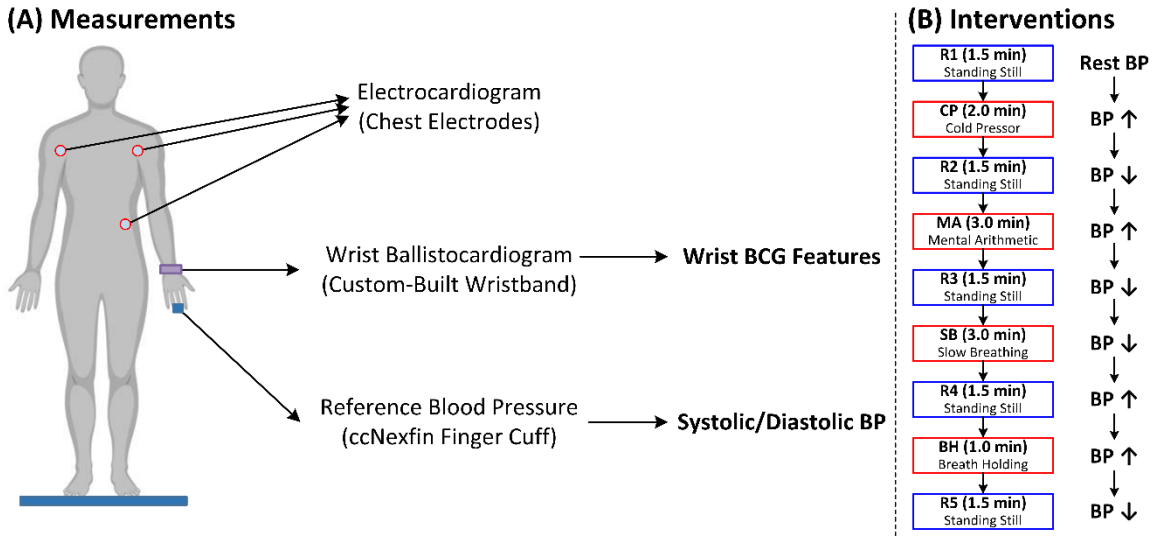

Fig. 4.1- Data collection for investigation of blood pressure trend tracking efficacy of wristband-based blood pressure surrogates. (A) Measured physiological waveforms. (B) Interventions to perturb subject's blood pressure.

Note that the interventions used in this study are known to effectively perturb BP through distinct changes in the cardiovascular parameters (including heart rate, stroke volume, and total peripheral resistance). In fact, CP is known to increase BP via an increase in heart rate and total peripheral resistance, often despite a decrease in stroke volume and cardiac output[77]–[83]; MA is known to increase BP via an increase in heart rate and total peripheral resistance (often along with a resulting increase in cardiac output)[77], [81]–[83]; SB is known to modestly decrease BP via a decrease in heart rate[84]–[89]; and BH is known to increase BP via an increase in TPR despite a decrease in heart rate, stroke volume, and cardiac output[90], [91].

Fig. 4.2 shows the experimental set-up for the human subject study.

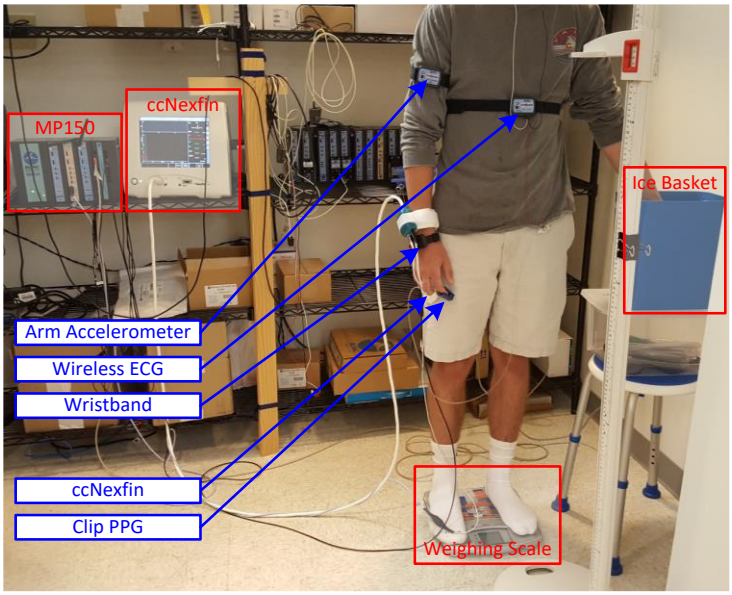

Fig. 4.2- Experimental set-up for human subject study.

4.2.2. Human Subject Statistics

Table 4.1 shows the subject demographics and ethnicity. Fig. 4.3 shows the perturbations in the reference DP and SP achieved with each intervention and all interventions.

Table 4.1: Subject demographics (mean+/-SD) and ethnicity.

(A) Demographics

Age [Years]	Gender	Weight [kg]	Height [cm]	SP Change [mmHg]	DP Change [mmHg]
23 +/- 5	M: 17 / F: 6	74 +/- 16	174 +/- 9	49.1+/-10.3	32.3+/-5.5

(B) Ethnicity

Hispanic Latin	American Indian Alaska Native	Black African American	Asian	Native Hawaiian Pacific Islander	White	Unknown
2	0	1	5	0	12	3

Table 4.2: T Maximum changes in reference diastolic (DP) and systolic (SP) pressures (mean+/-SE).

	R1→CP [mmHg]	CP→R2 [mmHg]	R2→MA [mmHg]	MA→R3 [mmHg]	R3→SB [mmHg]	SB→R4 [mmHg]	R4→BH [mmHg]	BH→R5 [mmHg]	All
DP	20+/-2	18+/-2	21+/-2	20+/-1	7+/-1	7+/-1	19+/-2	22+/-2	32+/-1
SP	26+/-2	25+/-2	30+/-3	30+/-2	10+/-2	8+/-2	31+/-4	31+/-3	49+/-2

Fig. 4.3 shows the group-average changes in the cardiovascular parameters (including DP and SP, heart rate, stroke volume, cardiac output, and total peripheral resistance) across the BP-perturbing interventions (here, the heart rate was derived by dividing the cardiac output by the stroke volume, both of which were obtained from the ccNexfin device). The results suggest that BP was changed as anticipated in the study design: BP increased in response to CP, MA, and BH, while it moderately decreased in response to SB. The results also indicate that the interventions changed BP through distinct alternations in the cardiovascular parameters: (1) CP by increasing heart rate and total peripheral resistance; (2) MA by largely increasing heart rate and total peripheral resistance while largely decreasing stroke volume; (3) SB by decreasing stroke volume and total peripheral resistance; and (4) BH by decreasing heart rate while increasing total peripheral resistance. Therefore, the collected data are expected to provide challenging tests for the BP trend tracking efficacy of the BP surrogates investigated in this study.

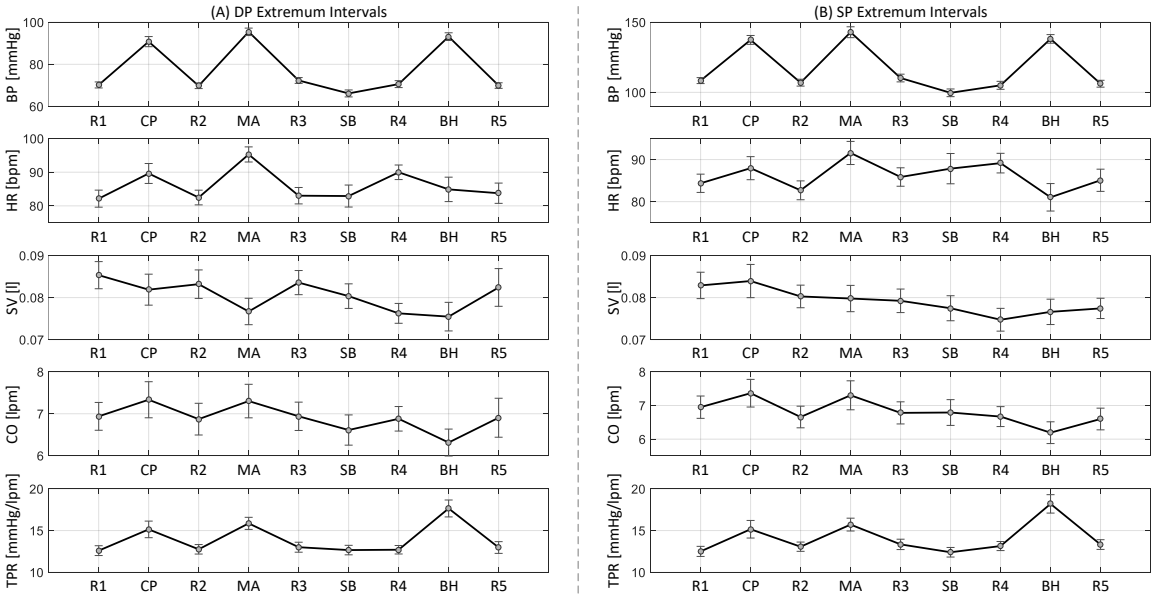

Fig. 4.3- Group-average changes in the cardiovascular parameters across BP-perturbing interventions (mean+/-SE).

4.3. Method

In this chapter, we investigated the association between PTT based on a wearable limb BCG (wrist BCG) and BP by the following steps: (i) requisite signals to construct PTT based on both whole-body BCG and wrist BCG as well as PAT, and the corresponding reference systolic (SP) and diastolic (DP) BP were acquired from the study participants under an array of BP-perturbing interventions; (ii) requisite features to construct PTT and PAT were extracted from the acquired signals, and then PTT and PAT were constructed; and (iii) the association between the PTT and PAT thus constructed versus reference BP was analyzed. Details follow.

4.3.1. Signal Processing

To extract the features, we need to process and clean the signal. In this regard, the collected data were first down-sampled to 250Hz. For each participant, the data were segmented into nine periods: R1, CP, R2, MA, R3, SB, R4, BH, and R5. In each period, the signals were processed as follows.

- First, the ECG R waves were detected as the local peaks in the ECG signal.

- Second, the scale and wrist BCG as well as PPG signals were band-pass filtered using a 1st-order Butterworth filter with nominal pass band of 0.5Hz~15Hz (in other words, the pass band of individual participants were varied around the nominal pass band).

- Third, the BCG and PPG beats were identified with the ECG gating.

- Fourth, individual beats were visually inspected and those associated with corrupted BCG (e.g., large-amplitude BCG due to non-negligible motion artifacts) and PPG (e.g., small signal-to-noise ratio PPG due to low-quality sensor-skin contact) signals were excluded from further analysis.

- Fifth, the scale and wrist BCG signals were smoothed using a causal 8-beat exponential moving average filter to suppress residual motion artifacts.

4.3.2. Construction of PTT and PAT

From the measured signals, PTT based on the scale and the wrist BCG as well as PAT were constructed based on the characteristic features extracted from the BCG, PPG, and ECG signals (Fig. 4.4). Details follow.

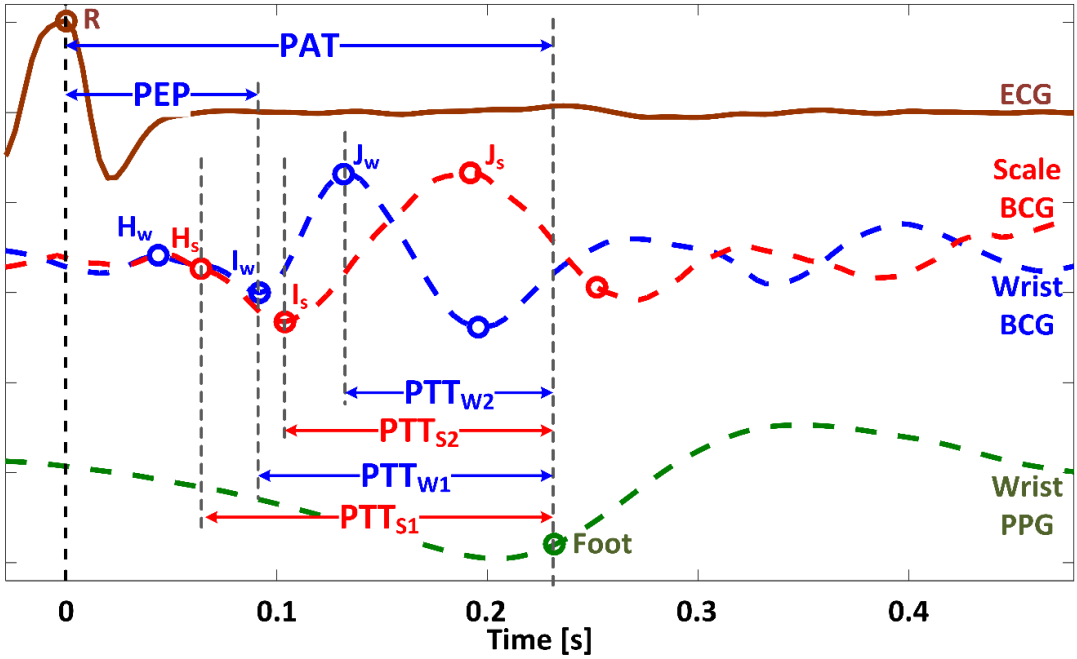

Fig. 4.4Fig. 2: Features extracted from ECG (R wave), BCG (HS, IS, JS, HW, IW, JW waves), and PPG (foot) signals, as well as scale PTT (PTTS1, PTTS2), wrist PTT (PTTW1, PTTW2), and PAT. Only green PPG signal is shown for the sake of illustration.

First, the PPG foot was extracted using the intersecting tangent method [31], [32]. Then, characteristic features (called the waves;Fig. 4.4) consistently available in the scale and wrist BCG signals were identified, which were then extracted from each beat as follows: (1) the scale J_S and wrist J_W waves were identified as the local maximum in the initial 15%~40% window of the beat; (2) the scale I_S and wrist I_W waves were identified as the nearest local negative waves before the J_S and J_W waves, respectively; and (3) the scale H_S and wrist H_W waves were identified as the nearest local positive waves before the I_S and I_W waves, respectively. The local waves were identified as local extrema, except for the H_S and I_W waves which were identified based on the intersecting tangent method.

From the consistently available features thus extracted, PTT and PAT were constructed as follows (Fig. 4.4). First, two scale PTTs were constructed as whole-body BCG-based PTT using the scale BCG and the wrist PPG as the proximal and distal timing references: PTT_{S1}

as the interval between the H_S wave and the PPG foot, and PTT_{S2} as the interval between the I_S wave and the PPG foot. Second, two wrist PTTs were likewise constructed as wrist BCG-based PTT using the wrist BCG and the wrist PPG as the proximal and distal timing references: PTT_{W1} as the interval between the I_W wave and the PPG foot, and PTT_{W2} as the interval between the J_W wave and the PPG foot. Third, PAT was constructed as the interval between the ECG R wave and the PPG foot. To examine the influence of the choice of the PPG signal on the efficacy of PTT and PAT, all the above PTTs and PAT were constructed using green and IR PPG signals, resulting in eight PTTs and two PATs for analysis. In addition to the above PTT and PAT, pre-ejection period (PEP) was constructed as the interval between the ECG R wave and the I_W wave similarly to our prior work [32].

4.3.3. Analysis of Association between PTT and PAT versus BP

To analyze the association between PTT and PAT versus BP, the reference DP and SP were extracted from each beat as the minimum (DP) and maximum (SP) of the height-compensated brachial BP signal. In addition, in each period, beat-to-beat fluctuations in the scale PTT, wrist PTT, and PAT were suppressed by removing outliers (defined as the PTT and PAT values outside of +/-3×SD from its mean value within each period) and smoothing the respective non-uniformly spaced beat-to-beat sequences using a quadratic Savitzky-Golay filter [92]. Then, the efficacy of the scale and wrist PTT as well as PAT in association with BP was analyzed in the maximum BP change regimes associated with all the resting and intervention periods as well as in the individual resting-intervention period pairs. Details follow.

First, the association between PTT and PAT versus BP in the maximum BP change regimes associated with all the resting and intervention periods was analyzed. The goal of the analysis was to comparatively assess the efficacy of scale PTT, wrist PTT, and PAT as surrogate of BP. In each period, the instant at which the reference BP attained extremum (minimum for resting and SB periods, and maximum for CP, MA, and BH periods) was identified. Then, the reference BP as well as the scale PTT, wrist PTT, and PAT representative of the period were determined as their respective median values within the five-beat interval around the extremum. Subsequently, up to nine pairs of reference BP and the corresponding scale PTT, wrist PTT, and PAT were obtained from the data collected from each participant. Considering that the pair of reference BP and the corresponding scale PTT, wrist PTT, and PAT could not be obtained in a subset of periods (especially BH due to the limited number of beats available from the collected data), only the participants equipped with the pair of reference BP and the corresponding PTT and PAT for ≥ 3 resting-

intervention period pairs (R1-CP, R2-MA, R3-SB, and R4-BH; thus ≥ 6 periods in total) were included for the analysis of PTT-BP and PAT-BP association.

Second, the association between the wrist PTT and PAT versus BP in the individual resting-intervention period pairs (R1-CP, R2-MA, R3-SB, and R4-BH) was analyzed. The goal of the analysis was to examine the robustness and consistency of the association between the wrist PTT and PAT versus BP across diverse BP-perturbing interventions. In each resting-perturbation period pair, the range of BP was segmented into 1 mmHg bins, and the median wrist PTT and PAT values contained in each bin were calculated. Then, the reference BP and the corresponding wrist PTT and PAT were included for analysis of wrist PTT-BP and PAT-BP association.

Table 4.3. Resting BP levels and overall BP changes (mean+/-SE). DP: diastolic BP. SP: systolic BP.

	Resting Level	Overall Change
DP	78+/-1	38+/-2
SP	119+/-2	56+/-3

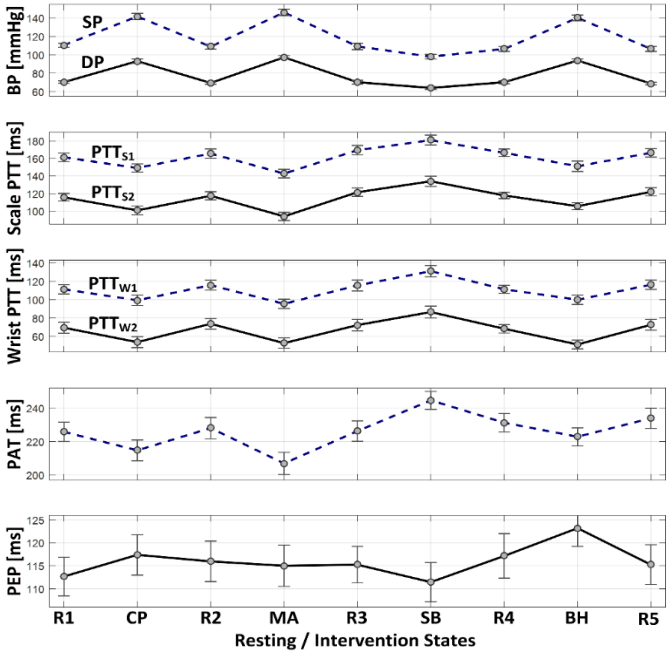

Fig. 4.5 Changes in BP, scale PTT based on green PPG, wrist PTT based on green PPG, pulse arrival time (PAT) based on green PPG, and pre-ejection period (PEP) in response to BP-perturbing interventions (mean+/-SE).

The efficacy of the scale PTT, wrist PTT, and PAT in their association with BP was quantified in terms of three metrics: correlation coefficient, root-mean-squared error (RMSE), and mean absolute error (MAE) between reference and calibrated BP. These

metrics were first computed in each participant and then summarized as mean and standard error (SE) across all participants. The Bland-Altman analysis was also conducted to assess the limits of agreement between reference and calibrated BP. In the analysis, the calibrated BP was computed as follows. In case of the analysis for the maximum BP change regimes, linear regression models to relate all the eight PTT (PTT_{S1}, PTT_{S2}, PTT_{W1}, and PTT_{W2}, all in conjunction with both green and IR PPG signals) and two PAT (in conjunction with both green and IR PPG signals) in the available (≥ 6) resting and intervention periods to reference DP and SP were obtained, and the calibrated DP and SP were computed by inputting each PTT and PAT to the respective regression model. Subsequently, the correlation coefficients, RMSEs, and MAEs between reference versus calibrated DP and SP were computed as measures of the best-case association. The significance in difference between wrist PTT and PAT was determined using the paired t-test with the Bonferroni correction for multiple comparisons (i.e., PTT_{W1} and PTT_{W2} versus PAT). As part of the analysis, the efficacy of PTT and PAT constructed with green and IR PPG signals was investigated in terms of the same quantitative metrics. In case of the analysis for the individual resting-intervention period pairs, linear regression models to relate the best-performing wrist PTT in the analysis of maximum BP change regimes and PAT to reference DP and SP were obtained, and the calibrated DP and SP were computed by inputting the best-performing PTT and PAT to the respective regression model. Then, the correlation coefficients, RMSEs, and MAEs between reference versus calibrated DP and SP were computed as measures of the best-case association.

4.4. Results

Table 4.3 summarizes the resting BP levels and overall BP changes associated with the study participants. Table 4.4 shows the maximum changes in BP in response to each BP-perturbing intervention as well as all interventions. Fig. 4.5 illustrates the changes in BP, scale and wrist PTT as well as PAT based on green PPG, and PEP in response to BP-perturbing interventions. Table 4.5 summarizes the correlation, RMSE, and MAE between reference BP versus BP calibrated from scale PTT, wrist PTT, and PAT based on green and IR PPG in all participants. Fig. 4.6 illustrates the correlation, RMSE, and MAE as well as the Bland-Altman plots between reference BP versus BP calibrated from scale PTT PTT_{S2}, wrist PTT PTT_{W2}, and PAT based on green PPG in all participants. Fig. 5 shows the correlation, RMSE, and MAE between reference BP versus BP calibrated from wrist PTT PTT_{W2} and PAT based on green PPG in all participants associated with individual resting-intervention pairs.

Table 4.4. BP changes in response to BP-perturbing interventions (mean+/-SE).

	R1→CP	CP→R2	R2→MA	MA→R3	R3→SB	SB→R4	R4→BH	BH→R5	Range
DP [mmHg]	+23+/-2	-24+/-2	+27+/-1	-26+/-2	-6+/-1	+6+/-1	+23+/-2	-25+/-2	38+/-2

SP [mmHg]	+31+/-3	-32+/-3	+37+/-2	-37+/-2	-10+/-2	+7+/-1	+33+/-3	-33+/-2	56+/-3

Table 4.5: Correlation, root-mean-squared error (RMSE), mean absolute error (MAE), and precision error (PE) between reference BP versus BP calibrated from scale PTT, wrist PTT, and pulse arrival time (PAT) (mean+/-SE). DP: diastolic BP. SP: systolic BP. ‡: $p<0.025$ with respect to PAT (paired t-test).

(a) Correlation

		DP		SP	
		Green PPG	IR PPG	Green PPG	IR PPG
Scale PTT	PTT_{S1}	0.70+/-0.04	0.60+/-0.04	0.67+/-0.04	0.55+/-0.07
	PTT_{S2}	0.73+/-0.03	0.59+/-0.05	0.67+/-0.04	0.54+/-0.07
Wrist PTT	PTT_{W1}	0.75+/-0.03	0.61+/-0.07‡	0.76+/-0.03	0.61+/-0.08
	PTT_{W2}	0.79+/-0.03‡	0.65+/-0.07‡	0.81+/-0.02‡	0.65+/-0.08
PAT		0.69+/-0.04	0.42+/-0.09	0.72+/-0.04	0.50+/-0.10

(b) RMSE

[mmHg]		DP		SP	
		Green PPG	IR PPG	Green PPG	IR PPG
Scale PTT	PTT_{S1}	7.2+/-0.5	7.5+/-0.4	10.9+/-0.8	10.8+/-0.5
	PTT_{S2}	7.1+/-0.4	7.4+/-0.4	10.8+/-0.7	10.7+/-0.6
Wrist PTT	PTT_{W1}	6.6+/-0.5‡	7.0+/-0.4‡	9.7+/-0.6	9.9+/-0.6
	PTT_{W2}	6.1+/-0.4‡	6.5+/-0.5‡	8.9+/-0.6	9.6+/-0.8
PAT		8.0+/-0.6	9.0+/-0.6	10.6+/-0.7	11.2+/-1.0

(c) MAE

[mmHg]		DP		SP	
		Green PPG	IR PPG	Green PPG	IR PPG
Scale PTT	PTT_{S1}	5.8+/-0.3	6.2+/-0.3	9.1+/-0.7	9.0+/-0.5
	PTT_{S2}	5.7+/-0.4	6.1+/-0.4	9.0+/-0.7	9.2+/-0.6
Wrist PTT	PTT_{W1}	5.5+/-0.4	5.8+/-0.3‡	8.3+/-0.5	8.4+/-0.5
	PTT_{W2}	5.1+/-0.3‡	5.3+/-0.4‡	7.6+/-0.5	8.0+/-0.7
PAT		6.5+/-0.4	7.4+/-0.5	8.6+/-0.6	9.4+/-0.9

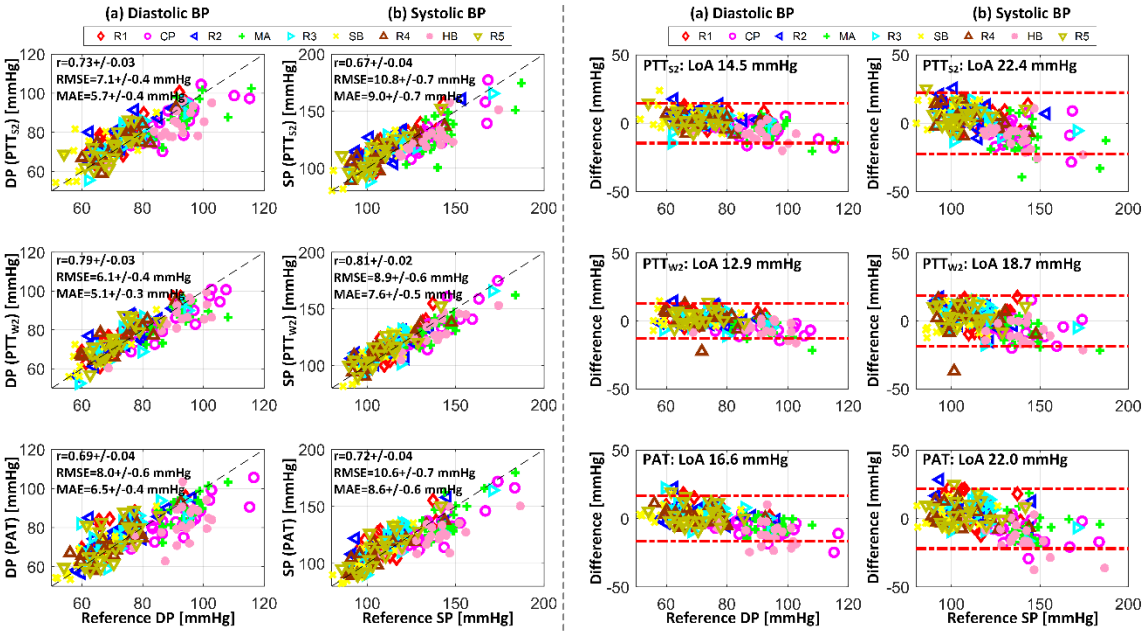

Fig. 4.6: Correlation (left) and Bland-Altman (right) plots for reference BP versus BP calibrated from scale PTT PTTS2, wrist PTT PTTW2, and pulse arrival time (PAT) based on green PPG in all participants. (a) Diastolic BP (DP). (b) Systolic BP (SP). LoA: limits of agreement.

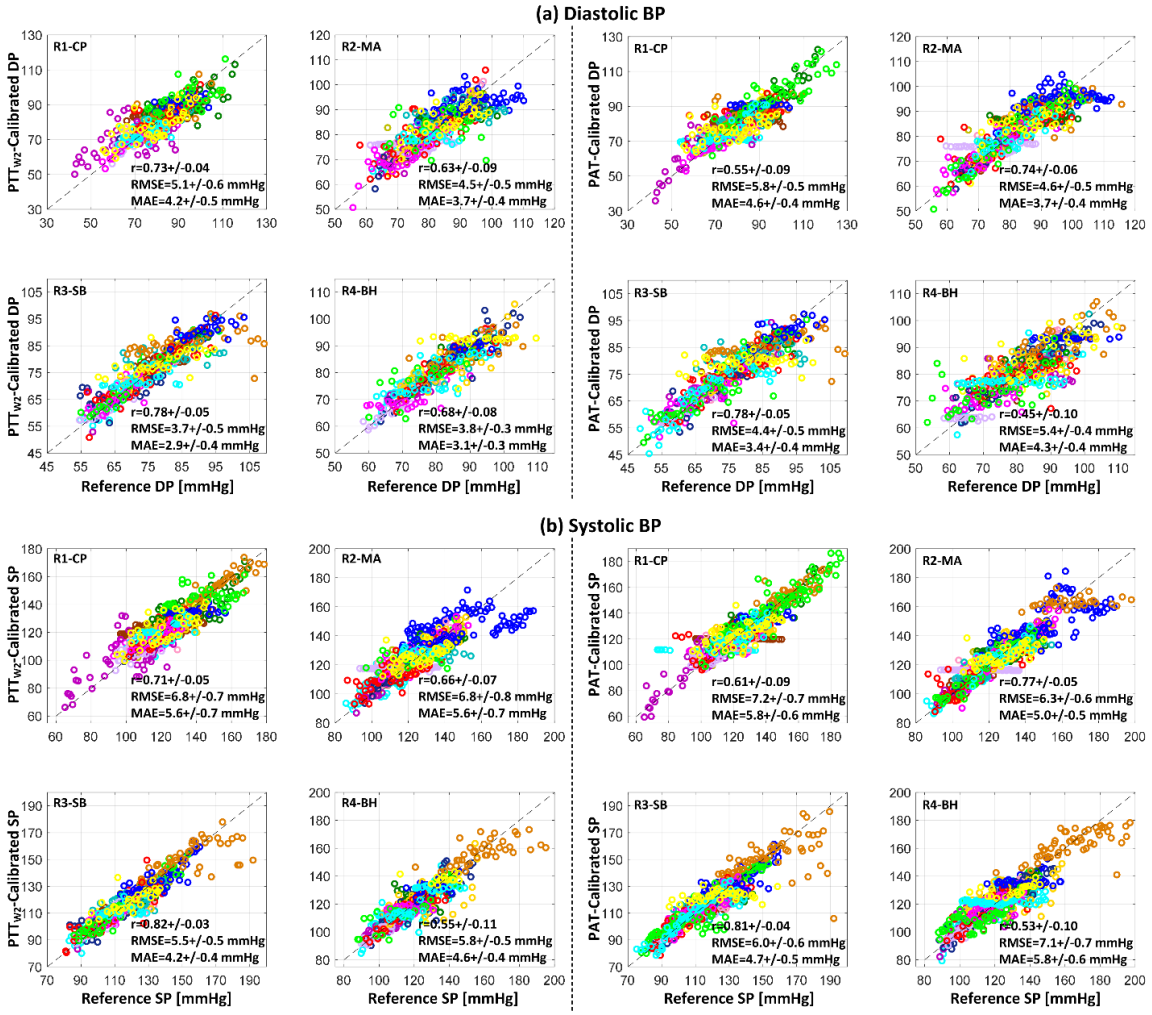

Fig. 4.7: Reference BP and BP calibrated from wrist PTT and pulse arrival time (PAT) based on green PPG in all participants associated with individual resting-intervention pairs. (a) Diastolic BP (DP). (b) Systolic BP (SP).

4.5. Discussion

Despite its potential for ultra-convenient BP monitoring with wide-ranging wearable devices, the limb BCG presents critical hurdles due to its unique yet unestablished morphology distinct from the relatively well understood whole-body BCG. To the best of our knowledge, no prior work has rigorously examined opportunities for the wearable limb BCG-based PTT and BP monitoring. In our initial attempt to tackle this challenge, this chapter intended to investigate the feasibility of ultra-convenient BP monitoring based on the PTT principle implemented using the BCG and PPG signals obtained from a single wrist-worn device. Our primary interests were (i) the overall association between the wrist PTT and BP with physiological justification and its consistency and robustness against diverse

perturbations in BP; (ii) comparative performance between the wrist PTT and PAT in association with BP, and (iii) the effect of the choice of PPG on the association between wrist PTT and BP.

4.5.1. BP Changes in Response to Interventions

Both DP and SP of all the participants could be varied widely with the BP-perturbing interventions employed in this chapter. On the average, 38 mmHg change in DP and 56 mmHg change in SP were observed (Table 4.3), while all the participants underwent the minimum changes of >24 mmHg in DP and >37 mmHg in SP. Each intervention contributed comparably to these overall BP changes with >23 mmHg change in DP and >31 mmHg change in SP on the average, except SB which decreased both DP and SP only modestly (Table 4.4). Further, cardiovascular mechanisms responsible for the BP changes due to each of the BP-perturbing interventions was distinct: (1) CP increased BP via an increase in heart rate and total peripheral resistance; (2) MA increased BP via a large increase in heart rate (with the associated decrease in stroke volume) and total peripheral resistance; (3) SB decreased BP via a decrease in stroke volume; and (4) BH increased BP via a large increase in total peripheral resistance despite a notable decrease in heart rate, stroke volume, and cardiac output (not shown). To a large extent, the cardiovascular mechanisms observed in this study accord with the findings from prior work: CP [77]–[83], MA [77], [81]–[83], and BH [90], [91]. Existing work suggests that SB decreases heart rate [84]–[89]. But, only a small decrease in heart rate was observed in response to SB in this study. Yet in sum, the experimental data used in this study has provided a quite challenging test for investigating the association between limb BCG-based PTT and BP under a wide range of changes in BP and cardiovascular mechanisms.

4.5.2. Association between Scale PTT and Wrist PTT versus BP

Remarkably, PTT constructed with consistent morphological features in the scale and wrist BCG exhibited good association with DP and SP (Table 4.5 and Fig. 4.5, Fig. 4.6). The PTT showed the desired inversely proportional behavior in response to changes in BP: it decreased when BP increased while it increased when BP decreased (Fig. 4.5). On the average, when green PPG was used as distal signal, correlation between scale PTT (PTT_{S1} and PTT_{S2}) versus DP and SP was ≥ 0.70 and 0.67, and as well, correlation between wrist PTT (PTT_{W1} and PTT_{W2}) versus DP and SP was ≥ 0.75 and ≥ 0.76. In addition to good correlation, both scale and wrist PTT achieved promising post-calibration BP error levels (Table 4.5). Specifically, the accuracy may not appear excellent (especially SP) when each BP measurement is viewed individually. However, noting that an important merit

associated with cuff-less BP monitoring is its compatibility for frequent measurement, the random errors in the individual BP measurements may be averaged out [93]. From this standpoint, both scale and wrist PTT achieved post-calibration RMSE levels to attain hypertension screening accuracy comparable to auscultation via measurement averaging (DP ≤ 8 mmHg and SP ≤ 12 mmHg) [93]. In addition, both achieved ≤ 7 mmHg MAE criterion required by the recent IEEE Standard for Wearable, Cuffless Blood Pressure Measuring Devices (IEEE Std 1708™-2014) for DP but not for SP. Comparing all the PTTs examined, PTT_{W2} exhibited the best association with both DP and SP in terms of all the metrics considered in this study.

The arterial path considered in this study (i.e., aorta to wrist) mainly involves large compliant vessels (including the aorta, subclavian artery, brachial artery, and radial artery, in which the influence of smooth muscle contraction (SMC) is small if not minimal) than local arteries whose tone is significantly affected by SMC. Hence, the imperfect PTT-BP association may be due to SMC rather than alterations in the BP dependence of arterial compliance (i.e., arterial stiffness). In particular, CP and MA maneuvers may have elicited a large degree of SMC.

It is also emphasized that the PTTs investigated in this study were not constructed randomly via trial and error. In fact, the notable association between the proposed scale and wrist PTT versus BP may be physiologically justified. In regards to the scale PTT, it has been elucidated that the timing associated with the onset of the I wave of the whole-body BCG may correspond to the onset of ascending aortic BP wave [70]. Noting that the scale BCG instrumented in this study may be regarded as a whole-body BCG, PTT_{S1} may serve as a viable PTT due to the proximity between the peak of the H_S wave and the onset of the I_S wave, while PTT_{S2} may as well serve as a viable PTT due to the proximity between the onset and peak of the I_S wave, in addition to the robustness in the detection of the peak of the I_S wave compared with its onset (in fact, the association between PTT_{S2} instrumented with a high-bandwidth force plate and BP has been demonstrated in our prior work ([31], [32]). In regards to the wrist PTT, the wrist BCG in this study was instrumented with an accelerometer. Thus, with a simplifying approximation that the human body is rigid (meaning that the whole-body and wrist movement responses to the heartbeat is exactly the same), the wrist BCG may be viewed as the second derivative of the whole-body BCG. Considering that the whole-body BCG is approximately inverted (i.e., vertically flipped) if differentiated twice, the I_W and J_W waves may approximately correspond to the H_S and I_S waves. For this reason, PTT_{W1} and PTT_{W2} may be viewed as equivalent to PTT_{S1} and PTT_{S2} and thus serve as viable PTT.

It is also worth mentioning that the wrist PTT outperformed the scale PTT in all the metrics considered in this study (Table 4.5 and Fig. 4.6). Although additional work must be conducted for complete understanding of this observation, this may be attributed to several reasons. First, it may be due to the possible distortion of the whole-body BCG when instrumented by the scale due to factors such as (i) dynamic characteristics of the scale and quality of the sensors (i.e., strain gauges) embedded in the scale as well as (ii) phase delay associated with the transfer of the whole-body BCG to the scale caused by the compliance of the human body (indeed, our recent work clearly showed that the scale BCG exhibited a non-negligible subject-dependent phase delay relative to the force plate BCG). In contrast to the scale BCG, the wrist BCG may have been subject to less instrumentation artifact due to the wide passband of the accelerometer used in this study (400 Hz). Second, it may also be due to the motion artifacts caused by breathing. We speculate that breathing may have more salient influence on the whole-body BCG than the wrist BCG because it originates from the main trunk. Hence, it may be of interest to further investigate the influence of breathing on the BCG signal quality.

4.5.3. Comparison of Wrist PTT and PAT

Both the wrist PTT PTT_{W1} and PTT_{W2} outperformed PAT in all the metrics for both DP and SP (Table 4.5 and Fig. 4.6). On the average, when green PPG was used as distal signal, correlation associated with PTT_{W2} was higher than PAT by 15% and 12% for DP and SP, respectively, while RMSE and MAE were smaller than PAT by 24% and 16% for DP, respectively, and 16% and 12% for SP, respectively. For DP, all the metrics for PTT_{W2} were significantly superior to those for PAT. On the other hand, only correlation was significantly superior as far as SP was concerned. Considering that PAT correlates quite well to SP [2], the efficacy of PTT_{W2} (in the sense that it significantly outperformed all the metrics for DP, plus a certain metric for SP) may still be viewed as promising if not superb.

In addition to its overall efficacy described above, PTT_{W2} exhibited more robust and consistent association with BP across diverse BP-perturbing interventions relative to PAT (Fig. 4.7). First, the correlation between PAT and BP varied 0.33 for DP and 0.28 for SP across the BP-perturbing interventions employed in this study (CP, MA, SB, and BH), whereas the correlation between PTT_{W2} and BP varied only 0.15 for DP and 0.27 for SP across the same interventions. Second, RMSE and MAE associated with PTT_{W2} were consistently lower than (or at least equal to) the same metrics associated with PAT in all the BP-perturbing interventions for DP and SP (except for SP in MA). On the other hand, PAT showed higher correlation than PTT in MA. It is speculated that the efficacy of PAT in MA may be attributed to the response of PEP to a large increase in heart rate invoked by

MA: an increase in cardiac output followed by a large increase in heart rate yielded a (albeit modest) decrease in PEP (Fig. 4.5), which, when synergistically combined with a decrease in PTT in response to MA, makes PAT more sensitive to change in BP than PTT_{W2}. But all in all, PTT_{W2} was more robust and consistent than PAT in terms of association with BP.

In addition to its remarkable performance relative to PAT, wrist PTT may also boast superior convenience to PAT: the measurement of ECG may require conventional electrodes or two-handed user maneuvers (e.g., [94]), whereas wrist BCG may be passively measured without requiring any user actions. Hence, wrist BCG may turn out to be an attractive alternative to PAT.

4.5.4. Effect of Choice of PPG on PTT-BP Association

All in all, green PPG resulted in superior association with BP (both DP and SP) than IR PPG (Table 4.5). This finding may be attributed to the anatomy of the wrist vasculature and the wavelengths of the green and IR PPG. First, the arterial bed in the back of the wrist is primarily composed of arterioles and capillaries while there is no major large artery passing through the back of the wrist. Second, green PPG is good at capturing capillary blood flow and perfusion at the level of skin, whereas IR PPG is more suited for capturing blood flow and perfusion deep under the skin (where relatively large arteries are often located) [95]. Hence, green PPG may possess superior signal quality than its IR counterpart at the wrist site and may thus be preferred for constructing PTT equipped with close association with BP.

4.6. Conclusion

Close and robust association between the wrist BCG-based PTT and BP was demonstrated. The finding may open up new opportunities for ultra-convenient BP monitoring based on the BCG instrumented at limb locations, using, e.g., wristband, armband, and smartphone. Future effort must be invested to (i) the translation of the findings from this study to innovative BP monitoring systems and algorithms applicable to real-world use, as well as (ii) the enhanced physiological understanding of limb BCG and its relationship to the whole-body BCG, and its application to independent monitoring of DP and SP.

5. Wearable BCG-Based Pulse Wave Analysis for Cuff-Less BP Monitoring

5.1. Introduction

As discussed in previous chapter, currently, the most popular approach to cuff-less BP monitoring is based on the principle of PTT[21], which is known to frequently exhibit an inversely proportional relationship to BP through the BP dependence of arterial stiffness. One main drawback of the PTT approach, especially from convenience standpoint, is that it requires the instrumentation of two arterial pulse waveforms to compute PTT. In the past, this requirement has been fulfilled by measuring arterial pulse waveforms from two distinct locations in the body (e.g., from carotid and femoral arteries for the well-known carotid-femoral PTT[6]), which is quite inconvenient and cumbersome. Hence, recent effort to enable ultra-convenient BP monitoring has focused on the development of techniques to infer BP from a single wearable device. Some of these efforts employ multiple pulse waveforms from a single device (e.g., an electrocardiogram and a PPG at an extremity site[7], [8], or multiple PPGs within a known short distance[9]) to still leverage the PTT principle for BP monitoring, while some other efforts strive to infer BP from the analysis of a single pulse waveform[10]–[12]. In both cases, PPG has been the preferred choice of modality for arterial pulse measurement due to its amenity to easy placement and stable instrumentation.

Previous studies demonstrated that the whole-body BCG measured with, e.g., a weighing scale-like platform, may be leveraged in conjunction with a second pulse waveform (e.g., PPG at an extremity location) for PTT-based BP monitoring[15], [68]. It is also demonstrated that whole-body BCG alone may suffice for cuff-less BP monitoring, where the use of waveform features in the whole-body BCG that (at least qualitatively) represent aortic PTT and distal aortic pulse pressure (PP) to achieve independent monitoring of diastolic (DP) and systolic (SP) BPs is perused[17]. Despite the potential of this whole-body-BCG-based approach to cuff-less BP monitoring explored thus far, there is room for improvement both in terms of convenience and accuracy. In terms of convenience, the measurement of whole-body BCG may require bulky devices such as scale and bed. Hence, a viable option to improve convenience may be to explore wearables that can be worn on limb locations (e.g., wrist watch and arm band) for instrumentation of the BCG. In terms of accuracy, the whole-body-BCG may be distorted by the dynamics of the measurement devices, like weighing scale. However, for the limb-BCG such problem does not exist due to the small weight of the MEMS acceleration sensor.

Motivated by the above rationale, the objective of this chapter was to investigate the association between a limb BCG and BP based on data mining. Like as the previous chapter, during four BP-perturbing interventions, the BCG and reference BP were measured from 23 young healthy volunteers using a custom-manufactured wristband equipped with a MEMS accelerometer and a commercial continuous BP measurement device. Then, both timing and amplitude features in the wrist BCG waveform were extracted, and significant features predictive of DP and SP were selected using stepwise linear regression analysis. The selected features were further compressed using principal component analysis to yield a small set of predictors for DP and SP. The association between the predictors thus obtained and BP was investigated by conducting multivariate linear regression analysis.

5.2. Method

Using the data from human subject study explained in section 4.2, in this section, we investigated the association between a limb BCG and BP by the following steps: (1) a number of timing and amplitude features were extracted from the BCG waveform; (2) significant features were selected and further compressed to form a small number of BP predictors; and (3) the BP predictors were correlated to reference BP. Details follow.

5.2.1. BCG Feature Extraction

From each subject record, the timings and amplitudes associated with an array of waves in the wrist BCG, including the G_w, H_w, I_w, J_w, K_w, and L_w waves in Fig. 5.1, were extracted based on the following procedure.

The subject records were segmented into nine periods: R1, CP, R2, MA, R3, SB, R4, BH, and R5. In each period, the waveform signals were processed as follows. First, the wrist BCG signal was band-pass filtered. For this purpose, a 1^{st}-order Butterworth filter with nominal cut-off frequencies of 0.5 Hz and 15 Hz was used (meaning that cut-off frequencies for individual subjects were tuned around the nominal frequencies to best filter the signals). Second, the ECG R waves were detected using the popular Pan-Tompkins method. Third, the wrist BCG beats were identified via the ECG gating. Fourth, the BCG beats were visually inspected and those associated with large motion artifacts (characterized by unusually large-amplitude beats) were excluded. Fifth, the BCG signal was then smoothed using a causal 8-beat exponential moving average filter to suppress the remaining random motion artifacts. Sixth, the BCG wave features of interest (i.e., the G_w, H_w, I_w, J_w, K_w, and L_w waves in Fig. 5.1) were extracted from each beat. Specifically, the J_w wave was identified as the local maximum within 100 ms to 300 ms after the ECG R

wave. The I_w and K_w waves were identified as the local minima before and after the J wave, respectively, that are nearest to the J_w wave. The H_w wave was identified as the local maximum before the I_w wave that is nearest to the I_w wave, and similarly, the G_w wave was identified as the local minimum before the H_w wave that is nearest to the H_w wave. Likewise, the L_w wave was identified as the local maximum after the K_w wave that is nearest to the K_w wave. We used the intersecting tangent method for detecting the G_w and I_w waves, because these waves were not often sharp enough. Seventh, the reference DP and SP were extracted from each beat as the minimum (DP) and maximum (SP) of the finger-cuff BP waveform. Then, all possible combinations of the timing intervals (16; including the heart period computed as the J_w-J_w interval (i.e., the time interval between the J_w waves associated with two consecutive beats – current beat and the beat ahead of it)) and amplitudes (21) were extracted as candidate features for association to BP.

Note that the naming of the wrist BCG waves followed that used for the whole-body BCG waves[76]. But, this way of naming is just for the sake of convenience; in fact, currently there is no commonly accepted naming convention for limb BCGs. Accordingly, it must be understood that the waves in a limb BCG does not have the same physiological implications as the corresponding whole-body BCG waves.

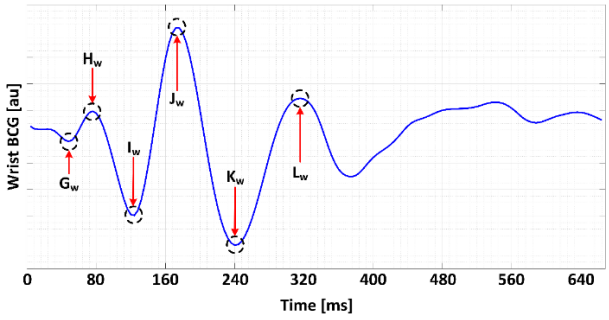

Fig. 5.1 Features extracted from a wrist BCG, which include the timings and amplitudes of Gw, Hw, Iw, Jw, Kw, and Lw waves.

5.2.2. BCG Feature Selection and Compression

From the 37 candidate features thus extracted, we selected significant features associated with DP and SP based on the stepwise linear regression analysis as follows. First, the range of DP (or SP) in each subject record was segmented into 1 mmHg bins, and the set of 37 median BCG feature values corresponding to each 1mmHg DP (or SP) bin was computed. Then, the pair of DP (or SP) and the computed median BCG feature values

associated with each subject was merged across all 23 subjects (note that the dimension of the DP (or SP) pair is determined by the range of DP (or SP)) and applied to the stepwise linear regression analysis to determine significant BCG features predictive of DP (or SP).

Due to the large number of significant BCG features selected from the stepwise linear regression analysis, the BCG features were further compressed using the principal component analysis (PCA) for dimensionality reduction. Specifically, the range of DP (or SP) in each subject record was again segmented into 1 mmHg bins, and the set of median values of the BCG features selected above with the stepwise linear regression corresponding to each bin was computed. Then, the pair of DP (or SP) and the corresponding median BCG feature values associated with each subject was merged across all 23 subjects. The BCG features were normalized with the respective feature's mean and standard deviation, and subsequently applied to the PCA to derive principal components (PCs) as predictors of DP (or SP).

5.2.3. Correlation Analysis

The association between the wrist BCG and BP was investigated using multivariate linear regression analysis. Specifically, the PCs predictive of DP and SP were correlated with the reference DP and SP, respectively, via the following calibration relationship:

$$P_X = \eta_0^X + \eta_1^X \phi_1^X + \cdots + \eta_N^X \phi_N^X \quad (1)$$

where P_X is reference BP, ϕ_k^X (k=1,…,N) the k-th PC, η_k^X (k=1,…,N) the calibration coefficient for the k-th PC, η_0^X the intercept, and N the total number of PCs included in the relationship (1) ($X = D$ for DP and $X = S$ for SP). Then, the association between the PCs derived from the wrist BCG and BP was analyzed in terms of three metrics: (1) correlation coefficient (r); (2) root-mean-squared error (RMSE); and (3) mean absolute error (MAE).

First, the association at the subject level was investigated. In each subject, the ranges of reference DP and SP across all BP-perturbing interventions were segmented into 1 mmHg bins, and the PCs associated with each DP and SP bins were computed from the set of median values of the BCG features recruited in the PCs corresponding to each bin. Then, these PCs were calibrated to the reference DP and SP by determining η_k^X (k=0,…,N) in the relationship (1) with least-squares fitting to yield a subject-specific calibration relationship. Then, correlation coefficients, RMSEs, and MAEs between the reference DP and SP versus DP and SP calibrated from the PCs were computed as measures of the best-case BCG-BP association in each subject.

Second, the association at the intervention level was investigated. In each rest-intervention pair in a subject (R1-CP, R2-MA, R3-SB, R4-BH), the ranges of reference DP and SP were likewise segmented into 1 mmHg bins, and the PCs associated with each DP and SP bins were computed from the set of median values of the BCG features recruited in the PCs corresponding to each bin. Then, these PCs were calibrated to the reference DP and SP by determining η_k^X (k=0,…,N) in the relationship (1) with least-squares fitting to yield a subject-specific calibration relationship pertaining to the rest-intervention pair under investigation. Then, correlation coefficients, RMSEs, and MAEs between the reference DP and SP versus DP and SP calibrated from the PCs were computed as measures of the best-case BCG-BP association in each intervention.

To investigate the number of requisite PCs for robust association of wrist BCG to BP, the above analysis was repeated for one to four PCs included in the calibration relationship (1), i.e., N=1, 2, 3, and 4. Significance of the difference in the association between reference versus calibrated DP and SP with respect to different N (specifically, N=1 versus N=2, N=2 versus N=3, and N=3 versus N=4) was assessed using the paired t-test with Bonferroni correction. The difference was deemed statistically significant if $p<0.016$.

Third, for the analysis with N=3 (the number of requisite PCs to achieve adequate association to both DP and SP; see Results), the association was investigated with all the calibration coefficients except two η_k^X (k=0,…,N) were regularized to constant values. This analysis was motivated by the practical consideration on the feasibility of building the calibration relationship with the conventional 2-point calibration method[2] (in which typically one slope coefficient and the intercept parameter in the calibration relationship are determined from the PCs-BP pairs obtained during rest and a BP-perturbing intervention). For this investigation, the PCs were calibrated to the reference DP and SP by determining just two η_k^X (which are associated with the largest coefficient of variations under subject-specific calibration) in (1) with least-squares fitting while the rest of the coefficients were fixed to respective mean values to yield a regularized (i.e., partially subject-specific) calibration relationship. Then, correlation coefficients, RMSEs, and MAEs between the reference DP and SP versus DP and SP calibrated from the regularized subject-specific calibration relationship were computed as measures of the practical BCG-BP association in each subject.

5.3. Results

Table 5.1 shows the wrist BCG features chosen by the feature selection. Fig. 5.2 and Fig. 5.3 show an example of subject-level and intervention-level associations between the

wrist BCG versus DP and SP in all subjects, in terms of correlation between reference versus calibrated DP and SP, when three most significant PCs are recruited for analysis. Fig. 5.4 shows the dependence of the degree of association between the wrist BCG and BP on the number of PCs recruited for analysis. Fig. 5.5 shows the composition of the four most significant PCs associated with DP and SP.

Table 5.1: Wrist BCG features for DP and SP selected by feature selection (stepwise linear regression). X_w-Y_w denotes timing between X_w and Y_w waves. $|X_w$-$Y_w|$ denotes the amplitude between X_w and Y_w waves.

	1	2	3	4	5	6	7	8	9	10	11	12
DP	J_w-J_w	G_w-H_w	H_w-I_w	I_w-J_w	$\|G_w$-$I_w\|$	$\|G_w$-$J_w\|$	$\|H_w$-$J_w\|$					
SP	J_w-J_w	G_w-H_w	H_w-I_w	H_w-J_w	H_w-K_w	I_w-J_w	I_w-L_w	$\|G_w$-$I_w\|$	$\|H_w$-$J_w\|$	$\|I_w$-$K_w\|$	$\|J_w\|$	$\|K_w\|$

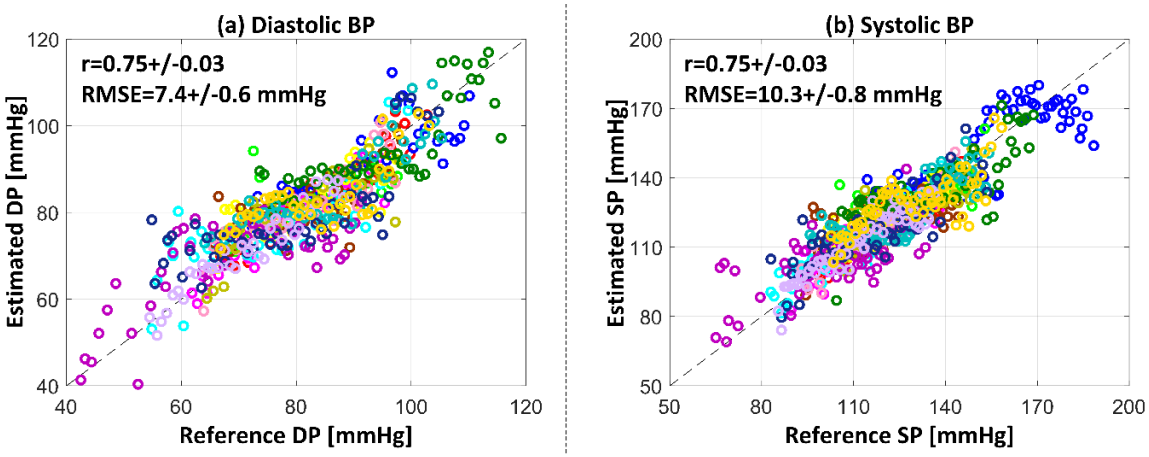

Fig. 5.2 Subject-level association between the wrist BCG versus diastolic (DP) and systolic (SP) pressures in all subjects. (A) DP. (b) SP.

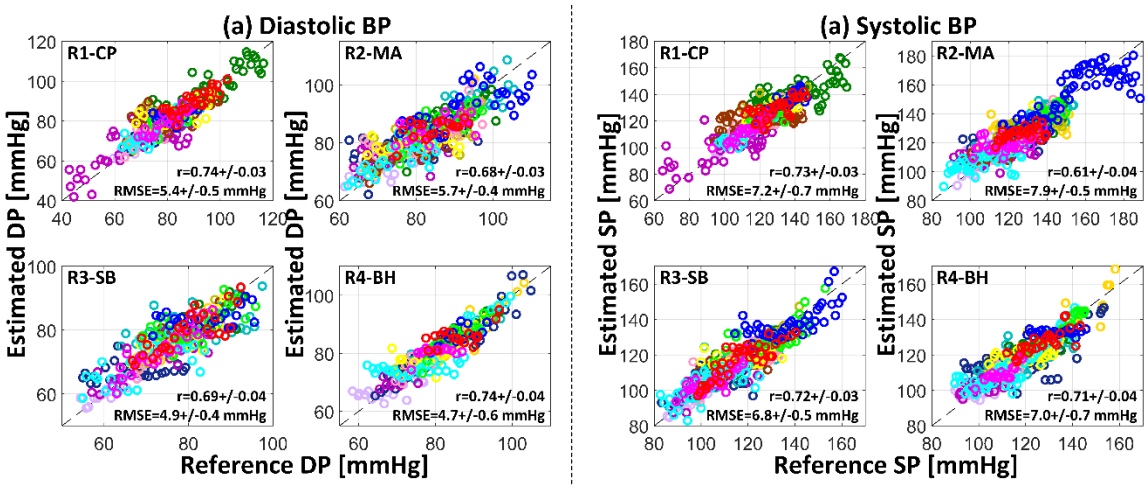

Fig. 5.3. Intervention-level association between the wrist BCG versus diastolic (DP) and systolic (SP) pressures in all subjects. (A) DP. (b) SP.

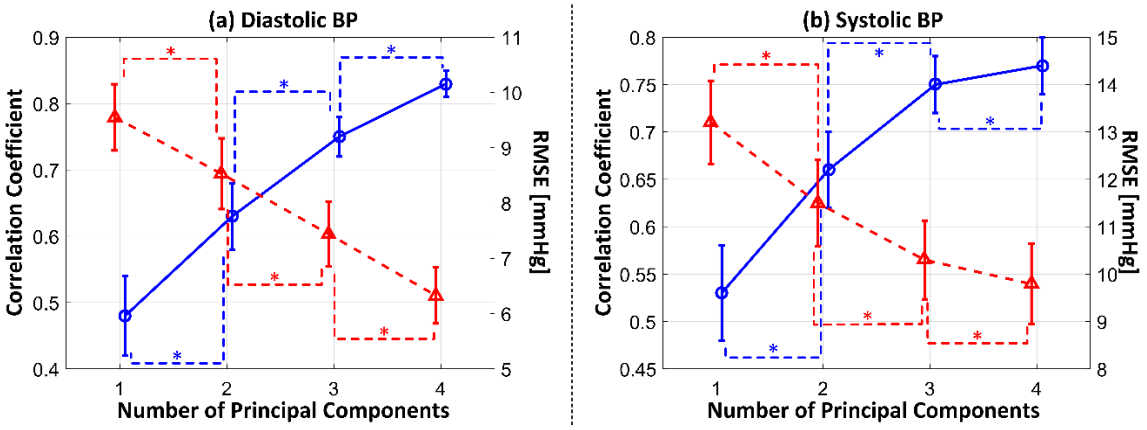

Fig. 5.4. The degree of association between the wrist BCG and BP with respect to the number of principal components (PCs) (mean+/-SE). *: p<0.016.

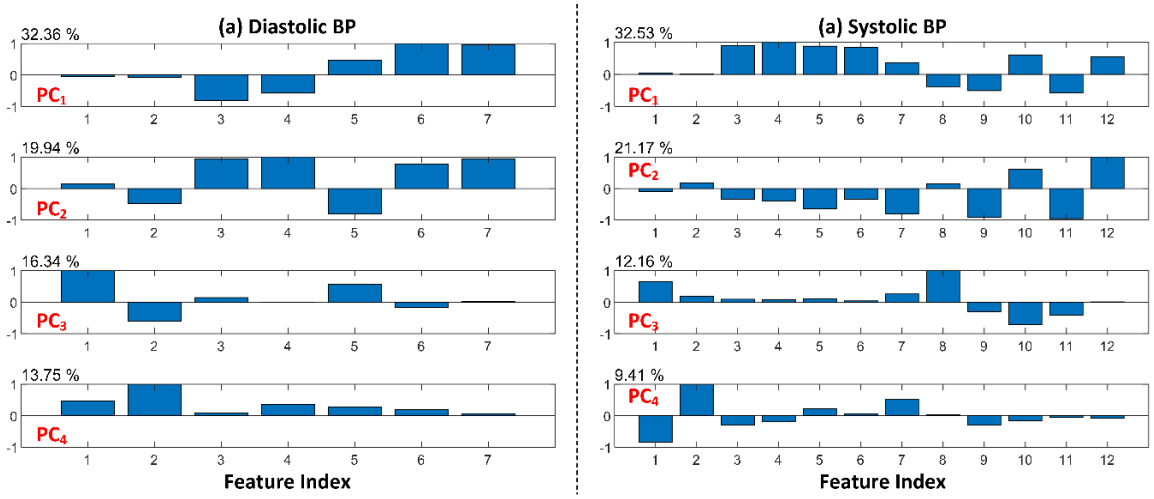

Fig. 5.5 Four most significant principal components (PCs) derived for (A) diastolic (DP) and (B) systolic (SP) pressures. See Table 3 for feature index.

5.4. Discussion

The objective of this chapter was to probe the feasibility of ultra-convenient BP monitoring based on a limb BCG by investigating the association between the morphological features in a limb BCG at the wrist and BP based on data mining. Of particular interests were overall subject-level association between the limb BCG and BP, variability in the association under a number of distinct BP-perturbation mechanisms, and practical considerations for realization of BP monitoring technologies based on a limb BCG.

5.4.1. Experimental Data

The interventions employed in this study widely varied both DP and SP. On the average, the maximum BP changes of >15 mmHg in DP and >25 mmHg in SP were achieved by each intervention (except SB which still modestly decreased DP and SP but not as widely as the other interventions), which added up to yield the overall maximum DP and SP changes of >30 mmHg and >45 mmHg at the subject level. Considering that the interventions employed in this study are known to effectively perturb BP through distinct changes in various cardiovascular parameters (including heart rate, stroke volume, and total peripheral resistance): (1) CP is known to increase BP via an increase in heart rate and total peripheral resistance, often despite a decrease in stroke volume and cardiac output[77]–[83]; (2) MA is known to increase BP via an increase in heart rate and total peripheral resistance (often along with a resulting increase in cardiac output)[77], [81]–[83]; (3) SB is

known to modestly decrease BP via a decrease in heart rate[84]–[89]; and (4) BH is known to increase BP via an increase in total peripheral resistance despite a decrease in heart rate, stroke volume, and cardiac output[90], [91], the experimental data used in this study has provided a quite challenging test for associating limb BCG and BP with wide-ranging BP ranges and physiological perturbation mechanisms.

5.4.2. Association between Limb BCG and Blood Pressure

The wrist BCG-based predictors exhibited meaningful associations with reference DP and SP at both subject level and intervention level. When three most significant predictors were used for DP and SP, correlation coefficient of r=0.75+/-0.03 (DP) and r=0.75+/-0.03 (SP), RMSE of 7.4+/-0.6 mmHg (DP) and 10.3+/-0.8 mmHg (SP), and MAE of 6.0+/-0.5 mmHg (DP) and 8.3+/-0.7 mmHg (SP) were obtained across all interventions (mean+/-SE). In addition, the association was consistent in all the individual interventions regardless of diverse physiological mechanisms invoked to perturb BP (on the average, $r \geq 0.68$, RMSE≤5.7 mmHg, and MAE≤4.5 mmHg for DP as well as $r \geq 0.61$, RMSE≤7.9 mmHg, and MAE≤6.4 mmHg for SP; note that $r \geq 0.71$ except for R2-MA (Fig. 5.3)). Hence, morphological features in the wrist BCG waveform may be equipped with valuable information contents for BP monitoring. In fact, this finding may not be surprising in that (1) the whole-body BCG is closely associated with aortic BP[70] and that (2) limb BCGs, including the wrist BCG, are elicited by the transmission of the whole-body BCG through compliant musculoskeletal elements in the body, although exact physical mechanism of this transmission is yet to be elucidated.

The three most significant PCs were responsible for 32%, 20%, and 16% of the total variance observed in the selected features corresponding to DP, and 33%, 21%, and 12% of the total variance observed in the selected features corresponding to SP. The degree of association between the wrist BCG versus DP and SP with respect to the number of PCs recruited for analysis (i.e., N in the calibration relationship (1); Fig. 5.4) shows that at least three most significant PCs may need to be employed for robust association of the wrist BCG features to BP. Overall, increasing N from 1 to 4 yielded statistically significant improvement in both correlation coefficient and RMSE. But, the degree of improvement tapered off as N increased. For DP, increasing N from 1 to 2, 2 to 3, and 3 to 4 resulted in 30%, 19% and 12% increase in correlation coefficient, while the reduction in RMSE was quite linear (11%, 13% and 15%). For SP, increasing N from 1 to 2, 2 to 3, and 3 to 4 resulted in 26%, 13%, and 4% increase in correlation coefficient as well as 13%, 11%, and 5% reduction in RMSE. Hence, it may be concluded that the use of one or two PCs for BP

monitoring may suffer from limited performance, while the use of more than four PCs may suffer from lack of robustness (e.g., by inducing overfitting).

The need for multiple requisite PCs to enable accurate and robust association of the wrist BCG to BP raises practical issues related to subject-specific calibration (i.e., how can the coefficients η_k^X (k=0,…,N) in (1) be realistically determined with minimal intervention?). The results obtained from regularized calibration suggest that the wrist BCG-based PCs derived in this study may still serve as viable predictors of BP even in conjunction with conventional 2-point calibration procedure. For example, across all subjects, correlation coefficients of r=0.63+/-0.05 and r=0.60+/-0.05, RMSEs of 9.3+/-0.8 mmHg and 14.7+/-1.4 mmHg, and MAEs of 7.6+/-0.7 mmHg and 11.9+/-1.1 mmHg were obtained between reference versus calibrated DP and SP, respectively, when three most significant predictors were used. These results may be regarded as an adequate association considering the challenging nature of the experimental data used in this study, although the results were relatively (and naturally) worse than the results from fully subject-specific calibration (Fig. 5.4).

Lastly, further scrutiny of the derived PCs indicates that monitoring of DP and SP may require independent and distinct predictors. Indeed, the composition of the PCs in Fig. 5.5 shows that significant PCs associated with DP and SP are largely different from each other. Most prior work on cuff-less BP monitoring, including both PTT-based techniques[2], [42]–[44] and techniques based on a single pulse waveform[45]–[47], tend to rely on the identical predictor(s) to infer both DP and SP. However, it is well known that SP depends not only on the arterial pressure-volume relationship (which dictates PWV) but also on cardiac functions (e.g., myocardial contractility determining pulse pressure). Hence, the results from this chapter provides us with an important insight: that independent and distinct predictors may indeed be needed to achieve superb association with both DP and SP, and that data mining may facilitate the selection of such effective predictors.

5.5. Conclusion

The morphological features in a limb BCG are associated with BP, offering promise for ultra-convenient BP monitoring based on a limb BCG alone. Future work must focus on (1) examining the generalizability of the findings from this chapter, (2) investigating alternative data-based approaches to further improve the efficacy of the limb BCG for predicting BP, and (3) understanding the physical basis of limb BCG in relation to BP and its fusion with data mining.

6. Hybrid Model Using BCG-Based PTT and PWA for Cuff-Less BP Monitoring

6.1. Introduction

Given the findings of the previous sections, it is illustrated that both PTT, and PWA features contain valuable information that can be used to estimate the blood pressure. The developed models in each of the two previous chapters, only utilize one source of the information which is either BCG-Based PTT or PWA features. In this section, the idea of combining the data from both sources is implemented. In this regard, three different analyses are practiced using the data from human subject study explained in section 4.2, and their results are reported. The first analysis is purely based on the machine learning techniques. In the second and third analyses, some physics based insights are utilized to define the predictors in addition to the machine learning methods.

6.2. Method

In the first analysis, pure machine learning approach is followed. In this regard, 38 features are utilized, from which 37 features are extracted from the BCG-based PWA and one more feature is the PTT, which is defined as the time interval between wrist J-peak and green PPG foot. From the 38 candidate features thus extracted, we selected significant features associated with PP, DP and SP based on the stepwise linear regression analysis as follows. First, the range of PP (or DP, SP) in each subject record was segmented into 1 mmHg bins, and the set of 38 median BCG feature values corresponding to each 1mmHg PP (or DP, SP) bin was computed. Then, the pair of PP (or DP, SP) and the computed median BCG feature values associated with each subject was merged across all 23 subjects (note that the dimension of the PP (or DP, SP) pair is determined by the range of PP (or DP, SP)) and applied to the stepwise linear regression analysis to determine significant features predictive of PP (or DP, SP).

Due to the large number of significant features selected from the stepwise linear regression analysis, the features were further compressed using the principal component analysis (PCA) for dimensionality reduction. Specifically, the range of PP (or DP, SP) in each subject record was again segmented into 1 mmHg bins, and the set of median values of the features selected above with the stepwise linear regression corresponding to each bin was computed. Then, the pair of PP (or DP, SP) and the corresponding median feature values associated with each subject was merged across all 23 subjects. The features were

normalized with the respective feature's mean and standard deviation, and subsequently applied to the PCA to derive principal components (PCs) as predictors of PP (or DP, SP).

The association between the created PCs and BP was investigated using multivariate linear regression analysis. Specifically, the PCs predictive of PP, DP and SP were correlated with the reference PP, DP and SP, respectively, via the following calibration relationship:

$$P_X = \eta_0^X + \eta_1^X \phi_1^X + \cdots + \eta_N^X \phi_N^X \quad (1)$$

where P_X is reference BP, ϕ_k^X (k=1,…,N) the k-th PC, η_k^X (k=1,…,N) the calibration coefficient for the k-th PC, η_0^X the intercept, and N the total number of PCs included in the relationship (1) ($X = P$ for PP, $X = D$ for DP and $X = S$ for SP). Then, the association between the PCs derived from the selected features and BP was analyzed in terms of three metrics: (1) correlation coefficient (r); (2) root-mean-squared error (RMSE); and (3) mean absolute error (MAE).

Having the population level predictors as described above, the association at the subject level was investigated. In each subject, the ranges of reference PP, DP and SP across all BP-perturbing interventions were segmented into 1 mmHg bins, and the PCs associated with each PP, DP and SP bins were computed from the set of median values of the selected features recruited in the PCs corresponding to each bin. Then, these PCs were calibrated to the reference PP, DP and SP by determining η_k^X (k=0,…,N) in the relationship (1) with least-squares fitting to yield a subject-specific calibration relationship. Then, correlation coefficients, RMSEs, and MAEs between the reference PP, DP and SP versus PP, DP and SP calibrated from the PCs were computed as measures of the best-case BCG-BP association in each subject.

To investigate the number of requisite PCs for robust association of the features to BP, the above analysis was repeated for one to four PCs included in the calibration relationship (1), i.e., N=1, 2, 3, and 4.

In the second type of analysis, a similar approach to the analysis #1 is followed, with one major difference. In this analysis, for the multivariate regression model, PTT is always selected to be one of the predictors, since it is known to be correlated with pulse wave velocity, which is directly correlated with the blood pressure, as discussed in previous chapters. Then, like as the analysis #1, we utilized the 37 features extracted from BCG-based PWA to create the second, third, and forth population level predictors. In sum 4 BP predictors are created, which are PTT and 3 PCs derived from BCG, and like as the analysis #1, these predictors are utilized to create and calibrate the subject level regression models.

In the third analysis, we add some more physics-based insights, using the developed model in chapter 3, to select and create the population level predictors. Like as the analysis #2, we force PTT to be one of the population level predictors. Then, to create the next predictors, we only use three BCG-based features, despite to analysis #2 that has used 37 features. The rational to select the three BCG-based features is as follow. Based on the illustrated results in Fig. 3.5, J-K interval is the most sensitive timing feature, and J-K (or J) amplitude is the most sensitive amplitude feature in the BCG signal in response to the BP perturbations. In addition to that, our analysis show that J-J timing, which could be interpreted as the heart period, is another strong predictor of blood pressure. Based on these insights, three BCG-based features are selected, and then PCA is applied to create the three PCs. Having 4 population level predictors, the rest of the procedure is like as the Analysis #2 or #1. The predictors are utilized to create and calibrate the subject level regression models and results are reported in the next section.

6.3. Results

Table 6.1 shows the utilized features in analysis #1 and #2 and the corresponding index number for each feature. Similarly, Table 6.2 illustrate the physics-based selected features utilized in analysis #3, and corresponding index numbers.

Fig. 6.1, Fig. 6.2, and Fig. 6.3 show the set of features chosen by the feature selection step, as well as the constructed PCs to predict SP, DP and PP in analysis #1, respectively. Fig. 6.4, Fig. 6.5 and Fig. 6.6 show the set of utilized features to predict SP, DP, and PP in Analysis #2. In these figures, PTT is the first independent predictor, as well as 3 other predictors constructed from BCG features by using of the feature selection and PCA analysis. Fig. 6.7 presents the set of utilized features to predict SP, DP, and PP in Analysis #3. In this figure, PTT is the first independent variable, and 3 other predictors are derived by applying PCA method on the three BCG-based features, selected using physics-based insights.

Table 6.3 summarizes the correlation, RMSE, and MAE between reference BP versus BP calibrated from wrist PTT and BCG-based PWA features in all participants.

Fig. 6.8, Fig. 6.9, Fig. 6.10 illustrate subject-level association between the estimated and measured SP, DP and PP in analysis #1, when 1, 2, 3, and 4 independent variables are recruited for modeling. In these figures, the data points for each subject are plotted with distinct colors. In the same way, Fig. 6.11, Fig. 6.12, Fig. 6.13 illustrate subject-level

association between the estimated and measured SP, DP and PP in analysis #2. Similar to the previous cases, Fig. 6.14, Fig. 6.15, Fig. 6.16 show the same information for analysis #3.

Fig. 6.17 summarizes the correlation coefficients for 1, 2, 3, and 4 variable models utilized in analyses #1, #2, #3 to predict PP, DP and SP. This figure is provided to facilitate the analyze of the data in Table 6.3 (a) by visualizing them.

Table 6.1. PTT and Wrist BCG features derived by pulse wave analysis, and corresponding index numbers used in analysis #1 and #2.

Index No	1	2	3	4	5	6	7	8	9	10	11	12	13	14	15	16	17
Timing Feature	PTT	J-J	G-H	G-I	G-J	G-K	G-L	H-I	H-J	H-K	H-L	I-J	I-K	I-L	J-K	J-L	K-L
Index No	18	19	20	21	22	23	24	25	26	27	28	29	30	31	32	33	34
Amplitude Feature	|G|	|G-H|	|G-I|	|G-J|	|G-K|	|G-L|	|H|	|H-I|	|H-J|	|H-K|	|H-L|	|I|	|I-J|	|I-K|	|I-L|	|J|	|J-K|
Index No	35	36	37	38													
Amplitude Feature	|J-L|	|K|	|K-L|	|L|													

Table 6.2. PTT and selected Wrist BCG features derived by pulse wave analysis and selected using physics-based insights, and corresponding index number used in analysis #3.

Index No	1	2	3	4
Selected Feature	PTT	J-J	|J-K|	|J-K|

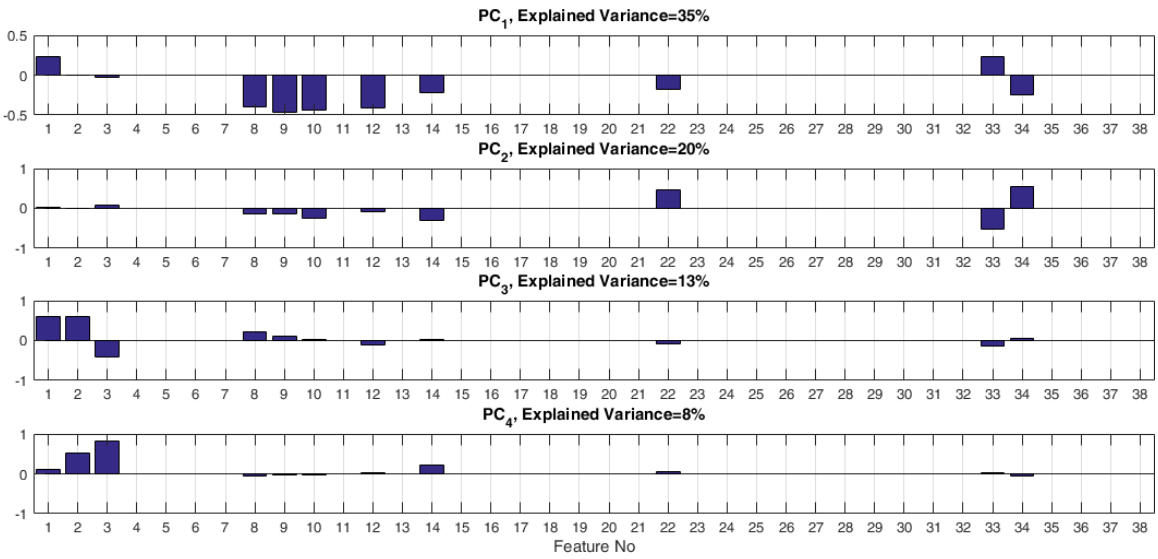

Fig. 6.1. Four most significant principal components (PCs) derived as independent predictors for systolic pressures estimation in Analysis #1. See Table 6.1 for feature index.

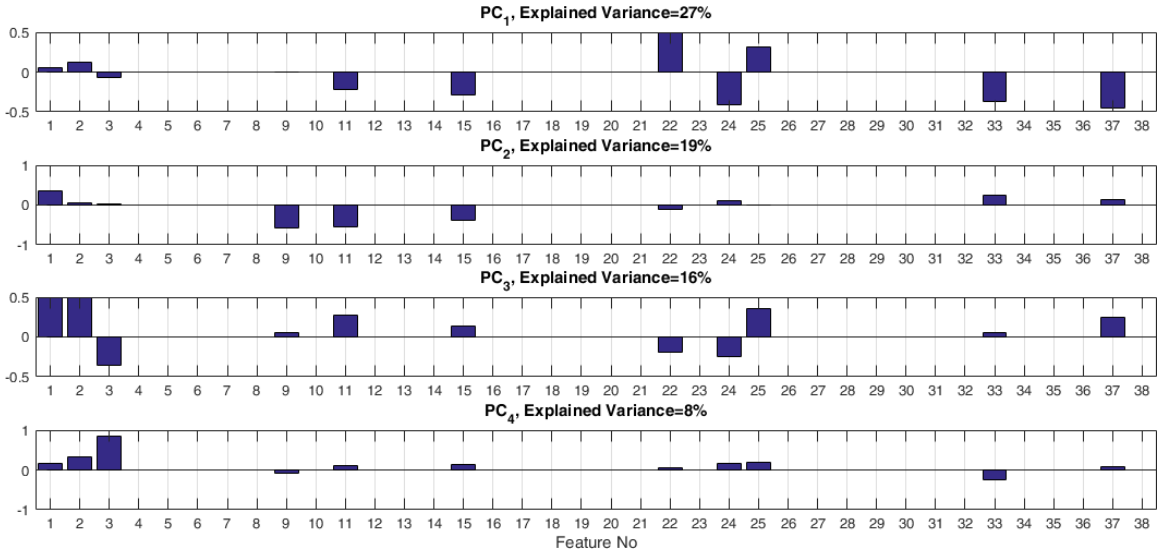

Fig. 6.2. Four most significant principal components (PCs) derived as independent predictors for diastolic pressures estimation in Analysis #1. See Table 6.1 for feature index.

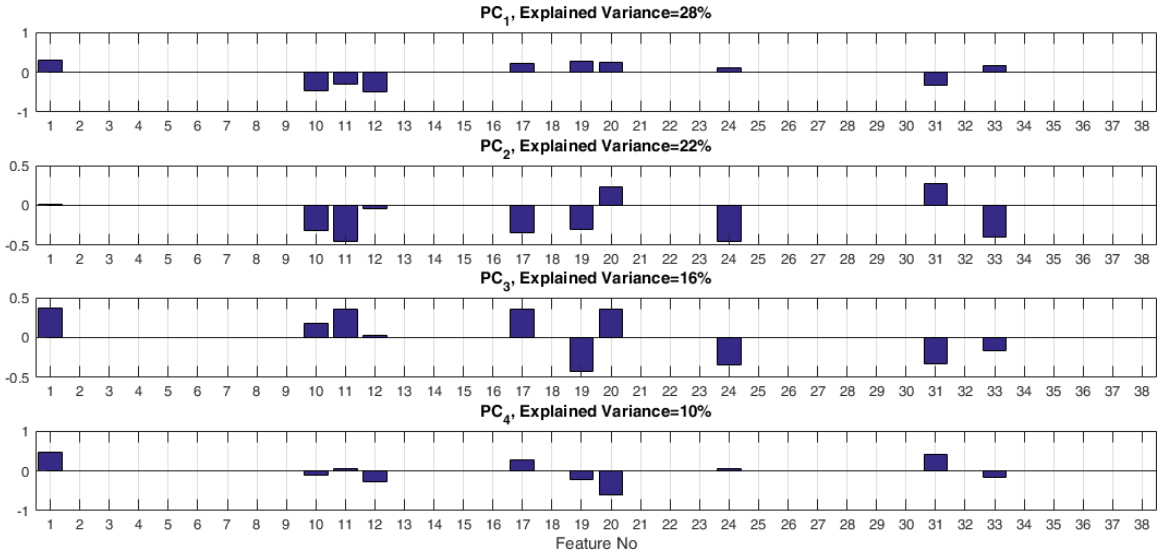

Fig. 6.3. Four most significant principal components (PCs) derived as independent predictors for pulse pressures estimation in Analysis #1. See Table 6.1 for feature index.

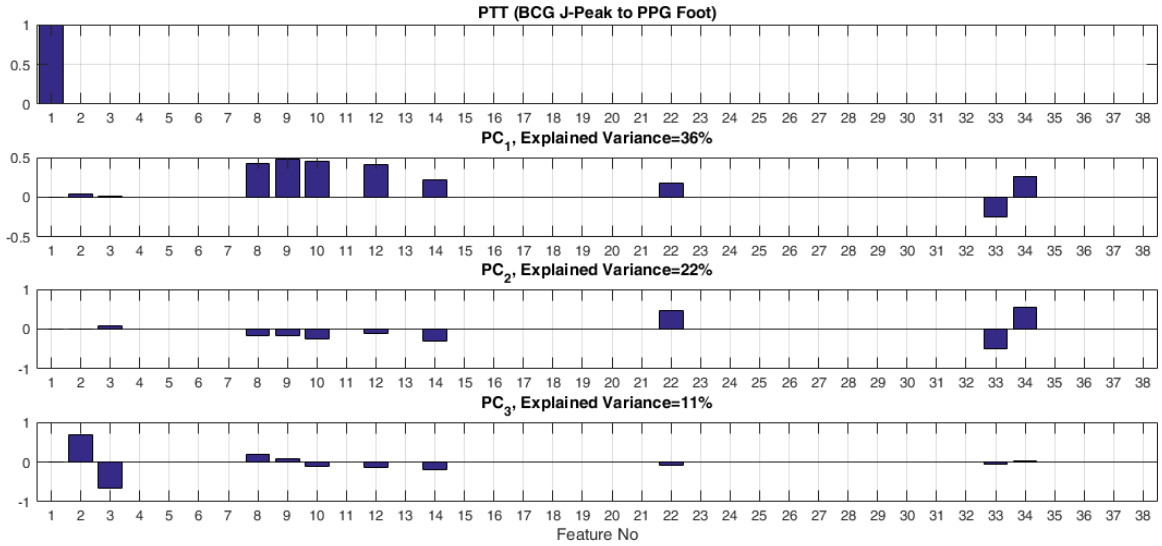

Fig. 6.4. PTT and three most significant principal components (PCs) derived as independent predictors for systolic pressures estimation in Analysis #2. See Table 6.1 for feature index.

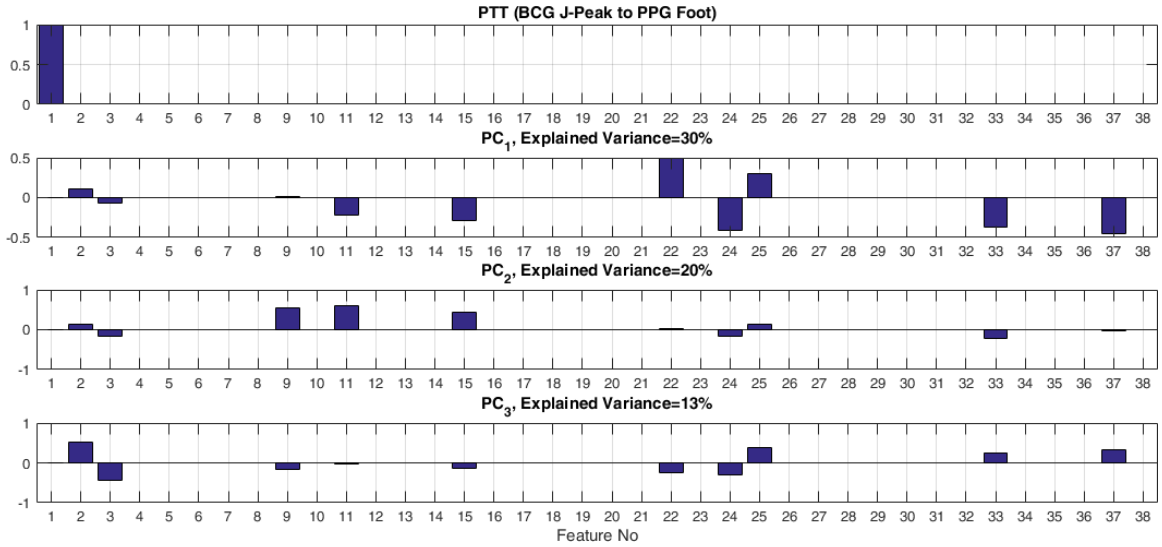

Fig. 6.5. PTT and three most significant principal components (PCs) derived as independent predictors for diastolic pressures estimation in Analysis #2. See Table 6.1 for feature index.

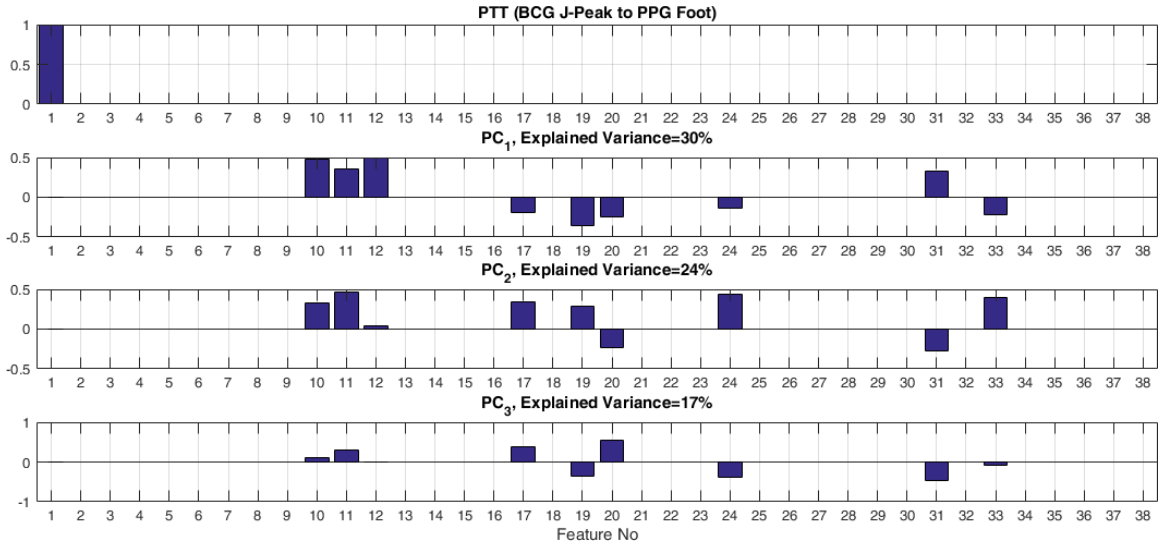

Fig. 6.6. PTT and three most significant principal components (PCs) derived as independent predictors for pulse pressures estimation in Analysis #2. See Table 6.1 for feature index.

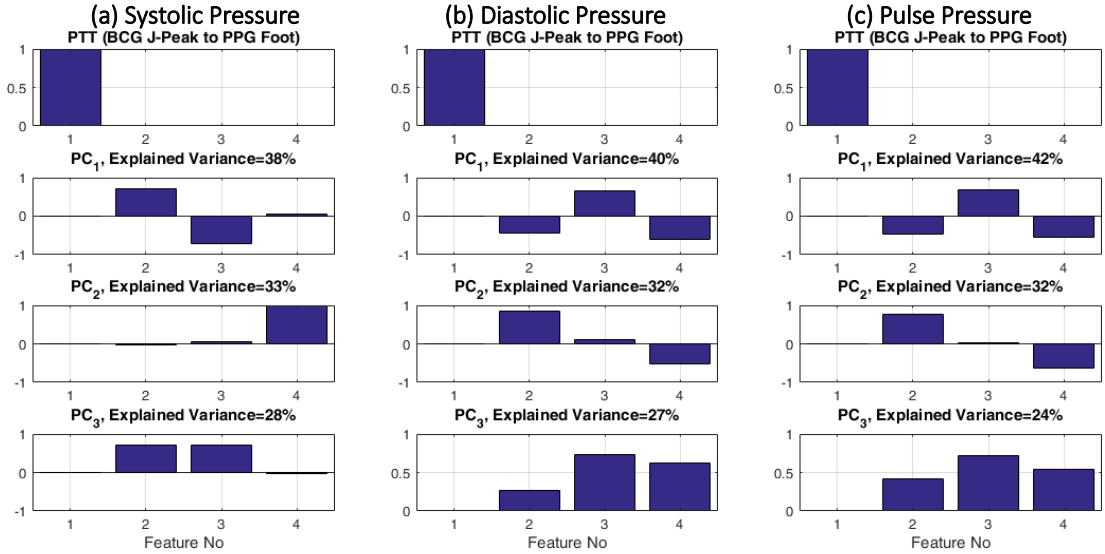

Fig. 6.7. PTT and three principal components (PCs) derived as independent predictors for pulse pressures estimation in Analysis #3. See Table 6.2 for feature index.

Table 6.3. Correlation, root-mean-squared error (RMSE), mean absolute error (MAE), and precision error (PE) between reference BP versus BP calibrated from constructed predictors. PP: pulse pressure DP: diastolic BP. SP: systolic BP.

(a) Correlation

	# of Independent Variables	Analysis #1	Analysis #2	Analysis #3
SP	1	0.50+/-0.07	0.72+/-0.06	0.72+/-0.06
	2	0.66+/-0.06	0.8+/-0.04	0.78+/-0.05
	3	0.75+/-0.04	0.83+/-0.04	0.81+/-0.04
	4	0.79+/-0.03	0.84+/-0.04	0.86+/-0.03
DP	1	0.44+/-0.06	0.72+/-0.07	0.72+/-0.07
	2	0.71+/-0.05	0.77+/-0.06	0.81+/-0.05
	3	0.8+/-0.04	0.84+/-0.04	0.87+/-0.03
	4	0.87+/-0.03	0.87+/-0.03	0.89+/-0.03
PP	1	0.52+/-0.07	0.66+/-0.06	0.66+/-0.06
	2	0.64+/-0.06	0.8+/-0.03	0.76+/-0.05
	3	0.77+/-0.04	0.84+/-0.03	0.82+/-0.04
	4	0.81+/-0.03	0.86+/-0.03	0.88+/-0.03

(b) RMSE (mmHG)

	# of Independent Variables	Analysis #1	Analysis #2	Analysis #3
SP	1	12.7+/-1.22	9.82+/-1.37	9.87+/-1.37
	2	11.09+/-1.25	8.65+/-1.23	9.02+/-1.33
	3	9.97+/-1.18	7.99+/-1.22	8.48+/-1.29
	4	9.11+/-1.07	7.72+/-1.2	7.66+/-1.02
DP	1	9.53+/-0.65	6.73+/-0.91	6.73+/-0.91
	2	7.12+/-0.85	6.21+/-0.89	5.84+/-0.82
	3	6.11+/-0.75	5.29+/-0.75	4.92+/-0.7
	4	5.14+/-0.62	4.88+/-0.7	4.57+/-0.68
PP	1	6.42+/-0.57	5.71+/-0.72	5.62+/-0.72
	2	5.85+/-0.56	4.56+/-0.55	4.9+/-0.71
	3	4.92+/-0.5	4.23+/-0.55	4.17+/-0.66
	4	4.56+/-0.49	3.96+/-0.54	3.58+/-0.6

(c) MAE (mmHG)

	# of Independent Variables	Analysis #1	Analysis #2	Analysis #3
SP	1	10.31+/-1.03	7.87+/-1.13	7.89+/-1.14
	2	8.8+/-1.04	6.87+/-1.01	7.2+/-1.12
	3	7.85+/-0.94	6.32+/-0.98	6.71+/-1.07
	4	7.16+/-0.81	6.13+/-0.97	6.02+/-0.83
DP	1	7.88+/-0.54	5.44+/-0.76	5.44+/-0.76
	2	5.75+/-0.71	4.98+/-0.74	4.71+/-0.68
	3	4.88+/-0.62	4.13+/-0.59	3.89+/-0.54
	4	4.03+/-0.48	3.82+/-0.55	3.57+/-0.52
PP	1	5.25+/-0.5	4.55+/-0.62	4.5+/-0.62
	2	4.64+/-0.5	3.58+/-0.45	3.88+/-0.57
	3	3.85+/-0.43	3.32+/-0.46	3.32+/-0.53
	4	3.61+/-0.41	3.14+/-0.45	2.81+/-0.46

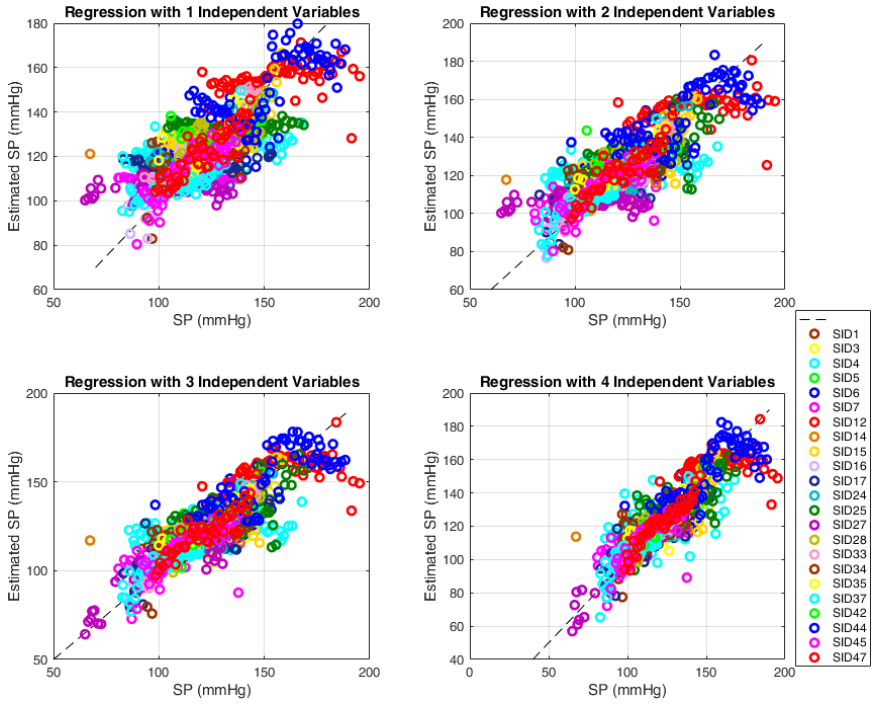

Fig. 6.8. Subject-level association between the estimated systolic pressure in analysis #1 (with 3 and 4 variable regression models) versus measured systolic pressures in all subjects.

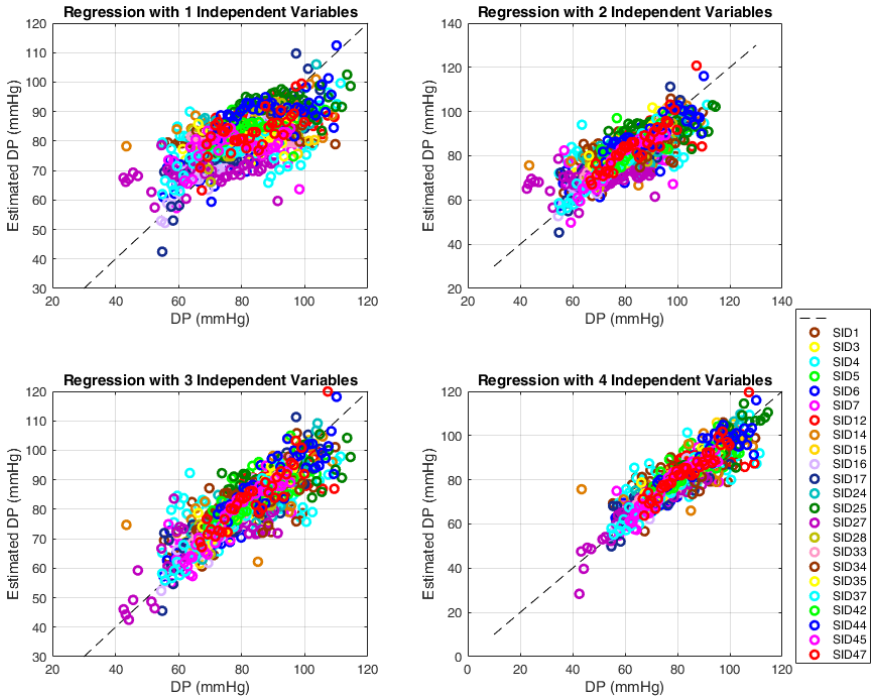

Fig. 6.9. Subject-level association between the estimated diastolic pressure in analysis #1 (with 3 and 4 variable regression models) versus measured diastolic pressures in all subjects.

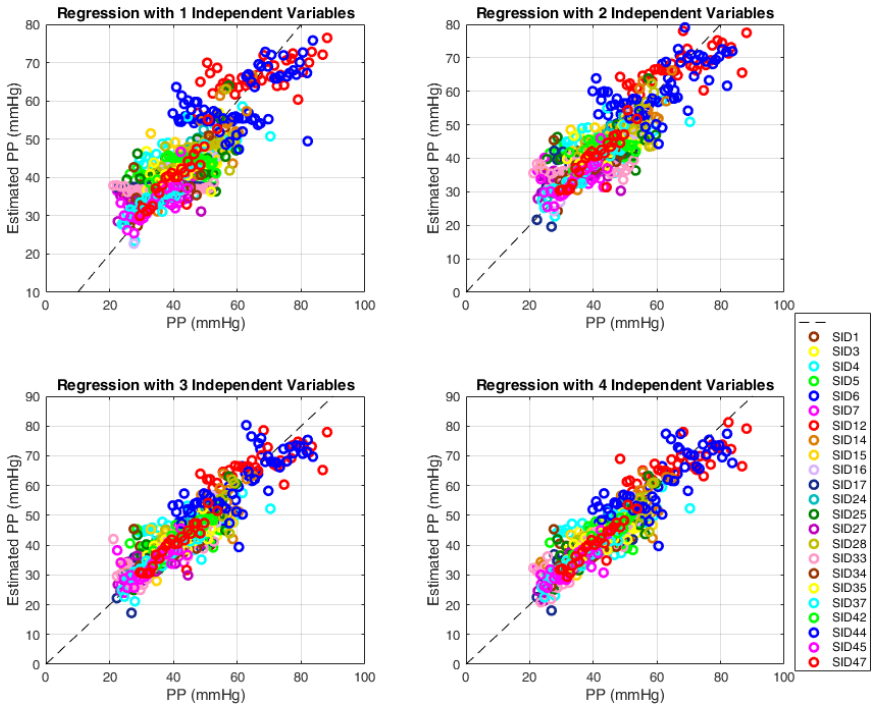

Fig. 6.10. Subject-level association between the estimated pulse pressure in analysis #1 (with 3 and 4 variable regression models) versus measured pulse pressures in all subjects.

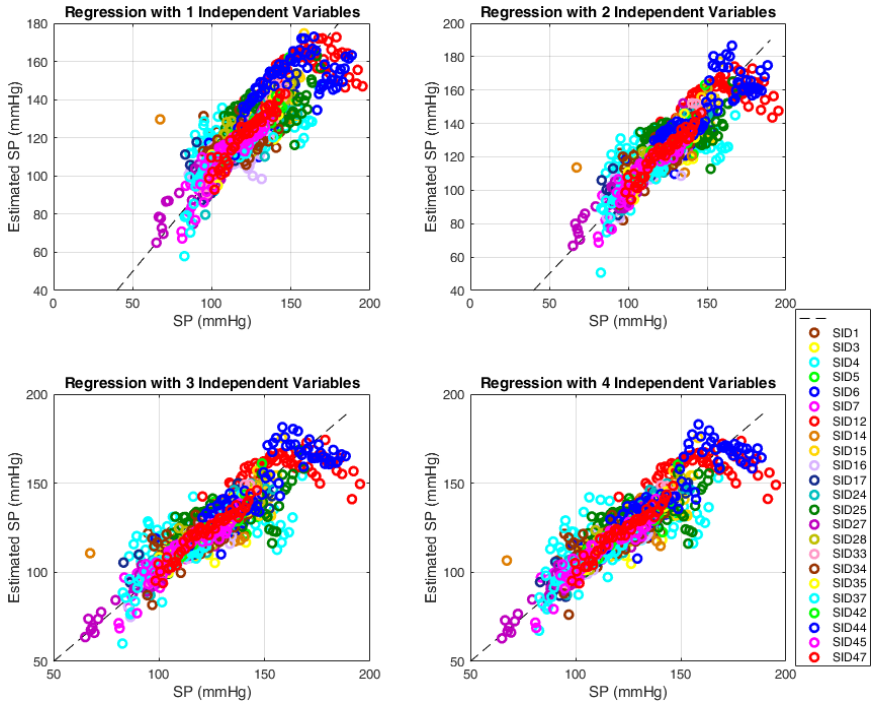

Fig. 6.11. Subject-level association between the estimated systolic pressure in analysis #2 (with 3 and 4 variable regression models) versus measured systolic pressures in all subjects.

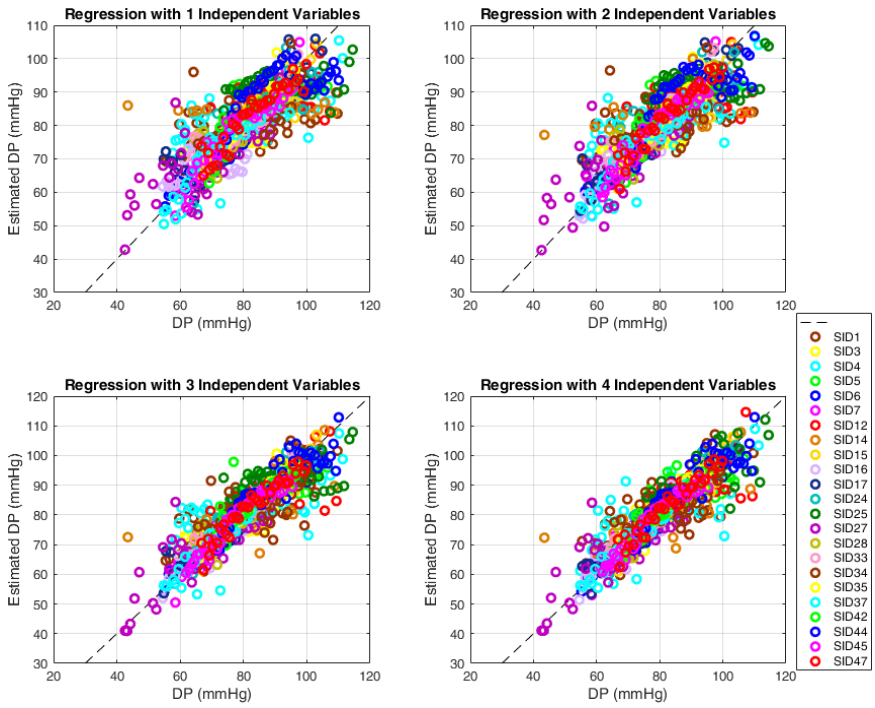

Fig. 6.12. Subject-level association between the estimated diastolic pressure in analysis #2 (with 3 and 4 variable regression models) versus measured diastolic pressures in all subjects.

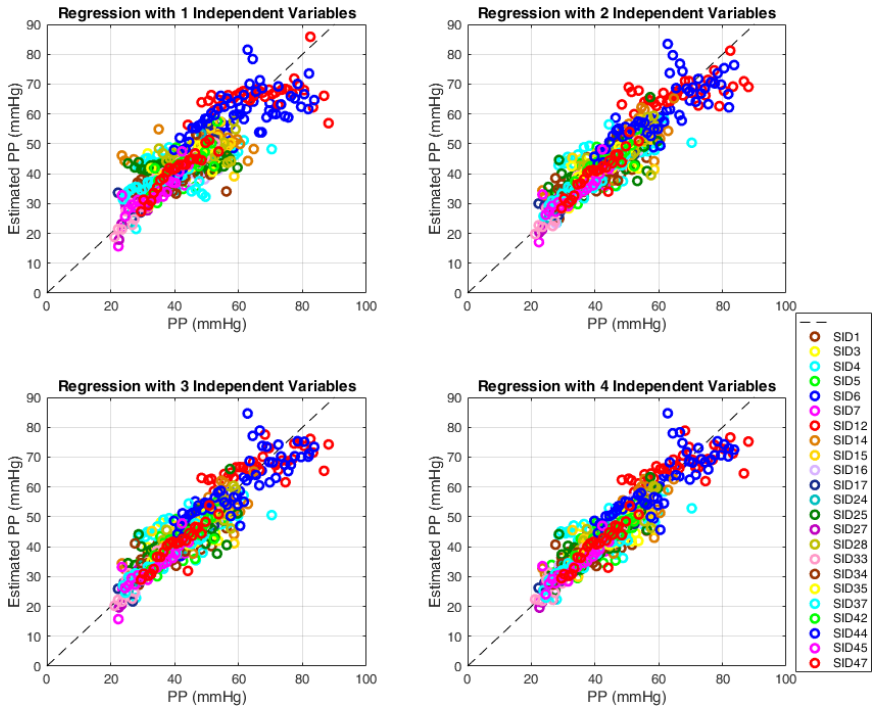

Fig. 6.13. Subject-level association between the estimated pulse pressure in analysis #2 (with 3 and 4 variable regression models) versus measured pulse pressures in all subjects.

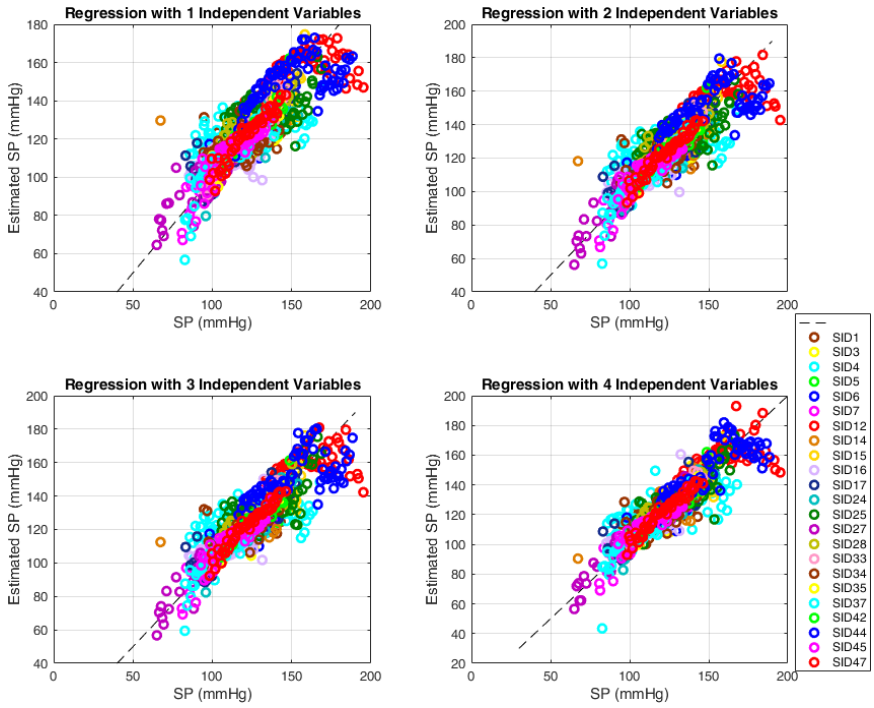

Fig. 6.14. Subject-level association between the estimated systolic pressure in analysis #3 (with 3 and 4 variable regression models) versus measured systolic pressures in all subjects.

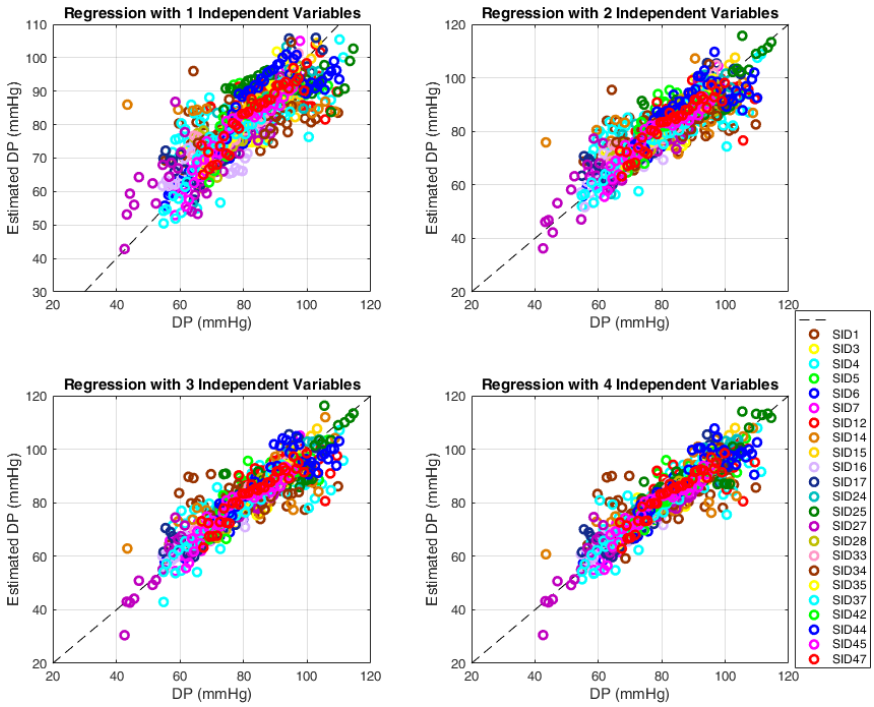

Fig. 6.15. Subject-level association between the estimated diastolic pressure in analysis #3 (with 3 and 4 variable regression models) versus measured diastolic pressures in all subjects.

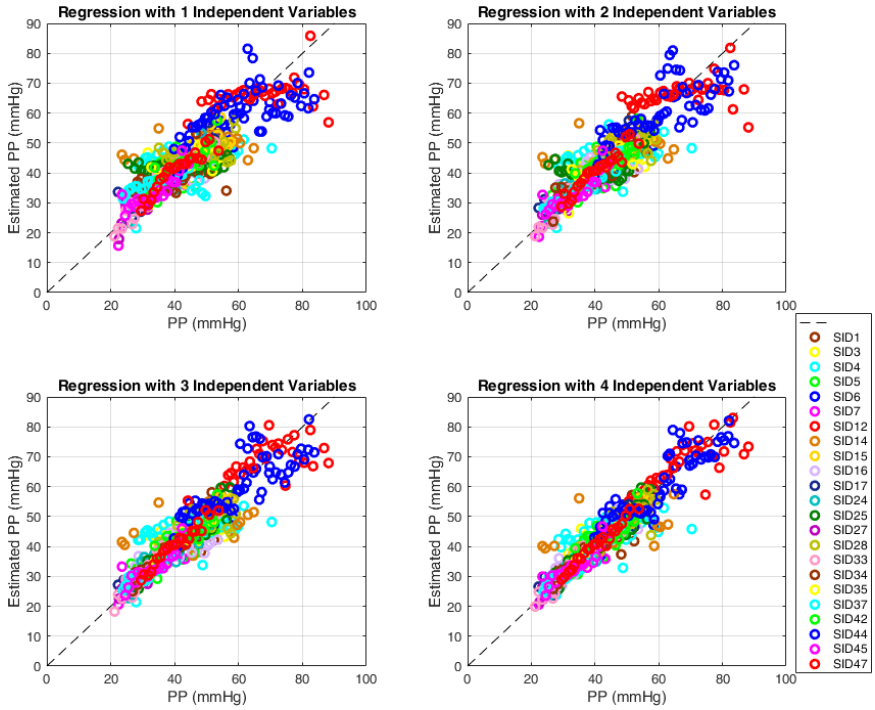

Fig. 6.16. Subject-level association between the estimated pulse pressure in analysis #3 (with 3 and 4 variable regression models) versus measured pulse pressures in all subjects.

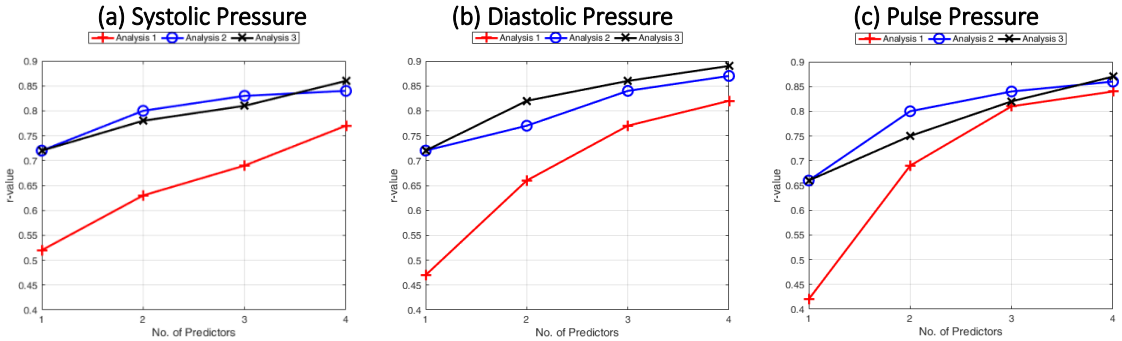

Fig. 6.17. Correlation coefficients for different types of analysis to estimate (a) systolic, (b) diastolic, (c) pulse pressure with respect to the number of the predictors in multivariate regression model.

6.4. Discussion

Comparing the results of analysis #1, with analyses #2 and #3 shows that pure machine learning is not completely successful in building the best estimation model. Fig. 6.17 clearly illustrates that correlation coefficients for all of the models in analysis #1, in which both feature selection and compression are done with machine learning techniques, are lower than either analysis #2 or #3, in which physics-based insights are mixed with the machine learning techniques. One of the important reasons that pure machine learning approach

doesn't work as good as the other two approaches could be the limited number of subjects. It is possible that by increasing the number of subjects and data, the results from analysis #1 could improve.

Results of the analysis #3 (or similarly analysis #2), shows that adding BCG specific features to the PTT helps to improve the accuracy of the BP estimation. More specifically in the analysis #3, when PTT is used as the only predictor (look at first predictor at Fig. 6.4, Fig. 6.5, Fig. 6.6) for PP, DP and SP estimation, correlation coefficient of r= 0.66+/-0.06 (PP), r= 0.72+/-0.07 (DP) and r= 0.72+/-0.06 (SP), RMSE of 5.71+/-0.72 mmHg (PP), 6.73+/-0.91 mmHg (DP) and 9.82+/-1.37 mmHg (SP), and MAE of 4.55+/-0.62 mmHg (PP), 5.44+/-0.76 mmHg (DP) and 7.87+/-1.13 mmHg (SP) were obtained across all interventions (mean+/-SE) according to Table 6.3. By adding more predictors, obtained from BCG signal, and constructing 4 variable regression model for PP, DP and SP estimation, correlation coefficient of r= 0.88+/-0.03 (PP), r= 0.89+/-0.03 (DP) and r= 0.86+/-0.03 (SP), RMSE of 3.58+/-0.6 mmHg (PP), 4.57+/-0.68 mmHg (DP) and 7.66+/-1.02 mmHg (SP), and MAE of 2.81+/-0.46 mmHg (PP), 3.57+/-0.52 mmHg (DP) and 6.02+/-0.83 mmHg (SP) were obtained across all interventions (mean+/-SE). This reads to improvement of correlation coefficient by 32%, 24% and 18%, RMSE by 36%, 32% and 22%, and MAE by 38%, 34% and 24% for PP, DP and SP, respectively.

By comparing the results from analysis #2 and #3, it is reasonable to assume that the analysis #3, which only utilizes 4 features selected by physics-based insights, has similar performance to the analysis #2, which uses 38 features. Reducing the number of the utilized features, without degrading the performance is favorable in the sense that it can facilitate the technological implementation of the algorithm, as the model with less features will need less data for calibration. Additionally, such a model is expected to be more generalizable, and robust when exposed to a new set of subjects.

As another interesting observation from analysis #3, from Fig. 6.7 we observe that DP and PP models utilizes very similar PCs. This means that with the given set of features using the physics-based insights, we can achieve a models that works best for both PP and DP prediction. Since SP can be calculated as the sum of the PP and DP, we can finally argue that with the illustrated set of features and PCs, we can estimate all BP variables. This support the previous argument that by narrowing down the number of the features we can develop generalizable models that works for a broad spectrum of the subjects and BP features. It worth to mention that, the reason of selecting different PCs for SP, is related to the binning of data. Because of the binning process in this analysis, SP data set does not exactly match with the sum of the DP and PP, and it results in different PCs.

6.5. Conclusion

In previous chapters we have illustrated that BCG-based PTT is a strong predictor of the BP. Additionally, in chapter 5 we demonstrated that BCG-based features derived from PWA, carry useful information regarding BP. In this chapter we illustrated that we can create more complicated models with higher accuracy by adding BCG-based PWA features on top of the PTT. Presented results show that a 4 variable model that uses PTT as one of the predictors, and BCG features as the other predictors could enhance the correlation coefficient by 32%, 24% and 18%, RMSE by 36%, 32% and 22%, and MAE by 38%, 34% and 24% for PP, DP and SP estimation, respectively.

In this chapter, we also discussed that with a limited number of subjects, pure machine learning based approaches may not be effective to achieve high performing predictive models. However, we can leverage physics-based and combine them with machine learning approaches to achieve strong BP predicting models. Moreover, reduced number of features seems promising to create a generic and robust model that can be used to estimate all of the BP variables, i.e. PP, DP, and SP. It can be highly useful in facilitating technological implementation of the cuff-less BP monitoring techniques in future.

7. Subject Specific Modeling for Cuff-Less BP Monitoring

7.1. Introduction

In the previous sections, we tried to develop population-level models by creating common features and PCs for the whole subjects within the population. The advantages of such a model is that it is more convenient for technological implementation, as it needs less data points to construct and calibrate the model. On the other hand, we need to include a large variety of the subjects, maybe thousands if not tens of thousands, in the database as one of the key requirements of creating such a model that works on a variety of subjects. In this sense, population-level models derived from the data of a limited number of subjects, may not show the full potential of the BCG-based approaches, due to the lack of enough data to create the best performing model. In this chapter, to get an idea about the full BP prediction potential of the wrist BCG and PPG signals, we have developed subject specific models. With such a model, the complete process of feature selection, feature compression, and regression model development is done on each subject separately. So, each subject could have different selected features, PCs, and regression model. With this approach, subject variation effects on the performance of the model is avoided by creating individual predictors for each subject.

Motivated by the above rational, three kinds of analysis are accomplished using the available data from the human subject study explained in section 4.2. In the first analysis, we attempt to show the ultimate association of the limb BCG with BP, by leveraging subject specific models. We will only use the features obtained from BCG pulse wave analysis, and develop a prediction models solely based on the BCG signal for the subject. With the second and third analysis, the idea of combining the data from BCG and BCG-based PTT is examined, with two different feature selection approaches.

7.2. Method

For each subject, the data is divided into the train and test sets. Out of the nine intervention that each subject has went through, the first and last rest interventions (R1 and R5) are selected as the test data, and the remained seven interventions (CP, R2, MA, R3, SB, R4, BH) are selected for training purpose. As mentioned above, three sets of analyses are developed in this section. The first analysis only uses BCG features. The second and third analyses are utilizing both PTT and BCG-based features. The difference between analysis #2 and #3 is on the feature selection process. More details are explained as follow.

In the first analysis (analysis #1), we only utilize 37 features BCG-based features. From the 37 candidate features thus extracted, we selected significant features associated with PP, DP and SP based on the stepwise linear regression analysis for each subject as follows. First, the range of PP (or DP, SP) at training interventions (CP, R2, MA, R3, SB, R4, BH) in each subject record was segmented into 1 mmHg bins, and the set of 37 median BCG feature values corresponding to each 1mmHg PP (or DP, SP) bin was computed. Then, applied the stepwise linear regression analysis to determine significant features predictive of PP (or DP, SP) for the subject.

Due to the large number of significant features selected from the stepwise linear regression analysis, the features were further compressed for each subject using the principal component analysis (PCA) for dimensionality reduction. Specifically, the range of PP (or DP, SP) at training intervention (CP, R2, MA, R3, SB, R4, BH) in each subject record was again segmented into 1 mmHg bins, and the set of median values of the features selected above with the stepwise linear regression corresponding to each bin was computed. Then, the features were normalized with the respective feature's mean and standard deviation, and subsequently applied to the PCA to derive principal components (PCs) as predictors of PP (or DP, SP).

The association between the created PCs for each subject and BP was investigated using multivariate linear regression analysis. Specifically, the PCs predictive of PP, DP and SP were correlated with the reference PP, DP and SP, respectively, via the following calibration relationship:

$$P_X = \eta_0^X + \eta_1^X \phi_1^X + \cdots + \eta_N^X \phi_N^X \quad (1)$$

where P_X is reference BP, ϕ_k^X (k=1,…,N) the k-th PC, η_k^X (k=1,…,N) the calibration coefficient for the k-th PC, η_0^X the intercept, and N the total number of PCs included in the relationship (1) ($X = P$ for PP, $X = D$ for DP and $X = S$ for SP). Then, the association between the PCs derived from the selected features and BP was analyzed in terms of three metrics: (1) correlation coefficient (r); (2) root-mean-squared error (RMSE); and (3) mean absolute error (MAE).

Having the subject specific level predictors constructed using the training data as described above, the association at the subject level was investigated. In each subject, the ranges of reference PP, DP and SP across all training interventions (CP, R2, MA, R3, SB, R4, BH) were segmented into 1 mmHg bins, and the PCs associated with each PP, DP and SP bins were computed from the set of median values of the selected features recruited in the PCs corresponding to each bin. Then, these PCs were calibrated to the reference PP,

DP and SP by determining η_k^X (k=0,…,N) in the relationship (1) with least-squares fitting to yield a subject-specific calibration relationship. Then, correlation coefficients, RMSEs, and MAEs between the reference PP, DP and SP versus PP, DP and SP calibrated from the PCs were computed as measures of the best-case BCG-BP association for the training data in each subject.

To investigate the number of requisite PCs for robust association of the features to BP, the above analysis was repeated for one to four PCs included in the calibration relationship (1), i.e., N=1, 2, 3, and 4.

After creating the predictive model for each individual, using subject specific features, PCs, and regression coefficients, the validity of the model is measured on the test data. As mentioned before, the test data is derived from the first and last interventions as follow. In each subject, the ranges of reference PP, DP and SP across the test interventions (R1, R5) were segmented into 1 mmHg bins, and the PCs associated with each PP, DP and SP bins were computed from the set of median values of the selected features recruited in the PCs corresponding to each bin. Then, correlation coefficients, RMSEs, and MAEs between the reference PP, DP and SP versus PP, DP and SP predicted from the model were computed as measures of the BCG-BP association for the test data in each subject.

Next step is to do analysis #2, in which the idea of combining PTT and BCG based features to achieve high performance models is implemented. In the analysis #1, we only utilized BCG specific features. In analysis #2, in addition to the BCG features, we utilize the BCG-based pulse transit time that is defined from the J-peak to PPG foot, which is already illustrated as a strong predictor of the BP. In this approach, the multi variate regression models with 1, 2, 3, and 4 predictors are constructed as follow. PTT is set to be as one of the independent variables. Then we use BCG based PCs calculated in analysis #1, as the second, third, and forth predictors. As an example, for the regression model with 3 variables, PTT is the first variable, PC_1 is the second variable, and PC_2 is the third variable. Note that PC_1, PC_2, and PC_3 in this analysis are purely calculated using BCG based features.

In analysis #3, again the idea of combining PTT and BCG features to achieve high performance BP predictive models is implemented, with a different method. In this analysis, first we create a feature pool with 38 features, in which 37 of them are BCG based features and the other one is PTT. Then the remaining steps in this method is exactly like as the analysis #1. Having 38 features, first BP binning is practiced for the training interventions. Then stepwise feature selection is used to decrease the number of features. Then PCA is applied to construct 4 most important PCs for each subject. Then the

regression models with 1, 2, 3, and 4 predictors are calculated for each subject. Afterward the model is used to calculate the correlation coefficients, RMSE, and MAE for the training and test data.

7.3. Results

Table 7.1 shows the utilized features in analysis #1, as well as the corresponding index number. Similarly Table 7.2 illustrates the features utilized in analyses #2 and #3, and corresponding index numbers.

Fig. 7.1, Fig. 7.2, and Fig. 7.3 show the features chosen by the stepwise feature selection, as well as the constructed PCs to predict SP, DP and PP for each subject in analysis #1, respectively. In these figures, each row corresponds to the constructed PCs for one of the subjects. Likely Fig. 7.4, Fig. 7.5, and Fig. 7.6 show the selected features and calculated PCs for each subject in analysis #2. As mentioned before, in this analysis PTT is chosen as the first independent predictor, as well as 3 other predictors constructed from BCG features by using of the feature selection and PCA analysis to predict SP, DP, and PP. Similarly, Fig. 7.7, Fig. 7.8, and Fig. 7.9 illustrates the selected features and calculated PCs for analysis #3.

Table 7.3 summarizes the correlation, RMSE, and MAE between reference BP versus BP calibrated from the developed models in all analysis #1, #2, and #3.

Fig. 7.10, Fig. 7.11, and Fig. 7.12 illustrate the subject-level association between the estimated and measured SP, DP and PP in analysis #1, for both train and test data using 1, 2, 3, and 4 variable models in analysis #1. In these figures, the data points for each subject are plotted with distinct colors. In the same way, Fig. 7.13, Fig. 7.14, and Fig. 7.15 illustrate the estimated vs measured values in analysis #2. Similar to the previous cases, Fig. 7.16, Fig. 7.17, and Fig. 7.18 show the same information for analysis #3.

Fig. 7.19 show the correlation coefficients for 1, 2, 3, and 4 variable models utilized in analyses #1 to predict PP, DP and SP. This figure is provided to facilitate the perception of the data presented in Table 7.3, to evaluate the performance of the developed models. In the same way, Fig. 7.20 and Fig. 7.21 are provided to show the similar information for analysis #2 and #3 respectively.

Table 7.1. Wrist BCG features derived by pulse wave analysis, and corresponding index numbers used in analysis #1.

Index No	1	2	3	4	5	6	7	8	9	10	11	12	13	14	15	16	17
Timing Feature	J-J	G-H	G-I	G-J	G-K	G-L	H-I	H-J	H-K	H-L	I-J	I-K	I-L	J-K	J-L	K-L	|G|
Index No	18	19	20	21	22	23	24	25	26	27	28	29	30	31	32	33	34
Amplitude Feature	|G-H|	|G-I|	|G-J|	|G-K|	|G-L|	|H|	|H-I|	|H-J|	|H-K|	|H-L|	|I|	|I-J|	|I-K|	|I-L|	|J|	|J-K|	|J-L|
Index No	35	36	37														
Amplitude Feature	|K|	|K-L|	|L|														

Table 7.2. PTT and Wrist BCG features derived by pulse wave analysis, and corresponding index numbers used in analysis #2 and #3.

Index No	1	2	3	4	5	6	7	8	9	10	11	12	13	14	15	16	17
Timing Feature	PTT	J-J	G-H	G-I	G-J	G-K	G-L	H-I	H-J	H-K	H-L	I-J	I-K	I-L	J-K	J-L	K-L
Index No	18	19	20	21	22	23	24	25	26	27	28	29	30	31	32	33	34
Amplitude Feature	|G|	|G-H|	|G-I|	|G-J|	|G-K|	|G-L|	|H|	|H-I|	|H-J|	|H-K|	|H-L|	|I|	|I-J|	|I-K|	|I-L|	|J|	|J-K|
Index No	35	36	37	38													
Amplitude Feature	|J-L|	|K|	|K-L|	|L|														

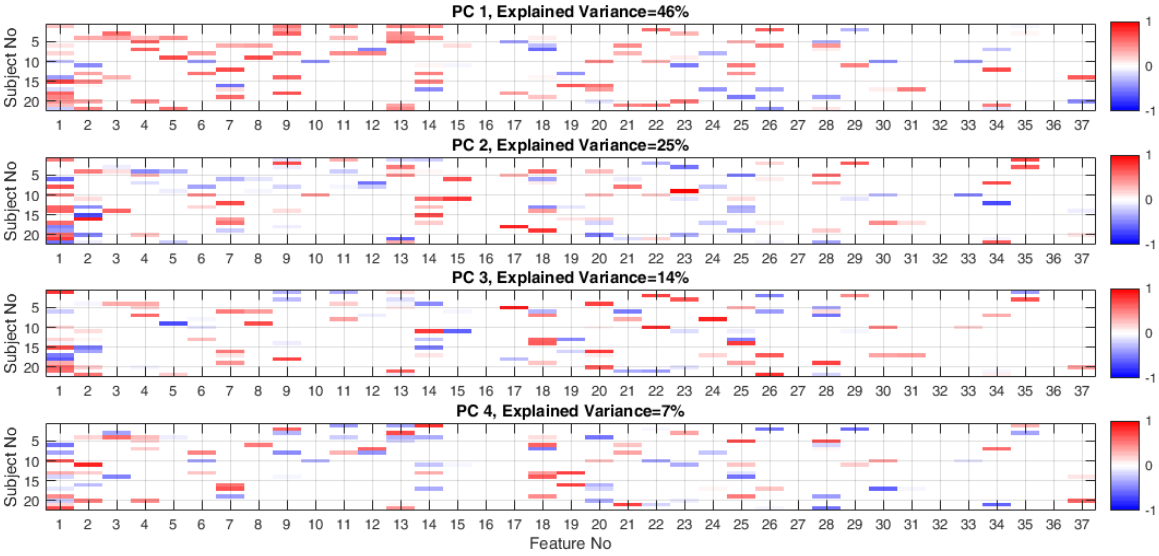

Fig. 7.1. Four most significant principal components (PCs) derived as independent predictors for subject specific systolic pressures estimation in Analysis #1. Table 7.1 for feature index.

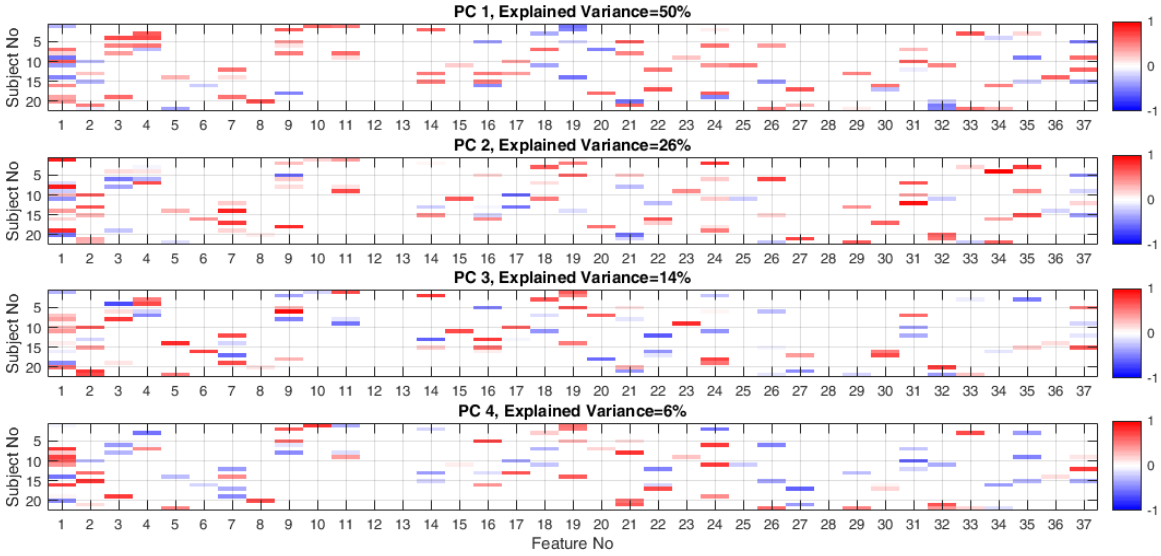

Fig. 7.2. Four most significant principal components (PCs) derived as independent predictors for subject specific diastolic pressures estimation in Analysis #1. See Table 7.1 for feature index.

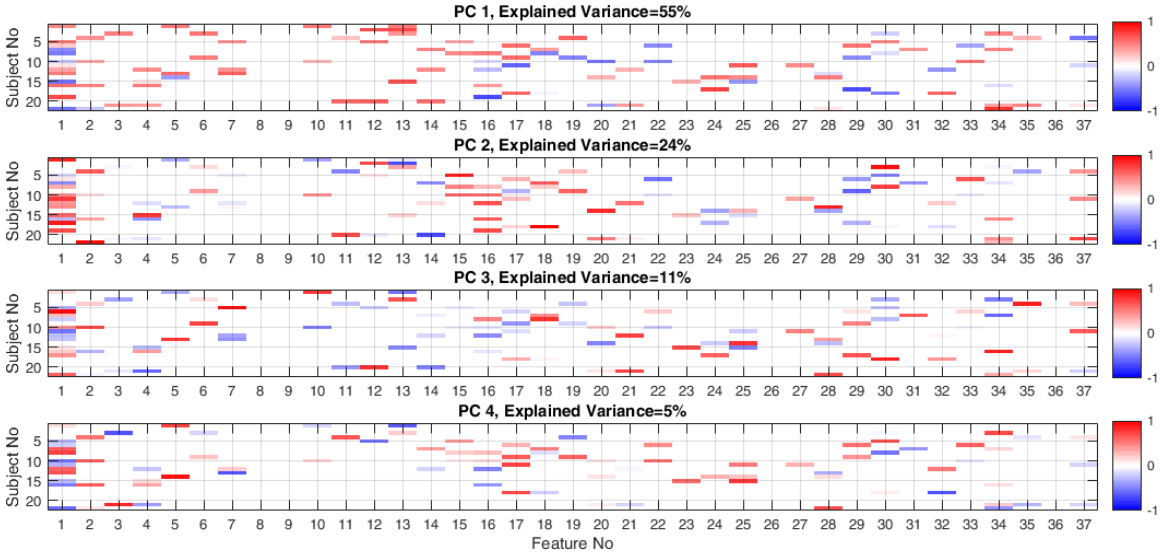

Fig. 7.3. Four most significant principal components (PCs) derived as independent predictors for subject specific pulse pressures estimation in Analysis #1. Table 7.1 for feature index.

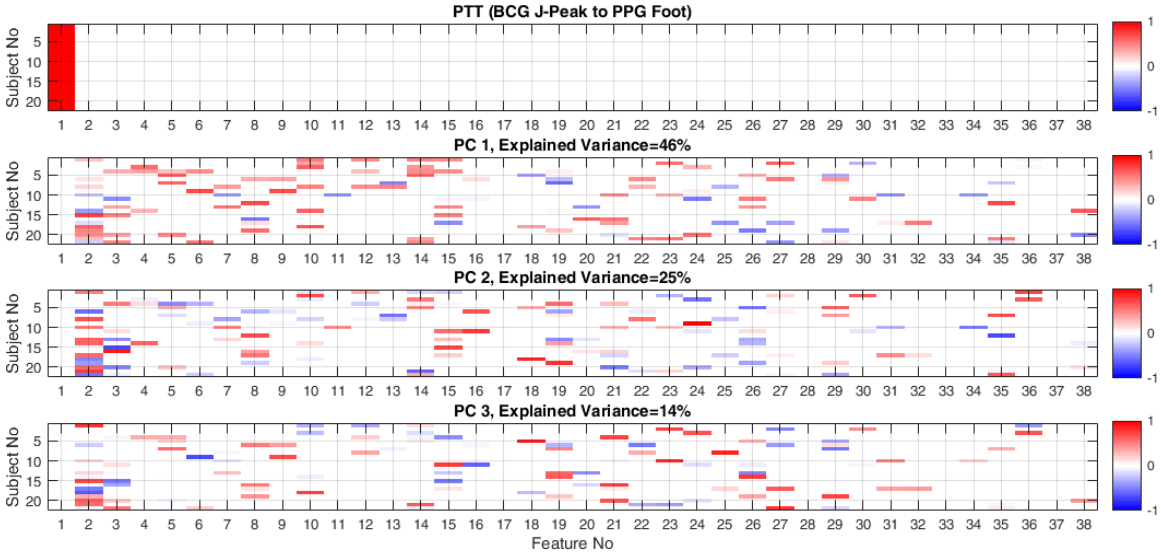

Fig. 7.4. PTT and three most significant principal components (PCs) derived as predictors for subject specific systolic pressures estimation in Analysis #2. See Table 7.2 for feature index.

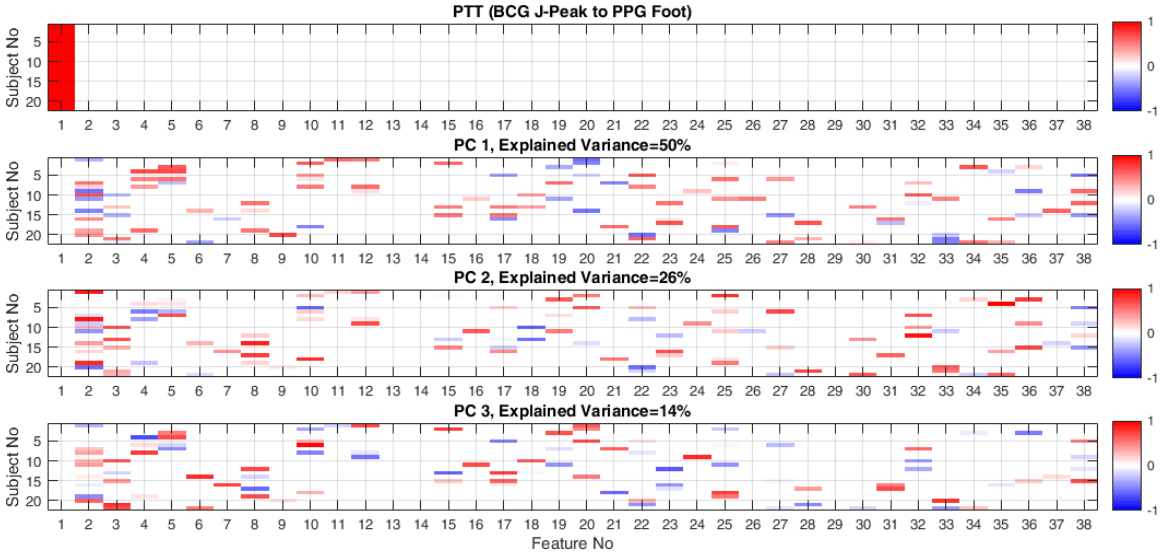

Fig. 7.5. PTT and three most significant principal components (PCs) derived as predictors for subject specific diastolic pressures estimation in Analysis #2. See Table 7.2 for feature index.

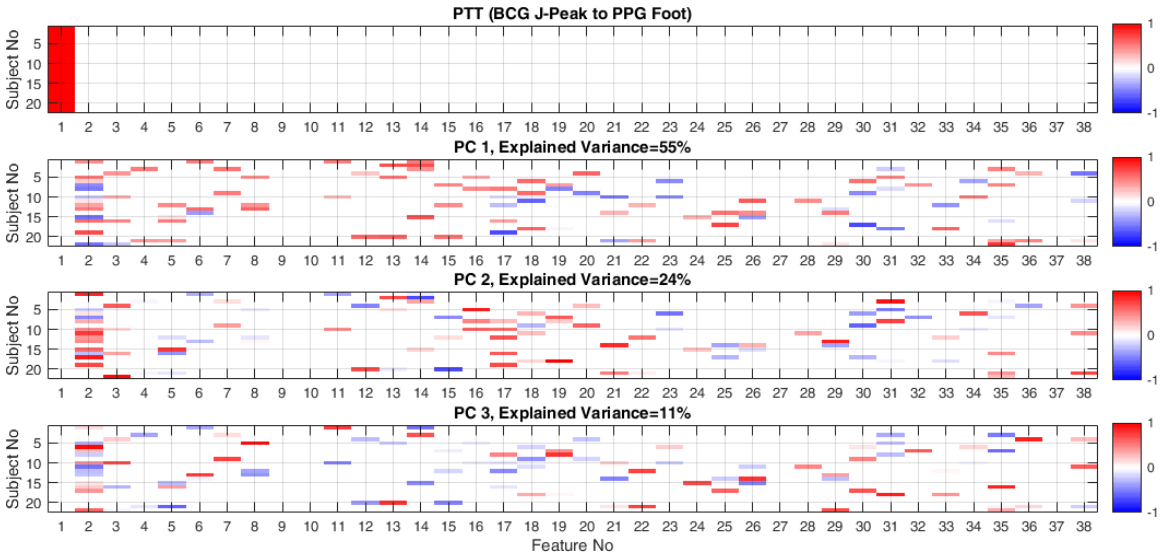

Fig. 7.6. PTT and three most significant principal components (PCs) derived as predictors for subject specific pulse pressures estimation in Analysis #2. See Table 7.2 for feature index.

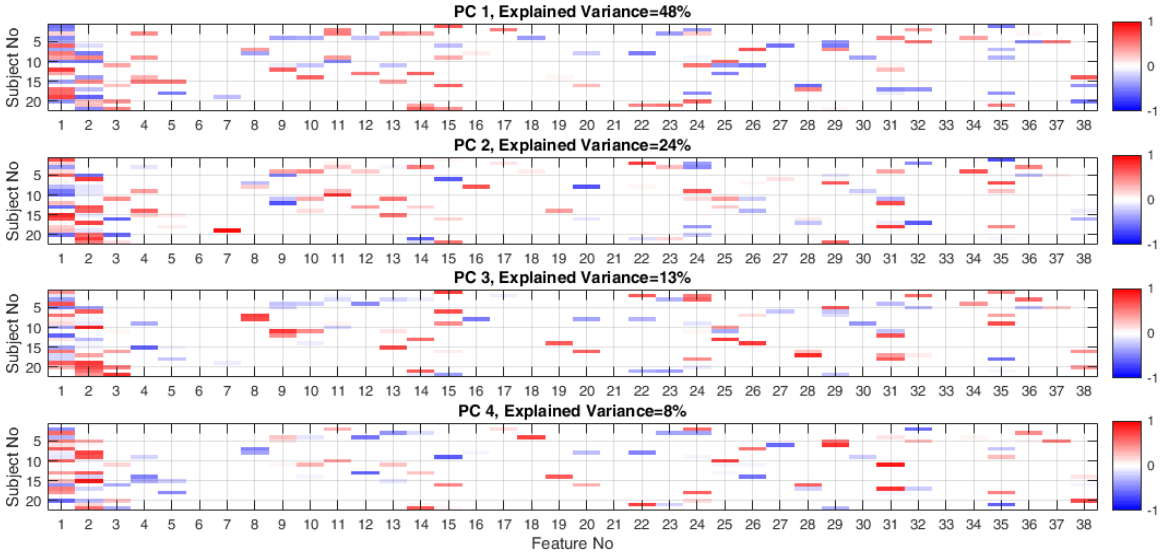

Fig. 7.7. Four most significant principal components (PCs) derived as independent predictors for subject specific systolic pressures estimation in Analysis #3. See Table 7.2 for feature index.

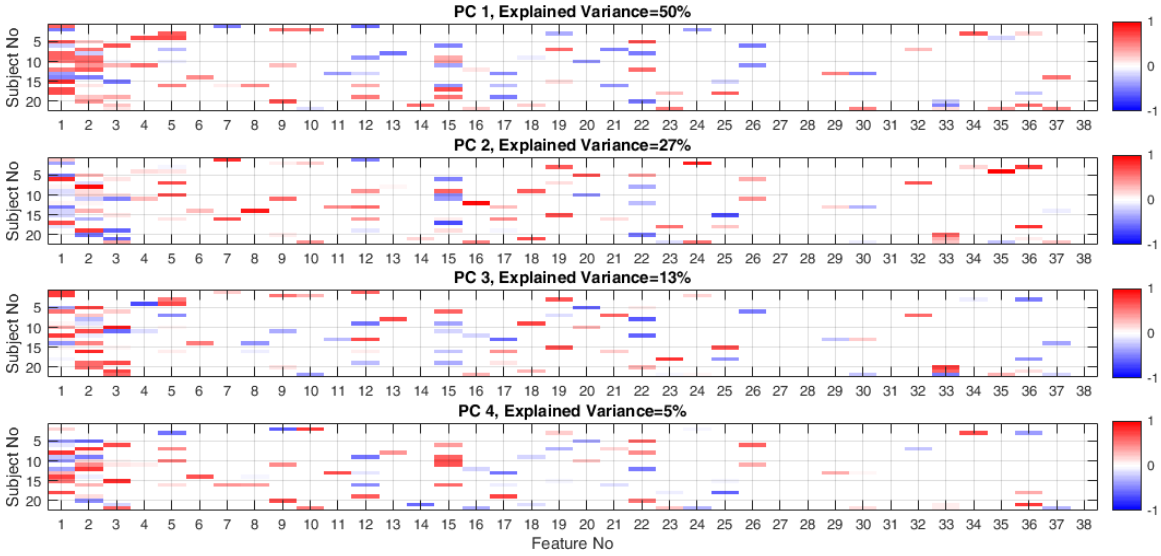

Fig. 7.8. Four most significant principal components (PCs) derived as independent predictors for subject specific diastolic pressures estimation in Analysis #3. See Table 7.2 for feature index.

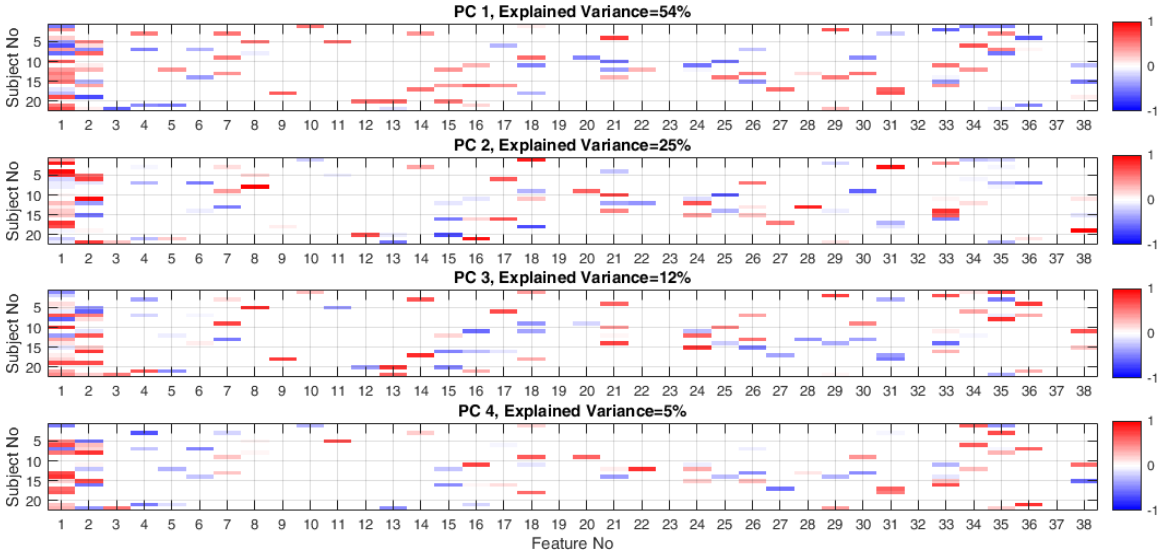

Fig. 7.9. Four most significant principal components (PCs) derived as independent predictors for subject specific pulse pressures estimation in Analysis #3. See Table 7.2 for feature index.

Table 7.3. Correlation, root-mean-squared error (RMSE), mean absolute error (MAE), and precision error (PE) between reference BP versus BP calibrated from constructed predictors. PP: pulse pressure DP: diastolic BP. SP: systolic BP. The results of all analysis #1, #2, #3 are presented in the table.

			SP			DP			PP		
			Analysis 1	Analysis 2	Analysis 3	Analysis 1	Analysis 2	Analysis 3	Analysis 1	Analysis 2	Analysis 3
r-val	Train	1-var	0.67+/-0.05	0.74+/-0.05	0.68+/-0.08	0.7+/-0.07	0.75+/-0.06	0.74+/-0.06	0.68+/-0.07	0.68+/-0.06	0.69+/-0.07
		2-var	0.78+/-0.04	0.85+/-0.03	0.82+/-0.05	0.84+/-0.04	0.86+/-0.05	0.87+/-0.04	0.85+/-0.02	0.87+/-0.03	0.85+/-0.04
		3-var	0.84+/-0.04	0.87+/-0.03	0.88+/-0.03	0.88+/-0.03	0.91+/-0.03	0.91+/-0.03	0.9+/-0.02	0.91+/-0.02	0.93+/-0.02
		4-var	0.86+/-0.03	0.89+/-0.02	0.9+/-0.02	0.91+/-0.02	0.92+/-0.02	0.93+/-0.02	0.94+/-0.01	0.93+/-0.01	0.94+/-0.01
	Test	1-var	0.31+/-0.11	0.72+/-0.05	0.59+/-0.08	0.66+/-0.06	0.75+/-0.06	0.56+/-0.11	0.54+/-0.09	0.61+/-0.08	0.51+/-0.12
		2-var	0.54+/-0.08	0.75+/-0.05	0.74+/-0.06	0.74+/-0.04	0.81+/-0.05	0.78+/-0.06	0.71+/-0.05	0.78+/-0.05	0.72+/-0.07
		3-var	0.66+/-0.06	0.78+/-0.05	0.83+/-0.03	0.78+/-0.04	0.85+/-0.03	0.83+/-0.04	0.81+/-0.03	0.82+/-0.04	0.86+/-0.03
		4-var	0.69+/-0.06	0.83+/-0.04	0.86+/-0.03	0.85+/-0.02	0.87+/-0.02	0.86+/-0.03	0.88+/-0.03	0.86+/-0.03	0.9+/-0.02
RMSE	Train	1-var	10.99+/-1.06	9.2+/-1.2	9.86+/-1.32	7.15+/-1.02	6.12+/-0.86	6.61+/-0.94	5.38+/-0.63	5.25+/-0.63	5.01+/-0.69
		2-var	9.01+/-1.09	7.42+/-0.97	7.74+/-1.23	5.62+/-0.86	4.72+/-0.78	4.96+/-0.87	4.04+/-0.46	3.61+/-0.49	3.82+/-0.63
		3-var	8.05+/-1.02	6.63+/-0.97	6.86+/-1.02	4.96+/-0.78	4.04+/-0.65	4.03+/-0.76	3.26+/-0.4	3.02+/-0.39	2.73+/-0.43
		4-var	7.3+/-0.95	6.2+/-0.91	6.11+/-0.83	4.23+/-0.67	3.66+/-0.58	3.69+/-0.74	2.49+/-0.38	2.58+/-0.32	2.32+/-0.43
	Test	1-var	11.08+/-1.17	10.33+/-1.49	10.43+/-1.84	7.27+/-1.23	6.82+/-1.12	7.75+/-1.47	4.56+/-0.38	4.85+/-0.45	4.92+/-0.39
		2-var	10.73+/-1.58	9.61+/-1.46	9.82+/-1.87	7+/-1.36	6.53+/-1.42	6.86+/-1.53	4.41+/-0.39	4.27+/-0.46	4.4+/-0.38
		3-var	10.31+/-1.57	9.92+/-1.77	9.34+/-1.74	6.96+/-1.46	6.52+/-1.51	6.73+/-1.5	4.13+/-0.36	4.24+/-0.51	3.95+/-0.42
		4-var	10.67+/-1.83	9.59+/-1.76	9.25+/-1.75	6.64+/-1.5	6.39+/-1.53	6.56+/-1.52	3.9+/-0.45	4.1+/-0.48	3.75+/-0.48
MAE	Train	1-var	8.8+/-0.94	7.47+/-1.08	7.98+/-1.15	5.78+/-0.91	5.04+/-0.76	5.37+/-0.82	4.28+/-0.54	4.23+/-0.56	4.07+/-0.58
		2-var	7.11+/-0.89	5.86+/-0.76	6.26+/-1.06	4.46+/-0.7	3.74+/-0.67	3.96+/-0.72	3.17+/-0.37	2.87+/-0.39	2.97+/-0.51
		3-var	6.4+/-0.84	5.19+/-0.74	5.41+/-0.81	3.93+/-0.63	3.21+/-0.53	3.19+/-0.61	2.6+/-0.32	2.42+/-0.32	2.13+/-0.34
		4-var	5.72+/-0.75	4.83+/-0.69	4.81+/-0.62	3.39+/-0.53	2.85+/-0.45	2.92+/-0.58	2.01+/-0.31	2.08+/-0.27	1.84+/-0.34
	Test	1-var	9.15+/-0.97	9.1+/-1.44	8.97+/-1.83	6.35+/-1.19	6.07+/-1.09	6.63+/-1.43	3.7+/-0.33	4.03+/-0.43	4+/-0.38
		2-var	8.97+/-1.45	8.3+/-1.44	8.6+/-1.88	6.06+/-1.31	5.88+/-1.39	6+/-1.51	3.66+/-0.35	3.62+/-0.44	3.67+/-0.36
		3-var	8.83+/-1.45	8.69+/-1.78	8.31+/-1.74	6.08+/-1.47	5.88+/-1.49	6.03+/-1.49	3.53+/-0.36	3.64+/-0.49	3.46+/-0.42
		4-var	9.33+/-1.77	8.55+/-1.78	8.3+/-1.78	5.94+/-1.52	5.79+/-1.53	5.92+/-1.51	3.45+/-0.44	3.58+/-0.48	3.36+/-0.48

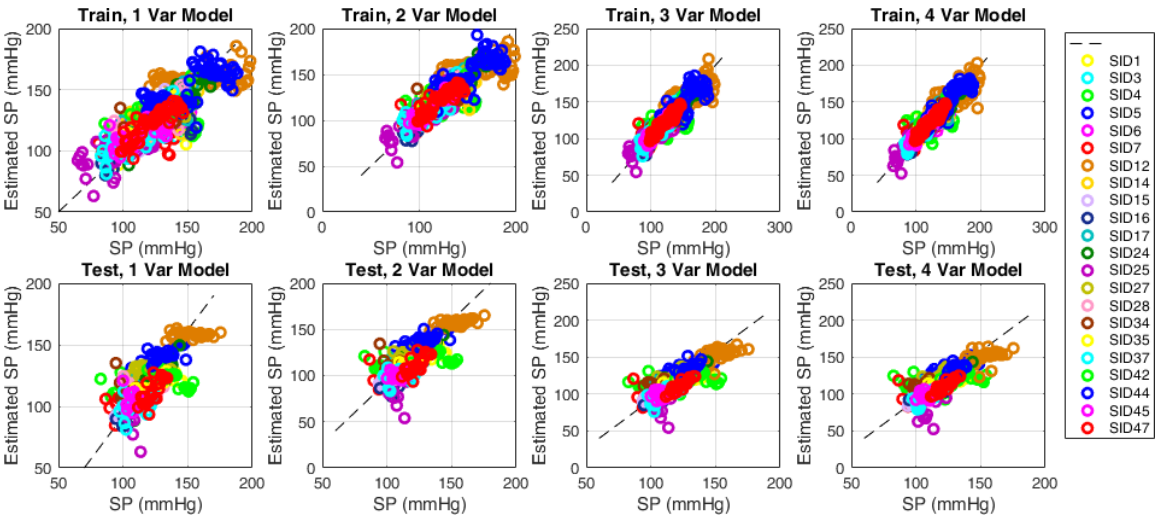

Fig. 7.10. Subject-level association between the estimated systolic pressure in analysis #1 (with 1,2,3, and variable regression models) versus measured systolic pressures in all subjects.

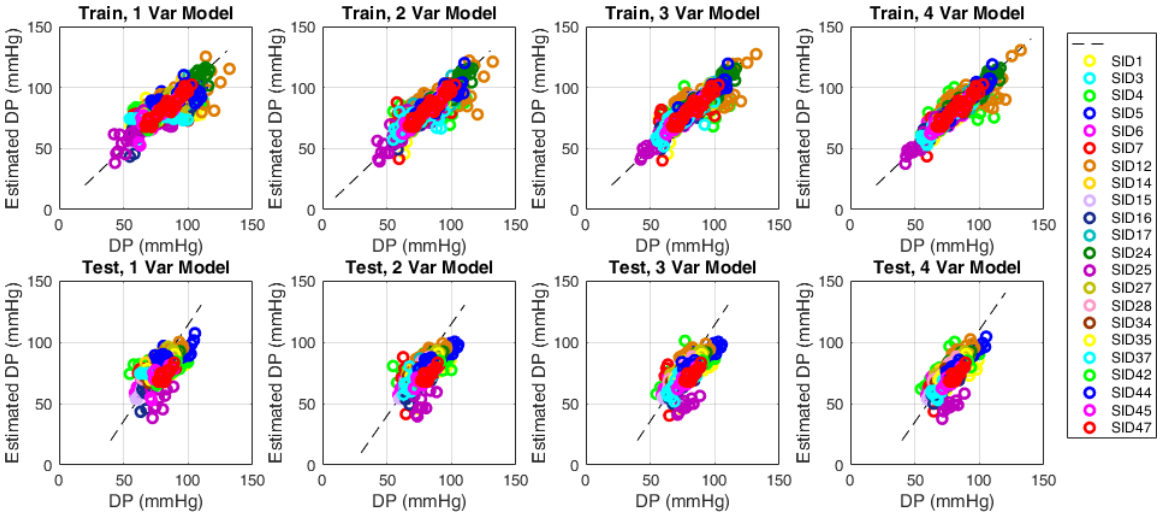

Fig. 7.11. Subject-level association between the estimated diastolic pressure in analysis #1 (with 1,2,3, and variable regression models) versus measured systolic pressures in all subjects.

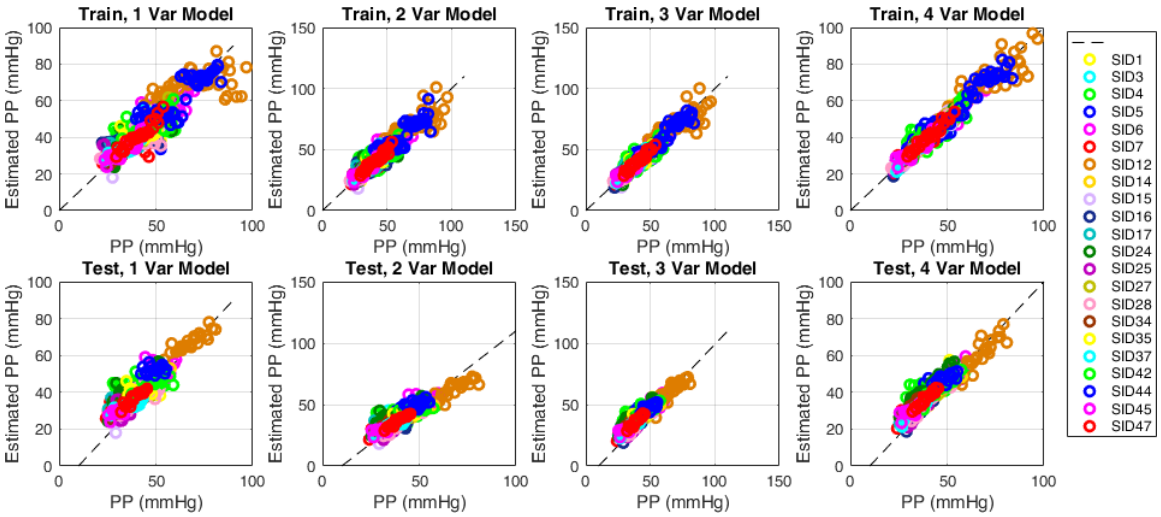

Fig. 7.12. Subject-level association between the estimated pulse pressure in analysis #1 (with 1,2,3, and variable regression models) versus measured systolic pressures in all subjects.

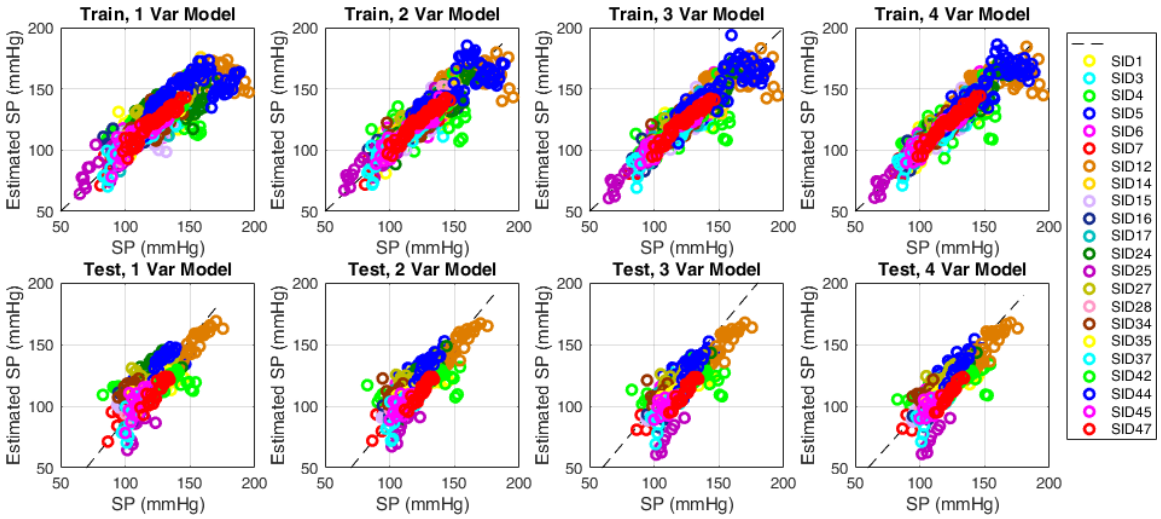

Fig. 7.13. Subject-level association between the estimated systolic pressure in analysis #2 (with 1,2,3, and variable regression models) versus measured systolic pressures in all subjects.

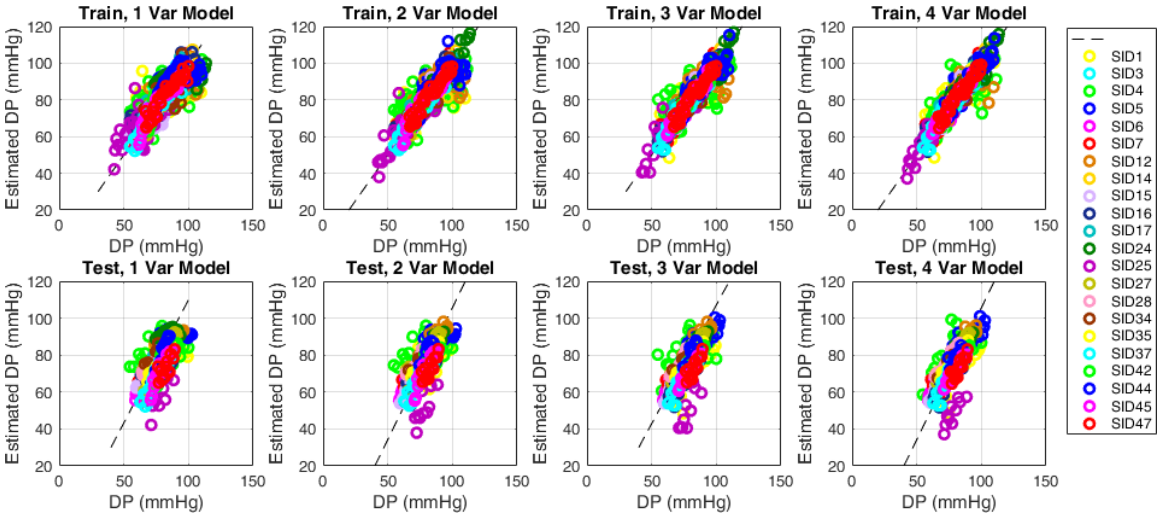

Fig. 7.14. Subject-level association between the estimated diastolic pressure in analysis #2 (with 1,2,3, and variable regression models) versus measured systolic pressures in all subjects.

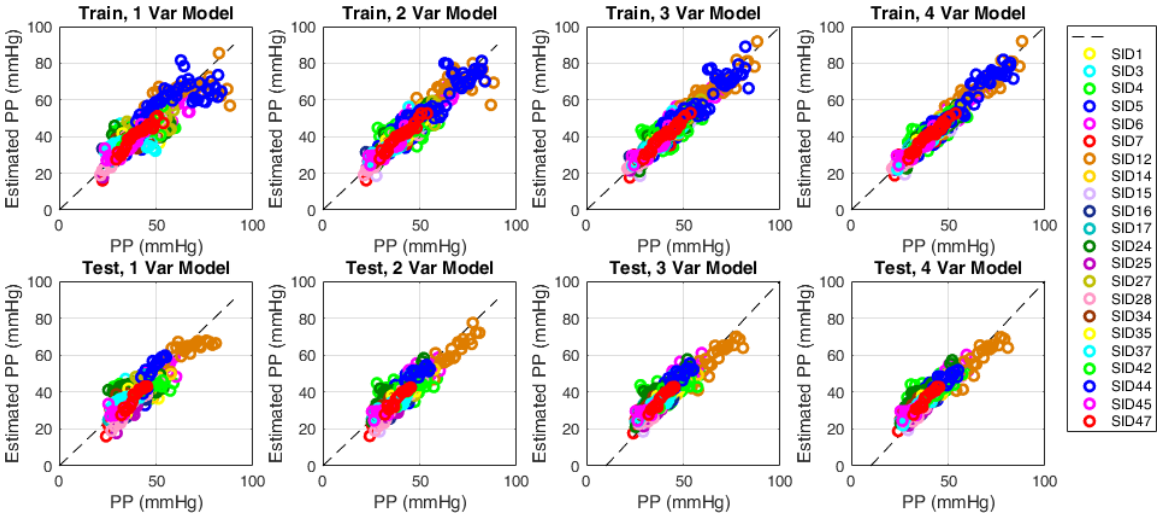

Fig. 7.15. Subject-level association between the estimated pulse pressure in analysis #2 (with 1,2,3, and variable regression models) versus measured systolic pressures in all subjects.

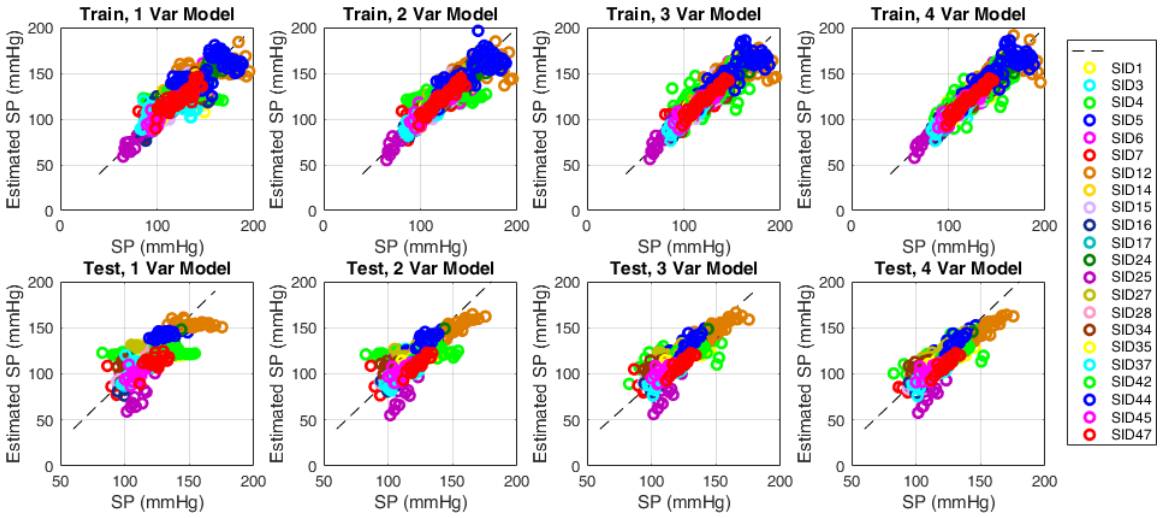

Fig. 7.16. Subject-level association between the estimated systolic pressure in analysis #3 (with 1,2,3, and variable regression models) versus measured systolic pressures in all subjects.

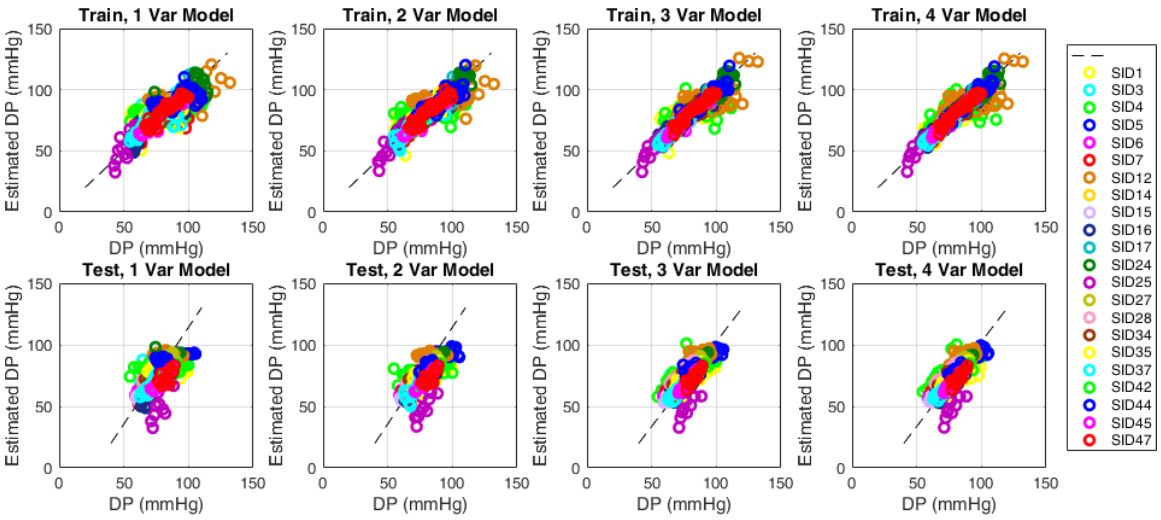

Fig. 7.17. Subject-level association between the estimated diastolic pressure in analysis #3 (with 1,2,3, and variable regression models) versus measured systolic pressures in all subjects.

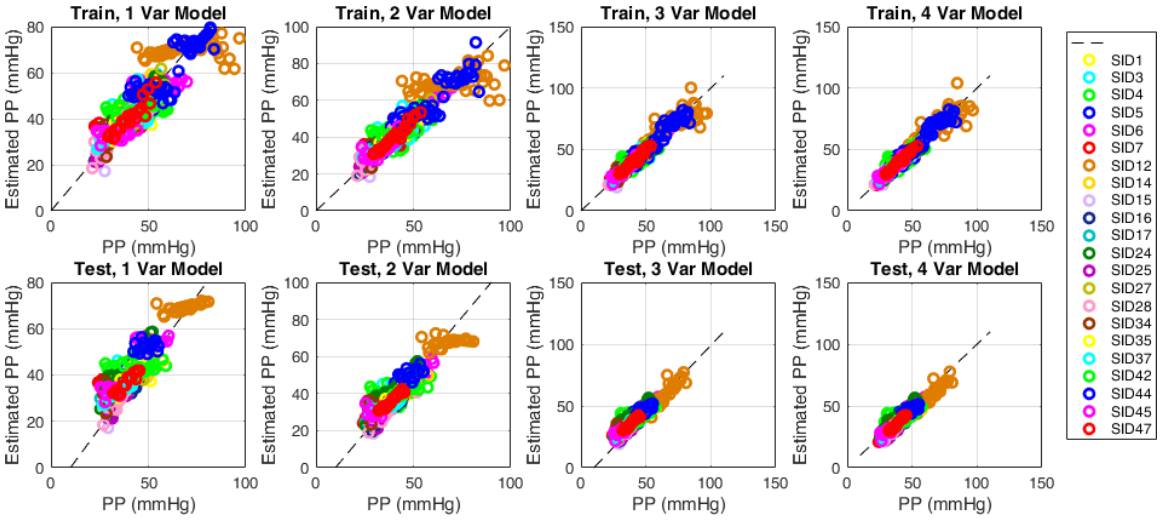

Fig. 7.18. Subject-level association between the estimated pulse pressure in analysis #3 (with 1,2,3, and variable regression models) versus measured systolic pressures in all subjects.

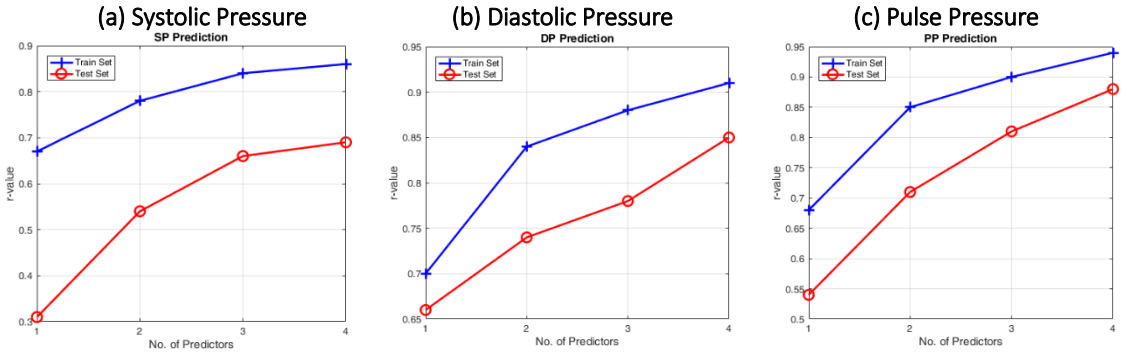

Fig. 7.19. Correlation coefficients variations to estimate (a) systolic, (b) diastolic, (c) pulse pressure with respect to the number of the predictors in the multivariate regression model in analysis #1.

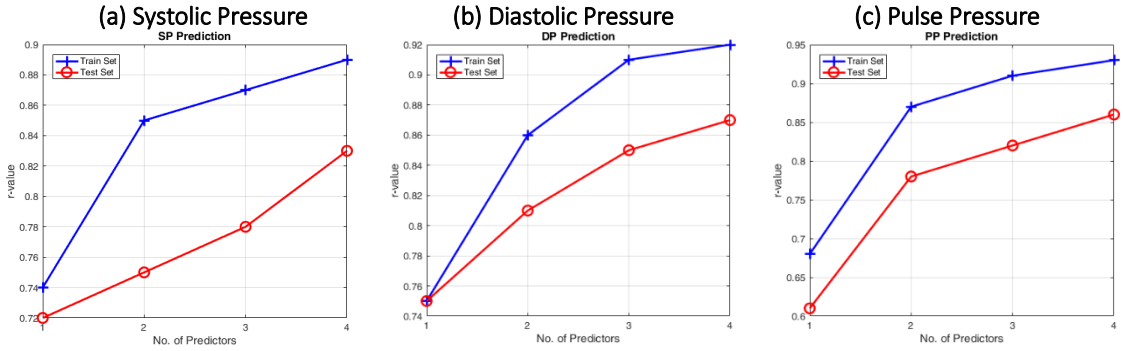

Fig. 7.20. Correlation coefficients variations to estimate (a) systolic, (b) diastolic, (c) pulse pressure with respect to the number of the predictors in the multivariate regression models in analysis #2.

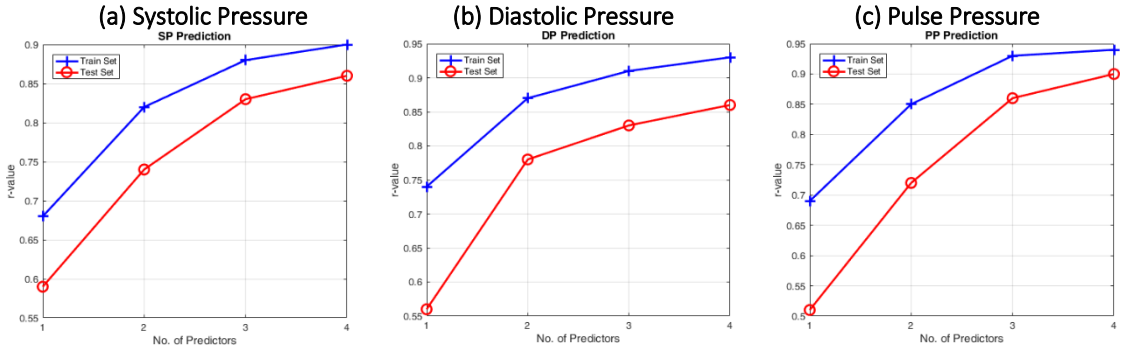

Fig. 7.21. Correlation coefficients variations to estimate (a) systolic, (b) diastolic, (c) pulse pressure with respect to the number of the predictors in the multivariate regression models in analysis #3.

7.4. Discussion

According to the results of analysis #1, BCG based features could be strong predictors of the BP. Based on the presented results in Table 7.3 for the 4 variable regression model (which has significantly higher accuracy than the other three models for both test and train data) using the constructed PCs (Fig. 7.1, Fig. 7.2, Fig. 7.3), when only BCG based features are utilized to construct the predictive models for PP, DP and SP estimation, correlation coefficient of r= 0.94+/-0.01 (PP), r= 0.91+/-0.02 (DP) and r= 0.86+/-0.03 (SP), RMSE of 2.49+/-0.38 mmHg (PP), 4.23+/-0.67 mmHg (DP) and 7.3+/-0.95 mmHg (SP), and MAE of 2.01+/-0.31 mmHg (PP), 3.39+/-0.53 mmHg (DP) and 5.72+/-0.75 mmHg (SP) were obtained across the training interventions (mean+/-SE). When the developed model is utilized for PP, DP, and SP estimation for the test interventions, correlation coefficient of r= 0.88+/-0.03 (PP), r= 0.85+/-0.02 (DP) and r= 0.69+/-0.06 (SP), RMSE of 3.9+/-0.45 mmHg

(PP), 6.64+/-1.5 mmHg (DP) and 10.67+/-1.83 mmHg (SP), and MAE of 3.45+/-0.44 mmHg (PP), 5.94+/-1.52 mmHg (DP) and 9.33+/-1.77 mmHg (SP) were obtained. More details of the subject level association between the estimated and measured BPs are provided in Fig. 7.10, Fig. 7.11, Fig. 7.12. We see that the performance on test data of SP, decreases considerably for SP. It could be due to the more complex nature of SP, compared to DP and PP, and it may require more sophisticated models with more predictors.

In analysis #2, the first variable in the regression model is assumed to be PTT (Fig. 7.4, Fig. 7.5, Fig. 7.6). So by looking at the results of the univariate regression model in this analysis, we can get the performance of a subject specific PTT based model on both train and test data. According to Table 7.3, correlation coefficient of r= 0.68+/-0.06 (PP), r= 0.75+/-0.06 (DP) and r= 0.74+/-0.05 (SP), RMSE of 5.25+/-0.63 mmHg (PP), 6.12+/-0.86 mmHg (DP) and 9.2+/-1.2 mmHg (SP), and MAE of 4.23+/-0.56 mmHg (PP), 5.04+/-0.76 mmHg (DP) and 7.47+/-1.08 mmHg (SP) were obtained across the training interventions. For the test intervention data, correlation coefficient of r= 0.61+/-0.08 (PP), r= 0.75+/-0.06 (DP) and r= 0.72+/-0.05 (SP), RMSE of 4.85+/-0.45 mmHg (PP), 6.82+/-1.12 mmHg (DP) and 10.33+/-1.49 mmHg (SP), and MAE of 4.03+/-0.43 mmHg (PP), 6.07+/-1.09 mmHg (DP) and 9.1+/-1.44 mmHg (SP) are obtained. Performance of the model on the test interventions is very close to the train data with slight degradation. This implies the robustness of the PTT feature as a BP predictor, specifically for DP which doesn't degrade on test data across all subjects.

According to the obtained results from both analysis #2 and #3, combining PTT and BCG-based features can improve the accuracy of subject specific models. In this regard, 4 variable regression model (Fig. 7.7, Fig. 7.8, Fig. 7.9), constructed in analysis #3, has the best performance and achieves significantly higher metrics than all other models in all of the other models for the test data. According to Table 7.3, correlation coefficient of r= 0.94+/-0.01 (PP), r= 0.93+/-0.02 (DP) and r= 0.9+/-0.02 (SP), RMSE of 2.32+/-0.43 mmHg (PP), 3.69+/-0.74 mmHg (DP) and 6.11+/-0.83 mmHg (SP), and MAE of 1.84+/-0.34 mmHg (PP), 2.92+/-0.58 mmHg (DP) and 4.81+/-0.62 mmHg (SP) is obtained across all training interventions. For the test interventions, correlation coefficient of r= 0.9+/-0.02 (PP), r= 0.86+/-0.03 (DP) and r= 0.86+/-0.03 (SP), RMSE of 3.75+/-0.48 mmHg (PP), 6.56+/-1.52 mmHg (DP) and 9.25+/-1.75 mmHg (SP), and MAE of 3.36+/-0.48 mmHg (PP), 5.92+/-1.51 mmHg (DP) and 8.3+/-1.78 mmHg (SP) is obtained using the same model.

Comparing the performance of the results described above, it is observed that hybrid model (which uses both BCG-based features and PTT) outperforms PTT based model by 19% (SP), 15% (DP), and 48% (PP) improvement in correlation coefficient. By comparison

of the hybrid model with purely BCG-based model, we observe that they have similar accuracy for DP and PP estimation. However, for SP estimation, the hybrid model outperforms the pure BCG-based model by 25% improvement of correlation coefficient in test data.

7.5. Conclusion

Close and robust association between of the wrist BCG-based PTT and PWA features with BP is demonstrated using subject specific models. The results show that for DP and PP can be estimated using both pure BCG-based models as well as hybrid models, which uses PTT in addition to BCG-based features. However, for SP estimation, hybrid model seems to be the only possible option.

8. Conclusion

By virtue of its direct association with the cardiovascular functions and compatibility to unobtrusive measurement during daily activities, the limb BCG is receiving an increasing interest as a viable means for ultra-convenient CV health and disease monitoring. However, limited insights on its physical implications have hampered disciplined interpretation of the BCG and systematic development of the BCG-based approaches for CV health monitoring. In this study, a mathematical model is developed that can explain the limp BCG waveform in response to the force generated by arterial blood pressure. The physical insights garnered by the analysis of the mathematical model may open up new opportunities toward the next generation of the BCG-based CV healthcare techniques embedded with transparency, interpretability, and robustness against the external variability.

Then the potential of wearable limb BCG as a basis to enable cuff-less blood pressure monitoring via pulse transit time is investigated. A wearable BCG-based PTT was constructed using the BCG and PPG signals instrumented by a wristband as a proximal and distal timing reference (wrist PTT). Its efficacy as a surrogate of BP was examined in comparison with PTT based on the whole-body BCG instrumented by a customized weighing scale (scale PTT) as well as pulse arrival time (PAT) using the experimental data collected from participants under multiple BP-perturbing interventions. Results illustrate that the wrist PTT exhibited a close association with both diastolic and systolic BP. The efficacy of the wrist PTT was superior to scale PTT and PAT for both diastolic and systolic BP. The association was consistent and robust against diverse BP-perturbing interventions. The wrist PTT showed superior association with BP when constructed with green PPG rather than infrared PPG.

The next step was to investigate the association between a limb BCG and blood pressure BP based on data mining. Both timing and amplitude features in the wrist BCG waveform were extracted, and significant features predictive of DP and SP blood pressure were selected and the association between the predictors thus obtained and BP was investigated by multivariate linear regression analysis. The predictors exhibited a meaningful association with BP. The minimum number of requisite predictors for robust yet practically realistic BP monitoring appeared to be 3. The requisite predictors for DP and SP were distinct from each other. The obtained results may provide a viable basis for ultra-convenient BP monitoring based on a limb BCG alone.

Ultimately, the idea of developing prediction models that utilize both wrist PTT and BCG-based feature is examined. The results show that adding BCG-based features on top of the PTT can improve the accuracy of BP monitoring. Additionally, it is illustrated that Physics based insights could be used to decrease the number of utilized features in such a complex model. A smaller set of utilized features can facilitate technological implementation by decreasing the number of data points required for model construction and calibration.

In the last chapter, subject-specific models were developed to obtain an estimated upper bound for the accuracy of BP monitoring models that could be achieved using the limb BCG and PPG signals. Based on these results it is possible to achieve correlation coefficient of r= 0.94+/-0.01 (PP), r= 0.93+/-0.02 (DP) and r= 0.9+/-0.02 (SP), RMSE of 2.32+/-0.43 mmHg (PP), 3.69+/-0.74 mmHg (DP) and 6.11+/-0.83 mmHg (SP), and MAE of 1.84+/-0.34 mmHg (PP), 2.92+/-0.58 mmHg (DP) and 4.81+/-0.62 mmHg (SP) is obtained across all training interventions. By applying the same model on the test interventions without any adjustment and calibration, correlation coefficient of r= 0.9+/-0.02 (PP), r= 0.86+/-0.03 (DP) and r= 0.86+/-0.03 (SP), RMSE of 3.75+/-0.48 mmHg (PP), 6.56+/-1.52 mmHg (DP) and 9.25+/-1.75 mmHg (SP), and MAE of 3.36+/-0.48 mmHg (PP), 5.92+/-1.51 mmHg (DP) and 8.3+/-1.78 mmHg (SP) is obtained. However, we should emphasize that subject-specific models are difficult to implement since they need a considerable number of data points for each subject to be created and calibrated. Maybe this problem could be addressed in the future by developing more advanced machine learning models for BP estimation.

9. Limitations and Future Work

Overall, the findings of this research shows that limb based BCG has the potential to realize convenient cuff-less BP monitoring. As a result, wearable limb BCG may open up new opportunities for convenient cuff-less BP monitoring via PTT and PWA in everyday life. However, to generalize the findings of this research for technological implementation, there are several limitations that should be addressed in future studies.

First, the participant pool was not diverse: all were healthy with no explicit indication of cardiovascular disease. Additionally, the sample size used in this study was not large. Hence, despite the demonstrated potential and opportunities, the generalizability of the findings to a broad range of subjects is yet to be shown. In the ideal, considering that the BCG waveform morphology is closely related to arterial BP waves[70], the variability in arterial mechanical properties may manifest itself in the BCG waveform through its impact

on the speed and morphology of arterial BP waves, thereby altering the BCG features. Hence, changes in arterial mechanical properties may be captured by the corresponding changes in the BCG features. But in reality, the relative significance of the BCG features (and thus the composition of the PCs) relevant to BP monitoring may vary with respect to age and disease. In addition, changes in smooth muscle tone and other artifacts may further complicate robust high-quality association of BCG with BP. It is our anticipation that the association between a limb BCG and BP may persistently exist in a wide range of subjects, but its pattern may vary. Future work on the rigorous evaluation of the efficacy of limb BCGs for BP monitoring, as well as the investigation of ideas to compensate for possible age- and disease-dependent variability in the association between a limb BCG and BP, must be conducted in a large number of diverse subjects.

Second, this study used the ECG for the sake of BCG and PPG gating. Being an initial feasibility study, it was deemed acceptable to employ ECG. However, ECG may need to be removed in the ultimate implementation of wearable wrist BCG-based BP monitoring so as to minimize the complexity associated with the device and its use. One reasonable option may be to replace ECG by PPG for BCG gating. We anticipate that PPG-based BCG gating will present non-trivial challenges due to the BP-dependent changes in the location of the PPG foot relative to the ECG R wave and the proximity between the PPG foot and the I-J-K complex in the BCG. Future work is required to develop PPG-based gating methods that can overcome these challenges.

Third, this study was limited to a specific posture (i.e., standing with the arms placed at the side). The shape of the wrist BCG (and in general any wearable limb BCG potentially) varies with respect to posture, since the change in posture alters the orientation of the sensors embedded in the wearable device [37]. Compensation of the impact of posture on the shape of the wrist BCG may require additional sensors (e.g., inertial sensors) and signal processing algorithms to determine the orientation of the wrist. In addition, additional consideration is needed if the wrist is artificially supported (e.g., if it is placed on a desk), in which the way the whole-body BCG is transferred to the wrist is altered by the reaction force exerted by the support. Rigorous future work is required to address this challenge to truly enable the wearable limb BCG-based PTT and BP monitoring.

Fourth, despite the notable potential of the wrist BCG in ultra-convenient PTT and BP monitoring, convenient PTT-BP calibration still remains an open challenge. Given that artery stiffens with aging and alters PTT-BP relationship, PTT-BP relationship must be continually calibrated. Existing PTT-BP calibration techniques typically involve the measurement of reference BP and PTT during BP-perturbing interventions. However, ideal

calibration must not require cumbersome interventions to maximize convenience. Future investigation needs to be conducted for the development of novel convenient PTT-BP calibration techniques.

Findings of this study suggest that certain characteristic features in the limb BCG waveforms may serve as viable surrogates of CV function, health, and potentially CVD. However, the convoluted and multi-faceted effects of the variability in the arterial BP waves on the limb BCG as well as the confounding impact of the bio-mechanical variability of the body may present challenges toward the development of novel techniques to decipher CV health and CVD from the limb BCG. Future effort must be invested to establish more rigorous physiological understanding of the limb BCG, examine the effect of CV pathophysiology on the morphology of the limb BCG waveforms, and investigate the opportunities to incorporate physiological insights derived from this study into CV health and CVD monitoring based on the limb BCG.

References

[1] E. J. Benjamin *et al.*, *Heart disease and stroke statistics - 2018 update: A report from the American Heart Association*, vol. 137, no. 12. 2018.

[2] R. Mukkamala *et al.*, "Toward Ubiquitous Blood Pressure Monitoring via Pulse Transit Time: Theory and Practice," *IEEE Trans. Biomed. Eng.*, vol. 62, no. 8, pp. 1879–1901, Aug. 2015.

[3] K. Hirata, M. Kawakami, and M. F. O'Rourke, "Pulse wave analysis and pulse wave velocity: a review of blood pressure interpretation 100 years after Korotkov," *Circ. J.*, vol. 70, no. 10, pp. 1231–1239, 2006.

[4] P. Salvi *et al.*, "Comparative study of methodologies for pulse wave velocity estimation," *J. Hum. Hypertens.*, vol. 22, no. 10, pp. 669–677, 2008.

[5] S. Laurent *et al.*, "Expert consensus document on arterial stiffness: Methodological issues and clinical applications," *Eur. Heart J.*, vol. 27, no. 21, pp. 2588–2605, 2006.

[6] E. Agabiti-Rosei *et al.*, "Central blood pressure measurements and antihypertensive therapy: A consensus document," *Hypertension*, vol. 50, no. 1, pp. 154–160, 2007.

[7] G. F. Mitchell *et al.*, "Changes in Arterial Stiffness and Wave Reflection With Advancing Age in Healthy Men and Women The Framingham Heart Study," 2004.

[8] T. J. Anderson and T. J. Anderson, "Assessment and Treatment of Endothelial Dysfunction in Humans," *J. Am. Coll. Cardiol.*, vol. 34, pp. 631–638, 1999.

[9] J. T. Kuvin *et al.*, "Assessment of peripheral vascular endothelial function with finger arterial pulse wave amplitude," vol. 8703, no. 03, pp. 0–6, 2003.

[10] A. E. Donald *et al.*, "Non-Invasive Assessment of Endothelial Function Which Technique ?," 2010.

[11] R. Rubinshtein *et al.*, "Assessment of endothelial function by non-invasive peripheral arterial tonometry predicts late cardiovascular adverse events," pp. 1142–1148, 2010.

[12] S. P. A. Nicolaï, L. M. Kruidenier, E. V Rouwet, M. E. L. Bartelink, M. H. Prins, and J. A. W. Teijink, "Ankle brachial index measurement in primary care : are we doing it right ?," no. June, pp. 422–427, 2009.

[13] J. A. Beckman, C. O. Higgins, M. Gerhard-herman, J. A. Beckman, C. O. Higgins, and M. Gerhard-herman, "Automated Oscillometric Determination of the Ankle – Brachial Index Provides Accuracy Necessary for Office Practice," 2006.

[14] N. Diehm, F. Dick, C. Czuprin, H. Lawall, I. Baumgartner, and C. Diehm, "Oscillometric measurement of ankle-brachial index in patients with suspected peripheral vascular disease : comparison with Doppler method," vol. 9, pp. 357–363.

[15] I. Starr, "The Relation of the Ballistocardiogram to Cardiac Function," *Am. J. Cardiol.*, vol. 2, pp. 737–747, 1958.

[16] O. Tannenbaum, J. A. Schack, and H. Vesell, "Relationship between Ballistocardiographic Forces and Certain Events in the Cardiac Cycle," *Circulation*, vol. VI, pp. 586–593, 1952.

[17] A. Noordergraaf and C. E. Heynekamp, "Genesis of Displacement of the Human Longitudinal Ballistocardiogram from the Changing Blood Distribution," *Am. J. Cardiol.*, vol. 2, no. 6, pp. 748–756, 1958.

[18] R. S. Gubner, M. Rodstein, and H. E. Ungerleider, "Ballistocardiography An Appraisal of Technic, Physiologic Principles, and Clinical Value," *Circulation*, vol. VII, pp. 268–287, 1953.

[19] W. R. Scarborough, R. E. Mason, F. W. Davis, M. L. Singewald, B. M. Baker, and S. A. Lore, "A ballistocardiographic and Electrocardiographic Study of 328 Patients with Coronary Artery Disease: Comparison with Results from a Similar Study of Apparently Normal Persons," *Am. Heart J.*, vol. 44, no. 5, pp. 645–670, 1952.

[20] L. M. Bargeron, "The Force Ballistocardiogram as an Index of Severity in Congenital Aortic Stenosis," *Circulation*, vol. 37, pp. 238–243, 1968.

[21] W. R. Scarborough, "Current Status of Ballistocardiography," *Prog. Cardiovasc. Dis.*, vol. 2, no. 3, pp. 263–291, 1959.

[22] D. W. Jung, S. H. Hwang, H. N. Yoon, Y. G. Lee, D. Jeong, and K. S. Park, "Nocturnal Awakening and Sleep Efficiency Estimation Using Unobtrusively Measured Ballistocardiogram," *IEEE Trans.*

Biomed. Eng., vol. 61, no. 1, pp. 131–138, 2014.
[23] J. H. Shin, Y. J. Chee, D. Jeong, and K. S. Park, "Nonconstrained Sleep Monitoring System and Algorithms Using Air-Mattress With Balancing Tube Method," *IEEE J. Biomed. Heal. Informatics*, vol. 14, no. 1, pp. 147–156, 2010.
[24] E. Pinheiro, O. Postolache, and P. Girão, "Non-Intrusive Device for Real-Time Circulatory System Assessment with Advanced Signal Processing Capabilities," *Meas. Sci. Rev.*, vol. 10, no. 5, pp. 166–175, 2010.
[25] A. Akhbardeh, S. Junnila, T. Koivistoinen, and A. Varri, "An intelligent Ballistocardiographic Chair using a Novel SF-ART Neural Network and Biorthogonal Wavelets," *J. Med. Syst.*, vol. 31, no. 1, pp. 69–77, 2007.
[26] O. T. Inan, M. Etemadi, R. M. Wiard, L. Giovangrandi, and G. T. A. Kovacs, "Robust Ballistocardiogram Acquisition for Home Monitoring," *Physiol. Meas.*, vol. 30, pp. 169–185, 2009.
[27] O. T. Inan, D. Park, S. Member, L. Giovangrandi, and G. T. A. Kovacs, "Noninvasive Measurement of Physiological Signals on a Modified Home Bathroom Scale," *IEEE Trans. Biomed. Eng.*, vol. 59, no. 8, pp. 2137–2143, 2012.
[28] J. H. Shin, K. M. Lee, and K. S. Park, "Non-constrained monitoring of systolic blood pressure on a weighing scale," *Physiol. Meas.*, vol. 30, no. 7, pp. 679–693, Jul. 2009.
[29] D. Da He, E. S. Winokur, and C. G. Sodini, "An Ear-Worn Vital Signs Monitor," *IEEE Trans. Biomed. Eng.*, vol. 62, no. 11, pp. 2547–2552, Nov. 2015.
[30] P. Yousefian *et al.*, "Data Mining Investigation of the Association between a Limb Ballistocardiogram and Blood Pressure," *Physiol. Meas.*, vol. 39, p. 075009, 2018.
[31] C.-S. Kim, A. M. Carek, R. Mukkamala, O. T. Inan, and J.-O. Hahn, "Ballistocardiogram as Proximal Timing Reference for Pulse Transit Time Measurement: Potential for Cuffless Blood Pressure Monitoring," *IEEE Trans. Biomed. Eng.*, vol. 62, no. 11, pp. 2657–2664, Nov. 2015.
[32] S. L.-O. Martin *et al.*, "Weighing Scale-Based Pulse Transit Time is a Superior Marker of Blood Pressure than Conventional Pulse Arrival Time.," *Sci. Rep.*, vol. 6, p. 39273, Dec. 2016.
[33] C. Kim, A. M. Carek, O. T. Inan, R. Mukkamala, and J.-O. Hahn, "Ballistocardiogram-Based Approach to Cuffless Blood Pressure Monitoring: Proof of Concept and Potential Challenges," *IEEE Trans. Biomed.*, 2018.
[34] D. Campo *et al.*, "Measurement of Aortic Pulse Wave Velocity With a Connected Bathroom Scale," *Am. J. Hypertens.*, vol. 33, p. 16351701, May 2017.
[35] M. Etemadi, O. T. Inan, L. Giovangrandi, and G. T. A. Kovacs, "Rapid assessment of cardiac contractility on a home bathroom scale," *IEEE Trans. Inf. Technol. Biomed.*, vol. 15, no. 6, pp. 864–869, 2011.
[36] H. Ashouri, L. Orlandic, and O. T. Inan, "Unobtrusive Estimation of Cardiac Contractility and Stroke Volume Changes using Ballistocardiogram Measurements on a High Bandwidth Force Plate," *Sensors (Switzerland)*, vol. 16, no. 6, p. 787, 2016.
[37] A. D. Wiens, M. Etemadi, S. Roy, L. Klein, and O. T. Inan, "Toward Continuous, Noninvasive Assessment of Ventricular Function and Hemodynamics: Wearable Ballistocardiography," *IEEE J. Biomed. Heal. Informatics*, vol. 19, no. 4, pp. 1435–1442, Jul. 2015.
[38] A. Q. Javaid, A. D. Wiens, N. F. Fesmire, M. A. Weitnauer, and O. T. Inan, "Quantifying and Reducing Posture-Dependent Distortion in Ballistocardiogram Measurements," *IEEE J. Biomed. Heal. Informatics*, vol. 19, no. 5, pp. 1549–1556, Sep. 2015.
[39] A. D. Wiens, S. Member, and O. T. Inan, "A Novel System Identification Technique for Improved Wearable Hemodynamics Assessment," *IEEE Trans. Biomed. Eng.*, vol. 62, no. 5, pp. 1345–1354, 2015.
[40] R. Mukkamala *et al.*, "Toward Ubiquitous Blood Pressure Monitoring via Pulse Transit Time: Theory and Practice," *IEEE Trans. Biomed. Eng.*, vol. 62, no. 8, pp. 1879–1901, Aug. 2015.
[41] S. C. Millasseau, A. D. Stewart, S. J. Patel, S. R. Redwood, and P. J. Chowienczyk, "Evaluation of carotid-femoral pulse wave velocity: Influence of timing algorithm and heart rate," *Hypertension*, vol. 45, no. 2, pp. 222–226, 2005.
[42] S. S. Thomas, V. Nathan, C. Zong, K. Soundarapandian, X. Shi, and R. Jafari, "BioWatch: A Noninvasive Wrist-Based Blood Pressure Monitor That Incorporates Training Techniques for Posture and Subject Variability," *IEEE J. Biomed. Heal. Informatics*, vol. 20, no. 5, pp. 1291–1300,

2016.
[43] Q. Zhang, D. Zhou, and X. Zeng, “Highly wearable cuff-less blood pressure and heart rate monitoring with single-arm electrocardiogram and photoplethysmogram signals,” *Biomed. Eng. Online*, vol. 16, no. 23, pp. 1–20, 2017.
[44] P. M. Nabeel, J. Jayaraj, and S. Mohanasankar, “Single-source PPG-based local pulse wave velocity measurement: A potential cuffless blood pressure estimation technique,” *Physiol. Meas.*, vol. 38, no. 12, pp. 2122–2140, 2017.
[45] N. Watanabe *et al.*, “Development and Validation of a Novel Cuff-Less Blood Pressure Monitoring Device,” *JACC Basic to Transl. Sci.*, vol. 2, no. 6, pp. 631–642, 2017.
[46] X. Xing and M. Sun, “Optical blood pressure estimation with photoplethysmography and FFT-based neural networks,” *Biomed. Opt. Express*, vol. 7, no. 8, p. 3007, 2016.
[47] K. Atomi, H. Kawanaka, M. S. Bhuiyan, and K. Oguri, “Cuffless Blood Pressure Estimation Based on Data-Oriented Continuous Health Monitoring System,” *Comput. Math. Methods Med.*, vol. 2017, 2017.
[48] S. L.-O. Martin *et al.*, “Weighing Scale-Based Pulse Transit Time is a Superior Marker of Blood Pressure than Conventional Pulse Arrival Time,” vol. 6.
[49] R. Shriram, A. Wakankar, N. Daimiwal, and D. Ramdasi, “Continuous cuffless blood pressure monitoring based on PTT,” in *2010 International Conference on Bioinformatics and Biomedical Technology*, 2010, pp. 51–55.
[50] L. S. Costanzo, *BRS Physiology*. .
[51] Mariana Ruiz Villarreal, “Human healthy pumping heart.” [Online]. Available: https://commons.wikimedia.org/wiki/File:Human_healthy_pumping_heart_en.svg. [Accessed: 07-May-2018].
[52] B. H. McGhee and E. J. Bridges, “Monitoring arterial blood pressure: what you may not know.,” *Crit. Care Nurse*, vol. 22, no. 2, p. 60–4, 66–70, 73 passim, Apr. 2002.
[53] D. Perloff *et al.*, “Human blood pressure determination by sphygmomanometry,” *Circulation*, vol. 88, pp. 2460–2470, 1993.
[54] B. S. Alpert, D. Quinn, and D. Gallick, “Oscillometric blood pressure: a review for clinicians,” *J. Am. Soc. Hypertens.*, vol. 8, pp. 930–938, 2014.
[55] G. Drzewiecki, R. Hood, and H. Apple, “Theory of the oscillometric maximum and the systolic and diastolic detection ratios,” *Ann. Biomed. Eng.*, vol. 22, pp. 88–96, 1994.
[56] B. P. Imholz, M. W. Wieling, G. A. van Montfrans, and K. H. Wesseling, “Fifteen years experience with finger arterial pressure monitoring: assessment of the technology,” *Cardiovasc. Res.*, vol. 38, no. 3, pp. 605–616, 1998.
[57] K. Wesseling, B. Wit, G. Hoeven, J. Goudoever, and J. J. Settels, “Physiocal, calibrating finger vascular physiology for Finapres,” *Homeostasis*, vol. 36, no. 2–3, pp. 67–82, 1995.
[58] G. M. Drzewiecki, J. Melbin, and A. Noordergraaf, “Deformational forces in arterial tonometry,” *IEEE Trans. Biomed. Eng.*, vol. 31, no. 8, p. 576, 1984.
[59] J. Eckerle, “Tonometry, arterial,” *Encycl. Med. devices Instrum.*, pp. 402–410, 2006.
[60] L. Peter, N. Noury, and M. Cerny, “A review of methods for non-invasive and continuous blood pressure monitoring: Pulse transit time method is promising?,” *IRBM*, vol. 35, no. 5, pp. 271–282, Oct. 2014.
[61] K. Shioya and T. Dohi, “Blood pressure measurement device based on the arterial tonometry method with micro triaxial force sensor,” in *2013 Transducers & Eurosensors XXVII: The 17th International Conference on Solid-State Sensors, Actuators and Microsystems (TRANSDUCERS & EUROSENSORS XXVII)*, 2013, pp. 2389–2392.
[62] Parry Fung, G. Dumont, C. Ries, C. Mott, and M. Ansermino, “Continuous noninvasive blood pressure measurement by pulse transit time,” in *The 26th Annual International Conference of the IEEE Engineering in Medicine and Biology Society*, 2004, vol. 3, pp. 738–741.
[63] Y.-L. Zheng *et al.*, “Unobtrusive Sensing and Wearable Devices for Health Informatics,” *IEEE Trans. Biomed. Eng.*, vol. 61, no. 5, pp. 1538–1554, May 2014.
[64] S. L. Martin *et al.*, “Weighing Scale-Based Pulse Transit Time is a Superior Marker of Blood Pressure than Conventional Pulse Arrival Time,” *Sci. Rep.*, vol. 6, pp. 1–8, 2016.
[65] R. A. Payne, C. N. Symeonides, D. J. Webb, and S. R. J. Maxwell, “Pulse transit time measured

from the ECG: an unreliable marker of beat-to-beat blood pressure," *J. Appl. Physiol.*, vol. 100, no. 1, pp. 136–141, Jan. 2006.
[66] C.-S. Kim *et al.*, "Ballistocardiogram: Mechanism and Potential for Unobtrusive Cardiovascular Health Monitoring," *Sci. Rep.*, vol. 6, no. 1, p. 31297, Nov. 2016.
[67] C.-S. Kim, A. M. Carek, O. Inan, R. Mukkamala, and J.-O. Hahn, "Ballistocardiogram-Based Approach to Cuff-Less Blood Pressure Monitoring: Proof-of-Concept and Potential Challenges," *IEEE Trans. Biomed. Eng.*, pp. 1–1, 2018.
[68] M. Wong, E. Pickwell-MacPherson, Y. Zhang, and J. C. Y. Cheng, "The effects of pre-ejection period on post-exercise systolic blood pressure estimation using the pulse arrival time technique," *Eur. J. Appl. Physiol.*, vol. 111, pp. 135–144, 2011.
[69] G. Zhang, M. Gao, D. Xu, N. B. Olivier, and R. Mukkamala, "Pulse arrival time is not an adequate surrogate for pulse transit time as a marker of blood pressure," *J. Appl. Physiol.*, vol. 111, no. 6, pp. 1681–1686, 2011.
[70] C.-S. Kim *et al.*, "Ballistocardiogram: Mechanism and Potential for Unobtrusive Cardiovascular Health Monitoring.," *Sci. Rep.*, vol. 6, p. 31297, Aug. 2016.
[71] N. Fazeli *et al.*, "Subject-specific estimation of central aortic blood pressure via system identification: preliminary in-human experimental study," *Med. Biol. Eng. Comput.*, vol. 52, no. 10, pp. 895–904, 2014.
[72] M. Rashedi *et al.*, "Comparative Study on Tube-Load Modeling of Arterial Hemodynamics in Humans," *ASME J. Biomech. Eng.*, vol. 135, no. March, p. 31005, 2013.
[73] P. Yousefian *et al.*, "The Association between Limb Ballistocardiogram-Based Pulse Transit Time and Blood Pressure," *IEEE Trans. Biomed. Eng.*, p. Under Review, 2018.
[74] D. P. Garg and M. A. Ross, "Vertical Mode Human Body Vibration Transmissibility," *IEEE Trans. Syst. Man. Cybern.*, vol. SMC-6, no. 2, pp. 102–112, 1976.
[75] S. G. Kelly, *Mechanical Vibrations: Theory and Applications*. Cengage Learning, 2011.
[76] W. R. Scarborough, F. W. Davis, B. M. Baker, R. E. Mason, and M. L. Singewald, "A REVIEW OF BALLISTOCARDIOGRAPHY," *Am. Heart J.*, vol. 44, pp. 910–946, 1952.
[77] J. Atterhog, K. Eliasson, and P. Hjemdahl, "Sympathoadrenal and cardiovascular responses to mental stress, isometric handgrip, and cold pressor test in asymptomatic young men with primary T wave abnormalities in the electrocardiogram," *Br. Heart J.*, vol. 46, pp. 311–319, 1981.
[78] P. G. Saab *et al.*, "The cold presser test: Vascular and myocardial response patterns and their stability," *Psychophysiology*, vol. 30, no. 4, pp. 366–373, 1993.
[79] S. B. Miller and A. Sita, "Parental history of hypertension, menstrual cycle phase, and cardiovascular response to stress," *Psychosom. Med.*, vol. 56, no. 1, pp. 61–69, 1994.
[80] A. Sita and S. B. Miller, "Estradiol, progesterone, and cardiovascular response to stress," *Psychoneuroendocrinology*, vol. 21, no. 3, pp. 339–346, 1996.
[81] G. Willemsen, C. Ring, D. Carroll, P. Evans, A. Clow, and F. Hucklebridge, "Secretory immunoglobulin A and cardiovascular reactions to mental arithmetic and cold pressor," *Psychophysiology*, vol. 35, pp. 252–259, 1998.
[82] E. S. Mezzacappa, R. M. Kelsey, E. S. Katkin, and R. P. Sloan, "Vagal rebound and recovery from psychological stress," *Psychosom. Med.*, vol. 63, no. 4, pp. 650–657, 2001.
[83] R. M. Kelsey, S. R. Ornduff, and B. S. Alpert, "Reliability of cardiovascular reactivity to stress: Internal consistency," *Psychophysiology*, vol. 44, no. 2, pp. 216–225, 2007.
[84] R. Adhana, M. Agarwal, R. Gupta, and J. Dvivedi, "Effect of slow breathing training on heart rate , spontaneous respiratory rate and pattern of breathing," *Int. J. Res. Med. Sci.*, vol. 4, no. 4, pp. 1027–1030, 2016.
[85] A. V. Turankar *et al.*, "Effects of slow breathing exercise on cardiovascular functions, pulmonary functions & galvanic skin resistance in healthy human volunteers - a pilot study," *Indian J. Med. Res.*, vol. 137, no. 5, pp. 916–921, 2013.
[86] Q. Chang, R. Liu, and Z. Shen, "Effects of slow breathing rate on blood pressure and heart rate variabilities," *Int. J. Cardiol.*, vol. 169, no. 1, pp. e6–e8, 2013.
[87] B. T. Engel and R. A. Chism, "Effect of Increases and Decreases in Breathing Rate on Heart Rate and Finger Pulse Volume," *Psychophysiology*, vol. 4, no. 1, pp. 83–89, 1967.
[88] Y. Zou *et al.*, "Meta-Analysis of Effects of Voluntary Slow Breathing Exercises for Control of

Heart Rate and Blood Pressure in Patients With Cardiovascular Diseases," *Am. J. Cardiol.*, vol. 120, pp. 148–153, 2017.
[89] C. N. Joseph *et al.*, "Slow breathing improves arterial baroreflex sensitivity and decreases blood pressure in essential hypertension," *Hypertension*, vol. 46, pp. 714–718, 2005.
[90] A. Grunovas, E. Trinkunas, A. Buliuolis, E. Venskaityte, J. Poderys, and K. Poderiene, "Cardiovascular Response to Breath-Holding Explained by Changes of the Indices and their Dynamic Interactions," *Biol. Syst. Open Access*, vol. 5, p. 152, 2016.
[91] F. Lemaître, F. Bernier, I. Petit, N. Renard, B. Gardette, and F. Joulia, "Heart rate responses during a breath-holding competition in well-trained divers," *Int. J. Sports Med.*, vol. 26, pp. 409–413, 2005.
[92] A. Savitzky and M. J. E. Golay, "Smoothing and Differentiation of Data by Simplified Least Squares Procedures," *Anal. Chem.*, vol. 36, no. 8, pp. 1627–1639, 1964.
[93] R. Mukkamala and J.-O. Hahn, "Toward Ubiquitous Blood Pressure Monitoring via Pulse Transit Time: Predictions on Maximum Calibration Period and Acceptable Error Limits," *IEEE Trans. Biomed. Eng.*, vol. 65, no. 6, pp. 1410–1420, 2018.
[94] J. M. Kang, T. Yoo, and H. C. Kim, "A wrist-worn integrated health monitoring instrument with a tele-reporting device for telemedicine and telecare," *IEEE Trans. Instrum. Meas.*, vol. 55, no. 5, pp. 1655–1661, 2006.
[95] J. Liu, B. P.-Y. Yan, W.-X. Dai, X.-R. Ding, Y.-T. Zhang, and N. Zhao, "Multi-wavelength photoplethysmography method for skin arterial pulse extraction," *Biomed. Opt. Express*, vol. 7, no. 10, p. 4313, Oct. 2016.